To the Graduate Council:

I am submitting herewith a thesis written by Steven M. Joslin entitled "The Feasibility of Rigid Die Bidimensional Compression For Consolidation of Metal Powders." I have examined the final copy of this thesis for form and content and recommend that it be accepted in partial fulfillment of the requirements for the degree of Master of Science, with a major in Metallurgical Engineering.

K H G Ashbee

Kenneth H. G. Ashbee, Major Professor

We have read this thesis
and recommend its acceptance:

Charlie R. Brooks

Dan I. Allen

Accepted for the Council:

Lee Minkel

Vice Provost
and Dean of The Graduate School

STATEMENT OF PERMISSION TO USE

In presenting this thesis in partial fulfillment of the requirements for a Master's degree at The University of Tennessee, Knoxville, I agree that the Library shall make it available to borrowers under rules of the Library. Brief quotations from this thesis are allowable without special permission, provided that accurate acknowledgment of the source is made.

Permission for extensive quotation from or reproduction of this thesis may be granted by my major professor, or in his absence, by the Head of Interlibrary Services when, in the opinion of either, the proposed use of the material is for scholarly purposes. Any copying or use of the material in this thesis for financial gain shall not be allowed without my written permission.

Signature Stan M Joslin

Date 11-30-89

THE FEASIBILITY OF RIGID DIE BIDIMENSIONAL COMPRESSION FOR CONSOLIDATION OF METAL POWDERS

A Thesis

Presented for the

Master of Science

Degree

The University of Tennessee, Knoxville

Steven M. Joslin

December 1989

ACKNOWLEDGEMENTS

I wish to thank my major advisor, Dr. K. H. G. Ashbee, for the opportunity to work on this project and the unhindered freedom to pursue it however I saw fit. I especially appreciate his overwhelming generosity in allowing me to procure all of the neccessary materials and equipment and to completely redesign the original apparatus, as well as his timely management of every aspect of the project and his concern for the success of the technique. His efforts will not soon be forgotten.

I would like to thank Dr. C. R. Brooks and Dr. B. F. Oliver for taking the time to review the manuscript and for their inputs to its content and organization.

I gratefully acknowledge the financial support provided by the Center For Materials Processing, The University of Tennessee.

I especially wish to thank the Machine Shop for their patience and perseverance during the entire ordeal. In particular, I wish to thank Doug Fielding for his intuition and help in working out the details of the apparatus designs, "Big" Michael Rogers for hours upon hours of machining, plumbing, fixing, and fiddling. I also wish to thank Larry Smith for his efforts to machine mechanical property specimens from the unpredictable billets produced

in this work, Ray "Junior" Bellamy for his efforts to weld the phase one cans, and Mike Ensor for fabrication of the idiot light system which prevented excessive out of plane deflection and further delays. They are the true heros behind this work. I will remember their dedication.

I would like to thank Bob Hale for the design of the working dies and for the personal support he and his wife Gene extended during this time.

ABSTRACT

The need to consider applied bidimensional stress fields for the consolidation of metal powders is supported by its absence in the literature. In this study, the feasibility of rigid-die bidimensional compression for the consolidation of metal powders is assessed. The apparatus is developed and tested as well as the success of the technique.

The apparatus developed is suitable for laboratory use. The limitations arise from the hydraulic system capacity (50,000 pounds force maximum), the friction between all of the moving parts (especially between the specimen and dies), and the absence of control over the movement of the individual components within the system.

Aluminum based powders are used to determine the success of the consolidation technique. The commercially pure aluminum, Al-123, powder developed mechanical properties equivalent to wrought 1060 aluminum. The alloyed powder, MB85, is intended for use in metal matrix composites with silicon carbide. The powder is used without reinforcement in this study. The baseline mechanical properties are not available for comparison, but the results of the tensile tests conducted in this study are encouraging.

The conditions providing maximum density range from room temperature to 450°C (840°F) and 300 MPa (43 ksi) to 63 MPa (9 ksi),respectively; all at a pressing time of 15 seconds.

TABLE OF CONTENTS

LIST OF FIGURES

LIST OF TABLES

CHAPTER I.

INTRODUCTION

From the advent of modern powder metallurgy in the 19th century to the present, the elusive potential of powder-based structural components has always met with a compromise between mechanical properties and economics, governed by the limitations inherent in the individual consolidation techniques. Progress in powder production techniques demands equal progress in consolidation technique, or else that which is gained by improved powder production may be lost during consolidation.

As powder production technology advances, more attention must be focused upon powder consolidation in order to develop the material's full potential in usable, bulk forms. A review of the history of powder consolidation techniques discloses a lack of consideration for applied bidimensional stress fields. The abundance of research performed in more conventional areas may be explained by the relative ease of designing a uniaxial press or an isostatic pressure chamber. A successful design and application of compressive force in only two dimensions has, for whatever reason, not been published. It is the purpose of this work to assess the viability of rigid-die bidimensional compression as a consolidation technique for powdered metals.

At the simplest level, the difficulty in achieving full potential from a powdered material stems from two fundamentally distinct phenomena; limitations in achieving interparticle bond integrity and microstructural degradation as a result of the consolidation process itself. The latter includes grain coarsening, segregation, and component interaction. By careful selection of the consolidation conditions, the microstructure of the final component can be controlled within the inherent limits of the consolidation technique employed. The extent to which the economics of the process affects the selection of the consolidation technique depends upon the application; often it takes the upper hand.

Since the consolidation technique developed in this work is unique, there are no references directly related to rigid-die bidimensional compression of powdered metals, the literature review will consist of: a summary of current consolidation techniques, a review of densification mechanisms and a review of powder metallurgy including the modes of pore closure and densification.

CHAPTER II.

LITERATURE REVIEW

CURRENT CONSOLIDATION TECHNIQUES

INTRODUCTION

Thermomechanical consolidation methods utilizing heat and/or external force include uniaxial pressing, isostatic pressing, forging, extrusion, and triaxial compaction. All of these methods may be performed hot or cold. For each method, the final properties of the compact depend on time, temperature, material, and state of applied stress. Consolidation under pressure produces superior microstructural integrity and is therefore the preferred method of production when dynamic structural properties are the controlling design factors. The consolidation methods to be reviewed are representative techniques which encompass the variations in the state of applied stress currently encountered in powdered metals processing.

UNIAXIAL COMPRESSION

Uniaxial pressing is the forerunner of modern consolidation techniques. The earliest techniques consisted of cold pressing by application of force along a single axis, followed by sintering. The initial pressing operation imparts sufficient "green" strength for handling. In conventional press and sinter consolidation, it is generally preferred that the green, cold pressed density be similar in magnitude to the final sintered density (1). High green density produces little shrinkage and increasing dimensional accuracy. This process generally produces parts with less than 95% theoretical density (1). The high flow stress and work hardening of the material at the low homologous temperatures employed usually limit the density obtained via cold pressing (2). Thus, sintering is generally required to eliminate residual porosity in cold pressed parts.

Tooling for uniaxial pressing generally consists of a cylindrical die cavity with one or two movable rams. Figure 1a shows a typical early press. Early on, the presses were single action; pressure was applied from the top only. Researchers soon realized, through density distribution studies (3,4,5), that die wall and interparticle friction limit the size of the compact. The interaction between friction and the application of uniaxial

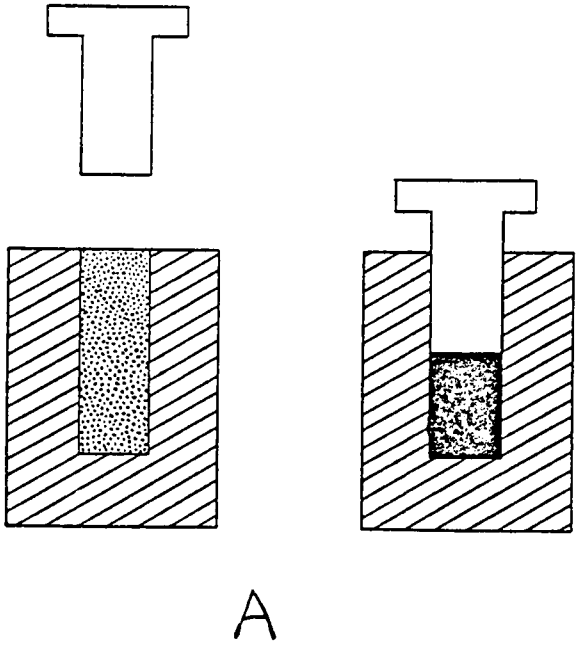

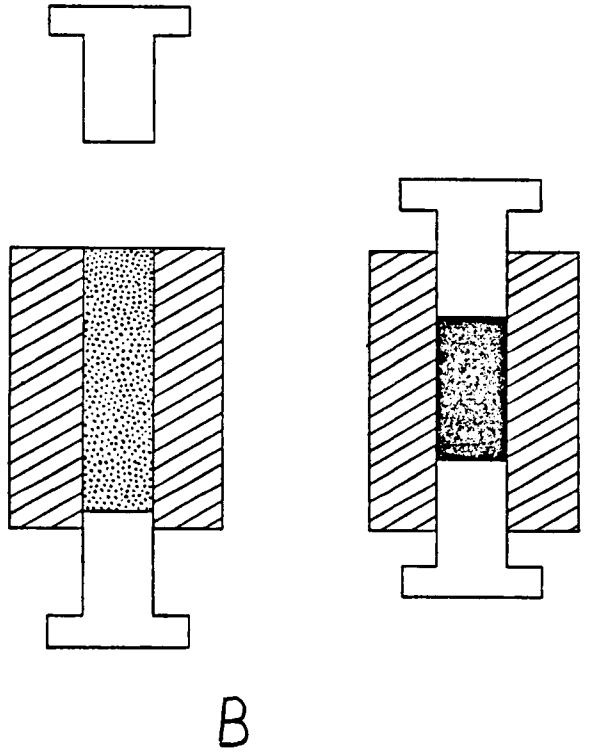

Figure 1: Schematic representation of: a) uniaxial press b) double action uniaxial press.

pressure results in appreciable density gradients within the compact (6). As the compression pressure increases, the average density increases, but variation in the density distribution also increases (7). When cold pressing is used in preparation of powders for sintering, these gradients manifest themselves as heterogeneous shrinkage or inconsistent mechanical properties in the sintered part. Cold compacted aluminum parts generally have densities in the range 50-80% of theoretical density leaving sufficient interconnected porosity for efficient degassing (8).

In 1912, the first hot pressing patent was issued (6) and full density via uniaxial pressing became feasible. Fischmeister (9) observed that friction in uniaxial hot pressing is not as critical as it is for uniaxial cold pressing. The lower flow stress reduces the reaction stresses against the die wall and hence the frictional stresses. Nevertheless, the uneven pressure propagation through any uniaxially pressed powder limits the homogeneity of the densification process and therefore the final properties of the part.

Based upon this finding, double-action presses were developed in which pressure is applied in opposite directions along the same axis, Figure 1b. In such a press, the compact height can be doubled over that of the single action press while maintaining the same degree of homogeneity (10). The additional ram may also facilitate

ejection from the die. In a study conducted on iron powders, Squire (3) observed a correlation between density and die geometry. An important result is that the static die wall area is the major source of friction which disrupts the propagation of uniform pressure, suggesting that this surface area should be minimized. The effects of die wall area-to-volume or height-to-diameter ratios are also evident in the work of Kamm, Steinberg, and Wulff (7).

Naturally, lubricants were tested to assess their ability to reduce friction. For particles smaller than the die surface roughness, the coefficient of friction is as high as 0.6, while for smooth die walls it ranges from 0.2 to 0.4 (11). The die wall friction leads to failures near the die wall/powder interface. Failure, in this case, indicates a plane across which discontinuous movement occurs; material on one side of the plane remains stationary, while material on the other side moves in a shearing mode. For rough-walled dies, the failure is localized in the powder, while it is the interface which fails for smooth dies (11). Failure at the die-wall interface is the desired senario. Squire (3) showed that die wall lubrication is more effective than lubricants blended with the powder, although mixing the lubricant with the powder is more typical in production (12). The absence of interparticle lubrication in the green part alleviates the problems associated with contamination by entrapment in

the final compact. The lubricant must be removed before internal voids are sealed from the surface. This requires an additional step prior to full densification, where the lubricant is burned off. However, better interparticle lubrication does allow a slightly more uniform density; this is a trade-off which must be evaluated. Figure 2 shows the density distribution found in rigid die pressed billets with and without lubrication (7). The highest density is found near the periphery of the moving ram(s). The lowest density is found at the bottom periphery for a single ram press and near the center periphery for a double-action press (7). Since the density of consolidated powders is indicative of their strength, the distribution should be as homogeneous and reproducible as possible. Establishing the design limits for parts made from the pressed billet is considerably more difficult, if at all plausible, when the properties are not homogeneous. In an effort to further improve homogeneity, Hammond and Schwarts (13) developed a rotating die which takes advantage of the lower dynamic coefficient of friction between the moving die wall and the powder.

Uniaxial pressing of aluminum powder typically involves pressure in the 6 to 10 ksi range at approximately 400°C for less than 2 minutes (14). The primary variables in uniaxial pressing for a given powder are pressure, temperature, height-to-diameter ratio, and lubricant. The

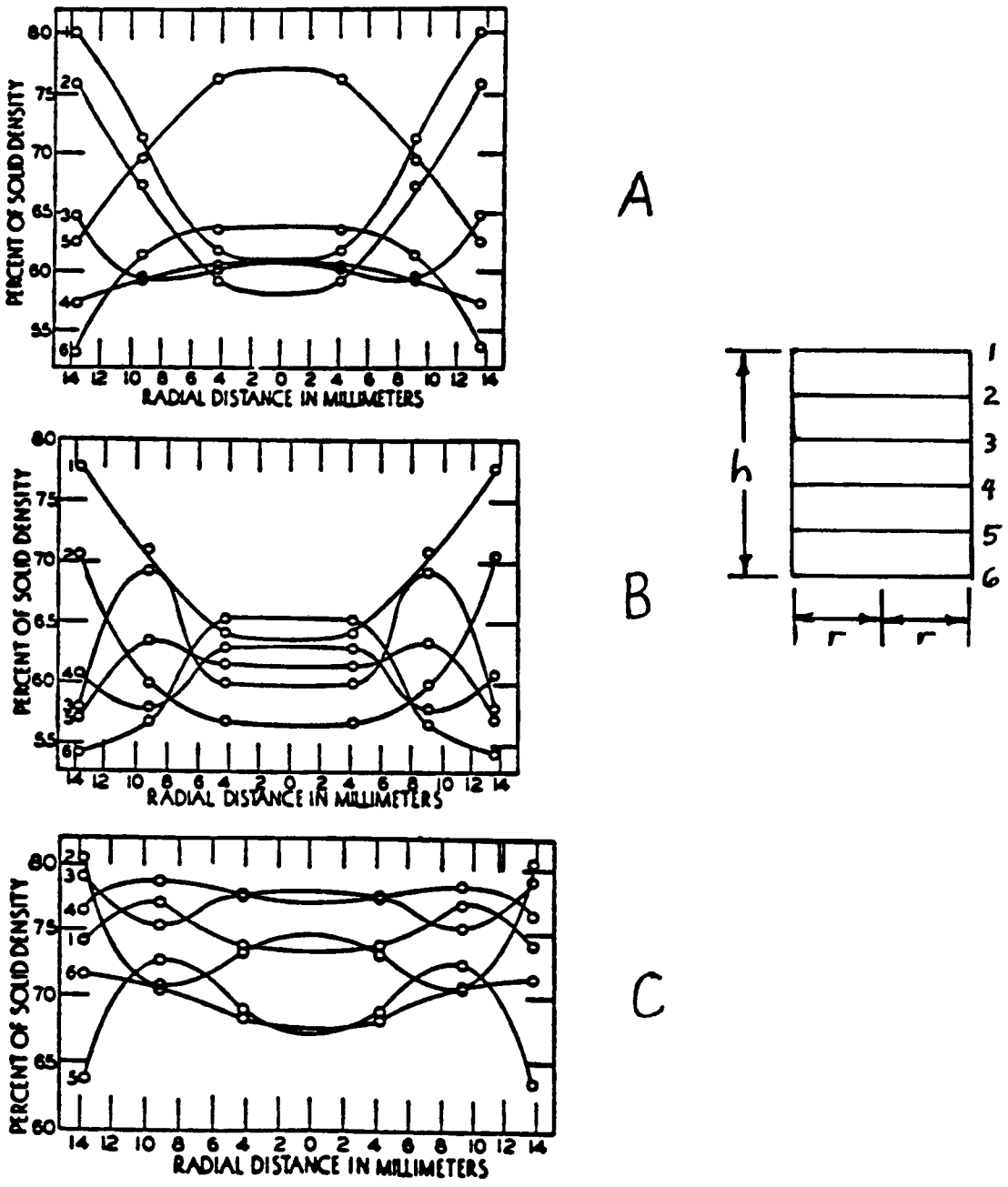

Figure 2: The relationship between density and position within the compact for uniaxial pressing of -300 mesh nickel at constant pressure (30 tons/sq.in.): a) No lubricant, b) Lubricant in the powder only, and c) Lubricant on the die walls only. (R. Kamm, M. Steinberg, Students, and J. Wulff, "Plastic Deformation in Metal-powder Compacts," Metals Technology (1947) 442)

initial packing of the powder may also affect the final properties (15) because friction can limit the axial strain and hence the final density.

ISOSTATIC PRESSING

Isostatic pressing virtually eliminates die wall friction. The process was developed in 1955 by Saller (16). In this technique, high pressure is applied to the powder via gaseous argon or nitrogen. The state of applied stress is purely hydrostatic because only the gas does work on the specimen. Encapsulation of the powder is usually required. For simple shapes, metal cans are used, while ceramic or glass molds are used for complex shapes. However, with sufficient green density or by application of a sealant to the green pressed part, containerless isostatic pressing is possible (17). Figure 3 is a schematic representation of a conventional hot isostatic pressing (HIP) system. Net and near-net shape parts with little distortion are common and have excellent uniformity of density and strength. However, irregular and fine powders must be precompacted to 70% of theoretical density to avoid warpage (9). Also, precompaction increases the interparticle contact area which increases the thermal conductivity from 1% to 27% of that for the solid at theoretical densities of 65% to 74%,

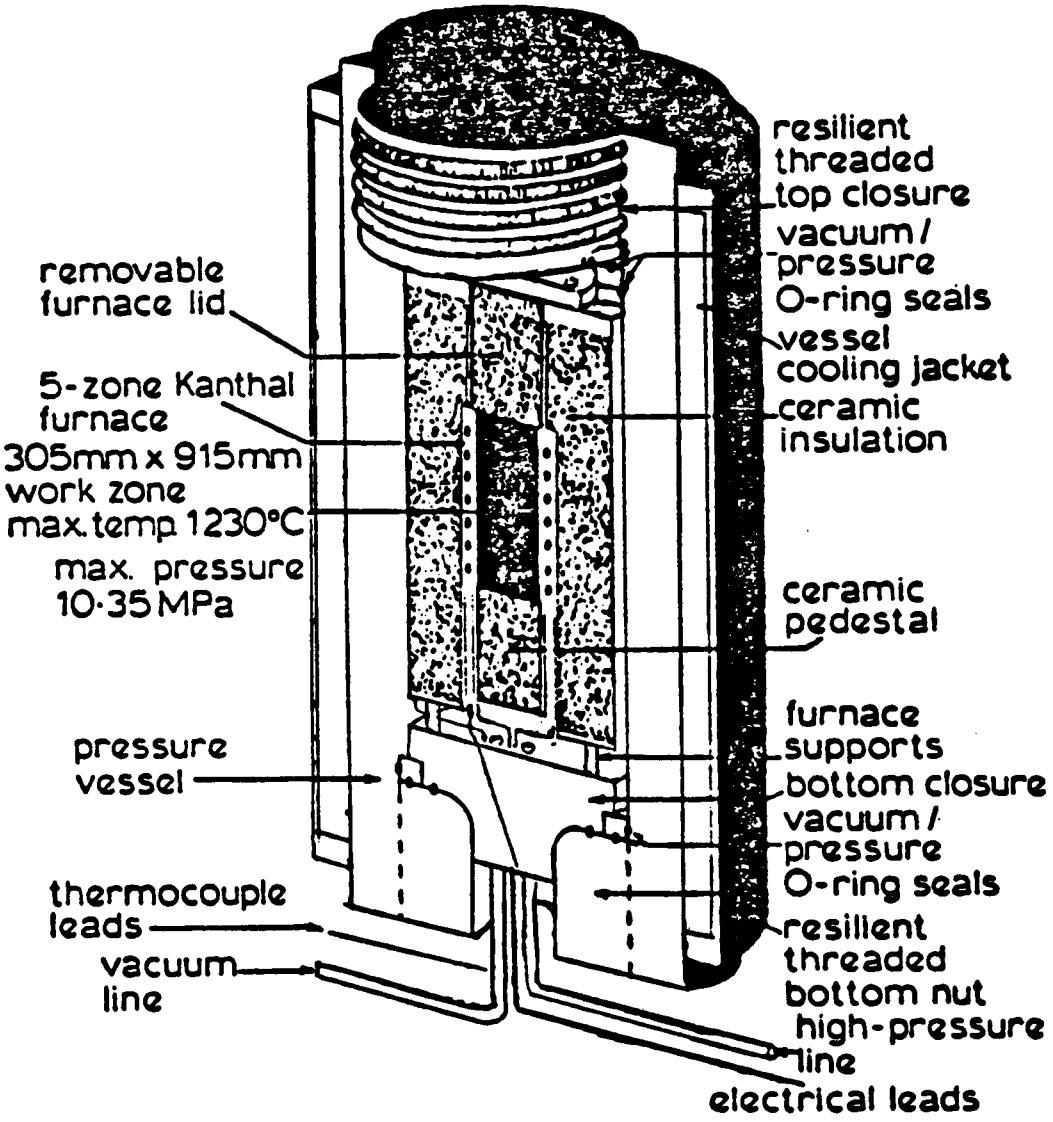

Figure 3: Conventional hot isostatic pressing system. (W. J. Huppman and M. Hirschvogel, "Powder Forging," International Metals Reviews, 5 (1978) 209)

respectively (9). Uniformity of the initial density is important to net shape parts. The dimensional accuracy depends on reproducible die or bag filling. Low initial density will cause more shrinkage during isostatic pressing in order to fill the voids. If the initial density is sufficient, buckling of the can is not a problem (9). Part sizes can be larger since die wall friction is not a limiting factor. Container design, entrapped gas, and outgassing of hydrides and adsorbed gases must be considered in the design of parts for HIP processing. Vacuum degassing is required for some powders, such as aluminum (8,14).

Cold isostatic compaction is usually performed under 8 to 20 ksi giving densities ranging from 60 to 80% of theoretical (18). At a pressure of 15 ksi, aluminum can be fully densified in 2 to 4 hours at 480 to 530 C (17). The time and temperature used are usually short enough and low enough to limit contamination from the can by solid state diffusion to superficial depths (9). The primary variables for a given powder include pressure, container design, temperature, time, and the heating and cooling rates. The densification rate under HIP conditions is exponentially dependent on temperature; pressure and temperature exhibit a power law dependence (1).

Current HIP systems are classified as wet bag or dry bag processes. The conventional process, also known as the wet bag process, entails loading individual containers, or green

parts, into a pressure chamber. The dry bag technique uses a different chamber, or mold, consisting of a flexible membrane and rigid end platens. Figure 4 illustrates the dry bag apparatus. The rigid ends make loading of the chamber faster and easier, hence improving productivity.

FORGING

Hot forging, sometimes called sinter forging, dates back to World War II. Interest died out but was renewed in the mid-sixties. Powder forging is usually a net shape process. The weight of the preform is tightly controlled; its dimensions are secondary to its mass (19). Ultimately, the part achieves full density as the die fully closes, resulting in no flash or material waste. The loads are much lower than for the forging of wrought stock, significantly reducing die wear.

Powder forging may be divided into two types: repressing and upsetting. The first type, repressing, constitutes the latter stages of closed-die forging where the die wall restricts lateral flow. In its simplest form, it is essentially net shape uniaxial pressing. There is little difference between axial and lateral stress; the difference decreases as consolidation progresses. Eventually the state of stress becomes isostatic. The second type, upsetting, is characterized by unconstrained lateral flow. Under this

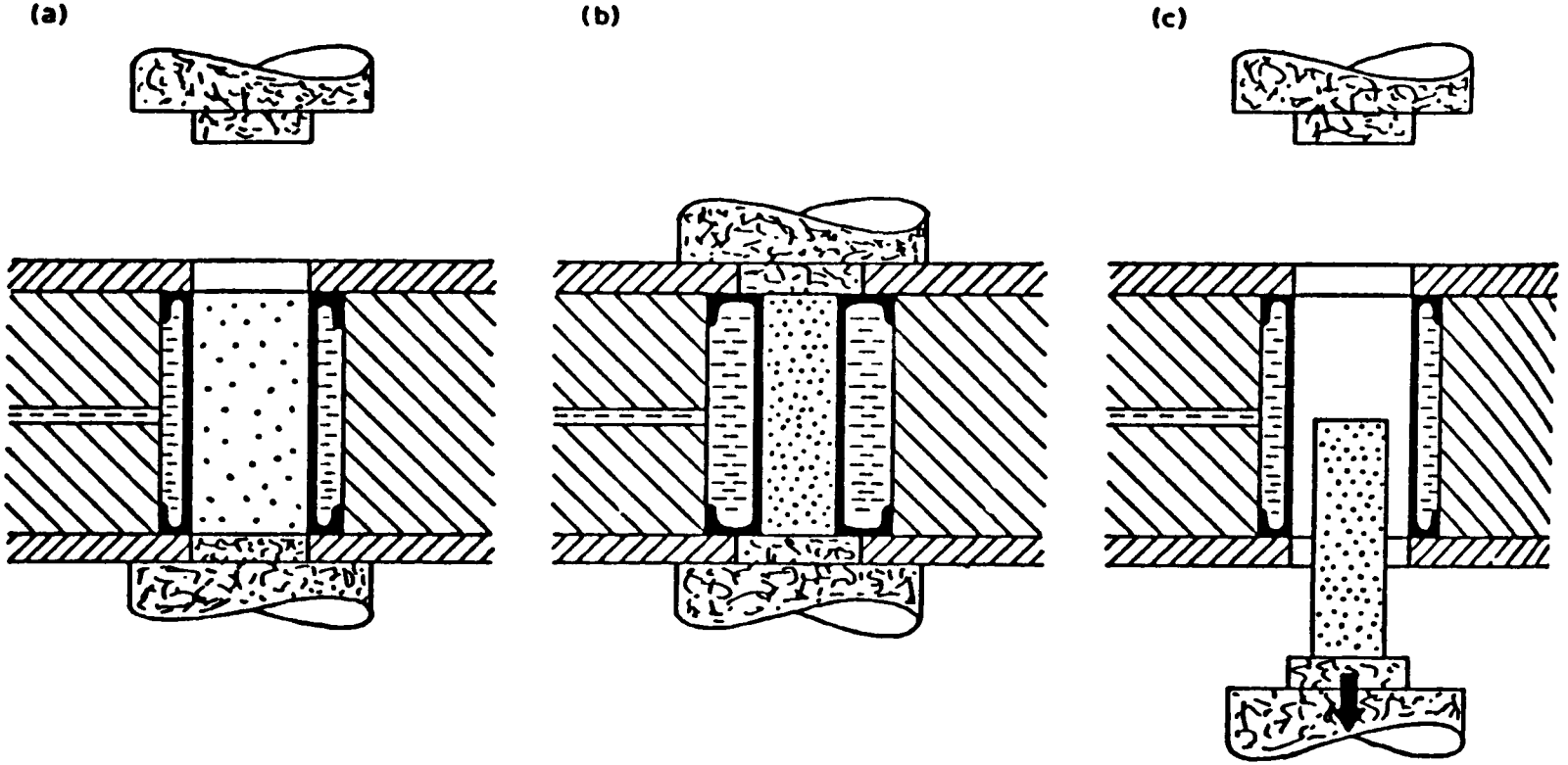

Figure 4: Dry bag isostatic compaction of a preform, a) fill, b) press, and c) eject. (W. J. Huppman and M. Hirschvogel, "Powder Forging," International Metals Reviews, 5 (1978) 209)

condition, shear stresses accompany the applied normal stress. In closed die forging, it is best to develop full density via the upsetting mode before the change in the state of stress, which occurs during the later stages, causes the dominant mode of pore closure to be repressing or isostatic (20). Higher forging loads are required under repressing conditions than under upset forging conditions to produce full density (21).

In most cases, a preform fabricated by a press and sinter procedure is used. Generally, the density of a preform used in hot forging is 70 to 85% of the theoretical density (22). Development of the preform shape can be difficult. The upset test, developed by Lee (23), is used to determine formability limits using a cylindrical powder compact. From these limits, the shape of the preform can be determined. The height-to-diameter (H/D) ratio is a major consideration. Barreling occurs as a result of friction between the preform and the forging dies (20). The effect of decreasing the H/D ratio is to increase the circumferential tensile stress, since the barreling of the cylinder wall would then have a smaller radius of curvature. This effect is illustrated in Figure 5 (22). The rule-of-thumb limit on the H/D ratio is 4 (6). Figure 6 shows the effect of friction on powder formability.

Strengths of forged aluminum parts are 40-60% higher than for non-forged equivalents (24). Fatigue and endurance

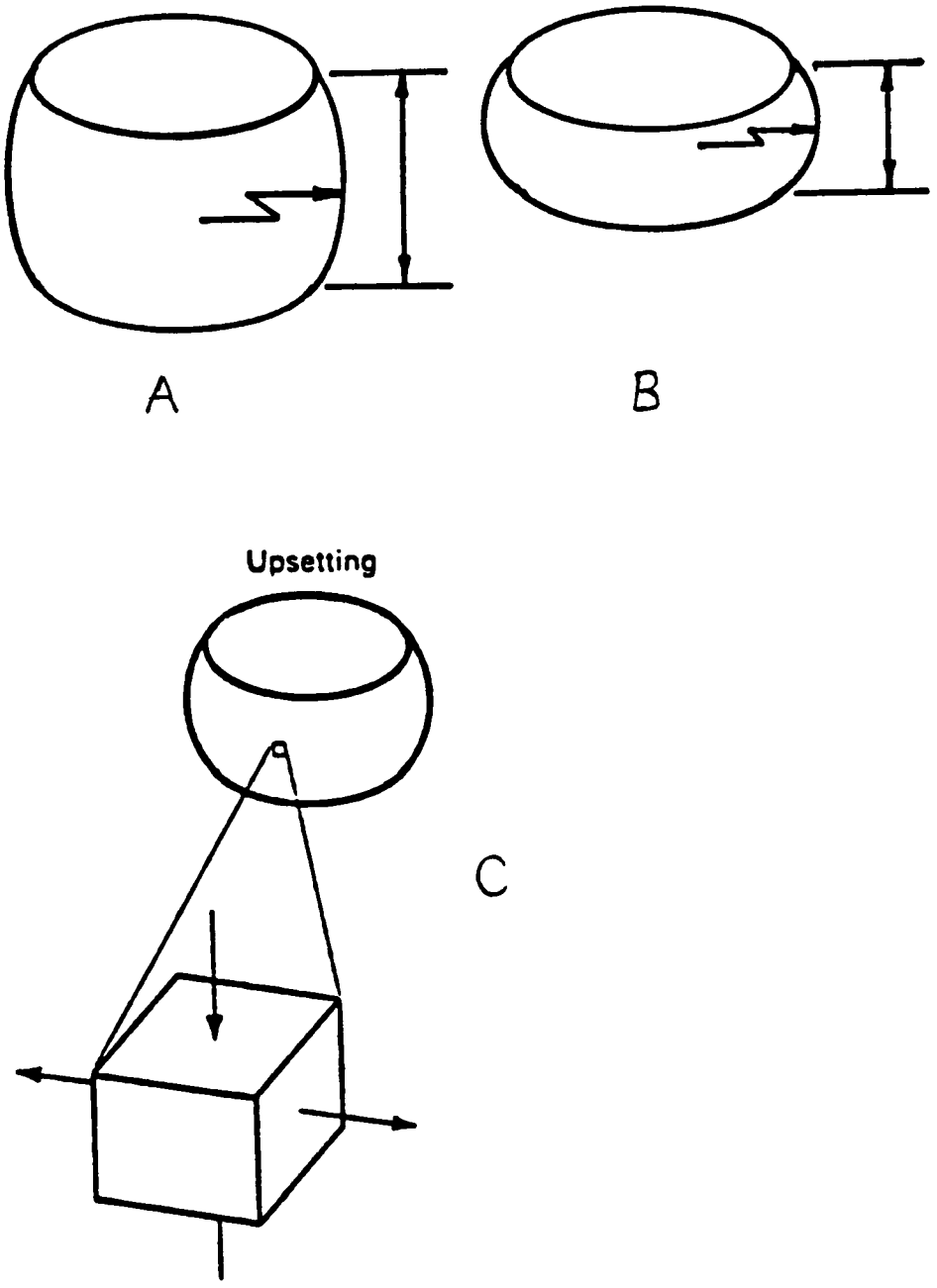

Figure 5: The barreling effect under upset forging conditions with friction at platens, a) Large H/D ratio, large radius of curvature, low hoop stress, b) Small H/D ratio, small radius of curvature, high hoop stress, and c) State of stress in bulged material.

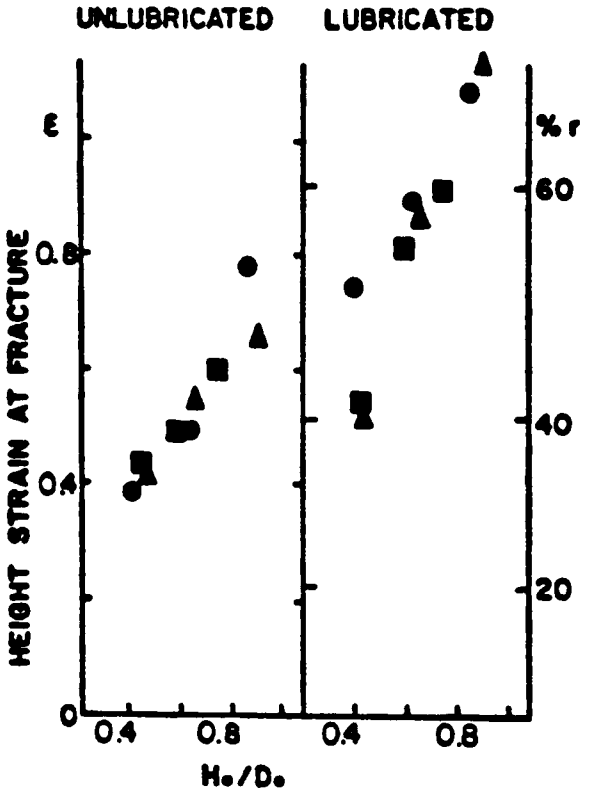

Figure 6: Height strain at fracture for hot upsetting of sintered (700°F) 601AB aluminum alloy powder compacts: ■ 76%, ● 88%, ▲ 93% initial density. (P. W. Lee and H. A. Kuhn, "P/M Forging," Metals Handbook, 9th Edition, Vol. 7, ASM, Metals Park, OH (1984) 410)

limits are doubled. Typical forging conditions for dispersion strengthened aluminum alloys are 90 ksi and 510 to 540°C (25). The primary variables are pressure, temperature, die design, and preform design. The mode of pore closure is important and will be discussed later.

EXTRUSION

Extrusion combines compaction and plastic work into one step. The starting billet may be loose or green pressed powder with or without encapsulation. If the powder is encapsulated, the material used for the can must have as close to the same stiffness at the extrusion temperature as the powder (14). The green billet is severely deformed under hydrostatic and deviatoric stresses. Deviatoric stress is defined as the non-isostatic component of the state of stress. Upon passing through the extrusion die the green billet is reduced in cross-section. The reduction in cross-sectional area establishes the amount of plastic work done on the material (26). Figure 7a (26) illustrates the process. Extrusion dies vary in cross-section and design; some produce a gradual reduction in area while others produce a very abrupt reduction. The angle in the die throat is an important parameter in the process (26).

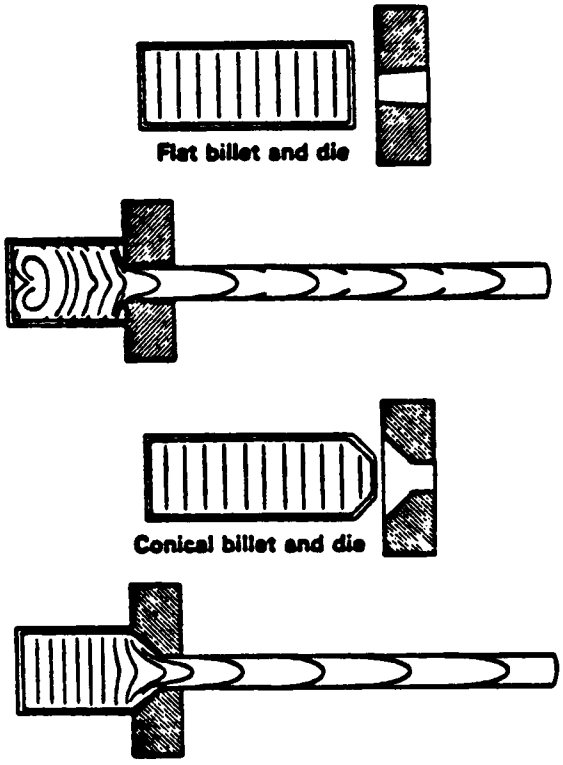

Figure 7: Schematic representation of extrusion for flat billet and die, conical billet and die, and the penetrator technique. The penetrator technique prevents can folding for loosely packed billets. (F. V. Lenel, "Hot Pressing - Appendix: Hot Extrusion," Metals Handbook, 9th Edition, Vol. 7, ASM, Metals Park, OH (1984) 515)

The shear stresses that develop result from friction between the die and the material. Nearly half of the work done is expended in shear deformation (26). It is generally accepted that large amounts of deformation by shearing is beneficial to the microstructural integrity of powder-based compacts (1,2,19,20,21,22,27). The overall die design is critical. Complex shapes may be produced by using inserts in simple cans. Figure 8 (26) shows two examples. For powders having low packing density, a penetrating ram is used, Figure 7b. The ram is designed to enter the inside diameter of the can so that sufficient densification of the powder occurs prior to extrusion which prevents the can from folding (26).

Mechanical properties are controlled by the extrusion ratio, pressure, temperature, die throat angle, and extrusion rate. For aluminum, extrusion ratios of at least 10:1 are required, with 20 or 50:1 being most common (25). Extrusion temperatures range from 340 to 480 C (25). The densification rate depends upon the rate of extrusion and die design. Strain rates are generally 10 to 30 inches per inch per second (25).

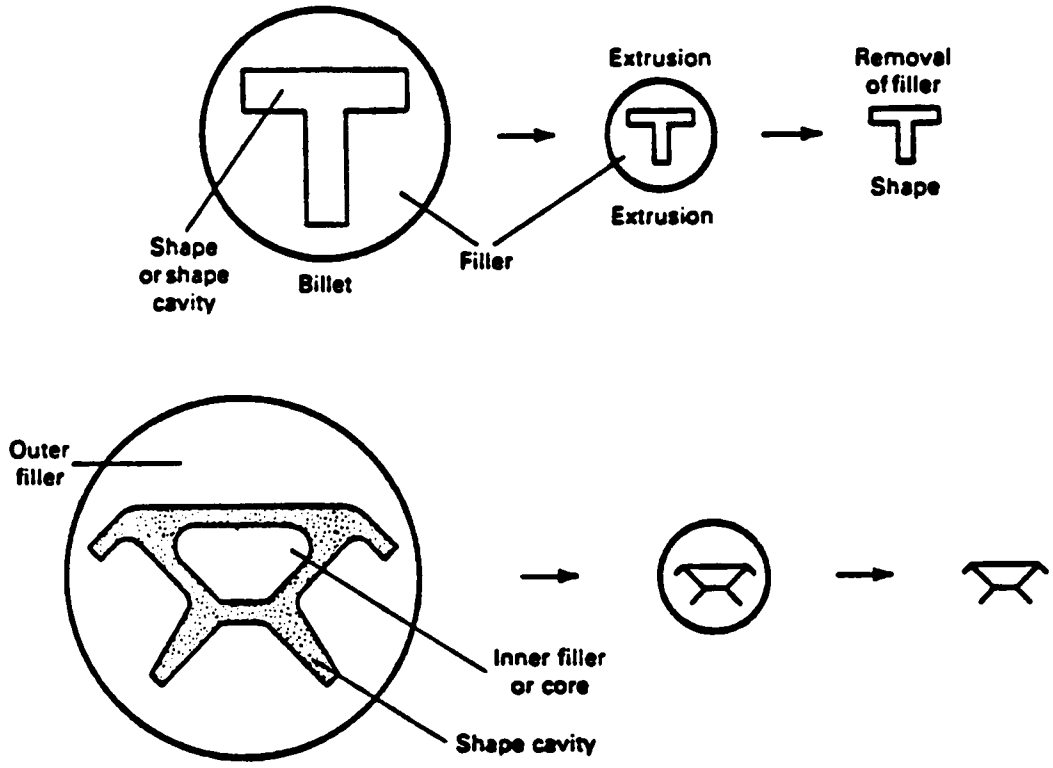

Figure 8: The use of inserts for extrusion of complex shapes in simple cans. (F. V. Lenel, "Hot Pressing - Appendix: Hot Extrusion," Metals Handbook, 9th Edition, Vol. 7, ASM, Metals Park, OH (1984) 515)

TRIAXIAL COMPACTION

Triaxial compaction is a more recent development than the previous techniques. It is a direct extension of both triaxial shear compression testing used in geotechnical engineering and dry bag isostatic pressing (28). The rigid upper and lower bag closures of a dry bag isostatic press are loaded via an axial piston. The axial and lateral pressures are therefore independently controllable. Hence, deviatoric stresses are created, resulting in higher green densities (28). Figure 9 illustrates the apparatus. The powder chamber is usually cylindrical (11) although other simple shapes are possible.

An important consideration is the sequencing of applied stresses. Isostatic pressure must be applied first, or simultaneously with the axial load, since loose powder has no shear strength (28). Figure 10 (28) shows some of the possible loading paths. The sustainable shear stress increases with increasing confining (lateral) pressure. The isostatic confining pressure becomes the minor principal stress. The axial pressure is the major principal stress. The shear stress developed depends on the relative magnitude

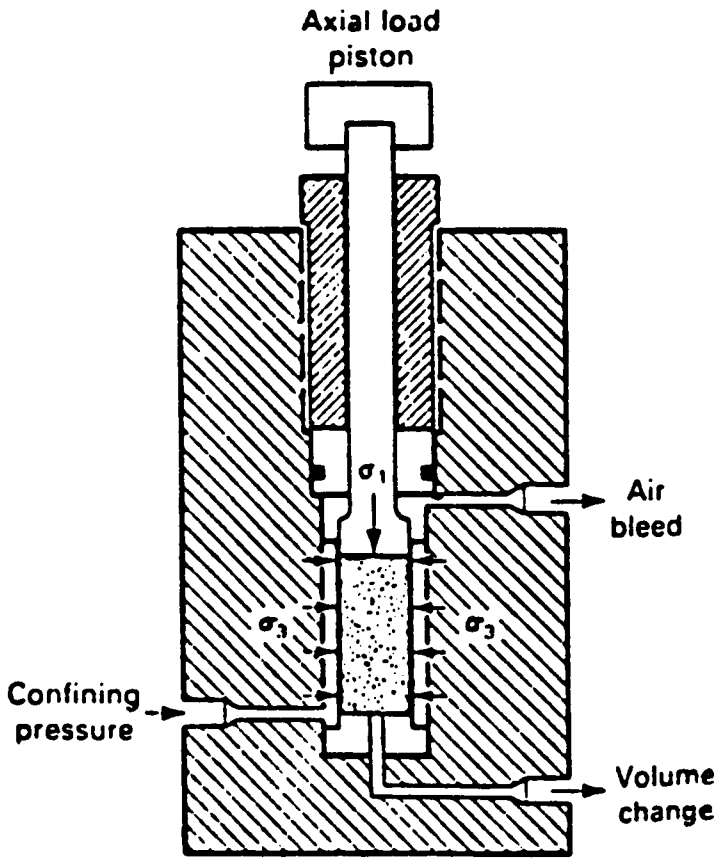

Figure 9: Schematic representation of triaxial compaction apparatus. (R. M. Koerner, "Triaxial Stress State Compaction of Powders," Powder Metallurgy Processing - New Techniques and Analysis, eds. H. A. Kuhn and A. Lawley, Academic Press, New York (1978) 33)

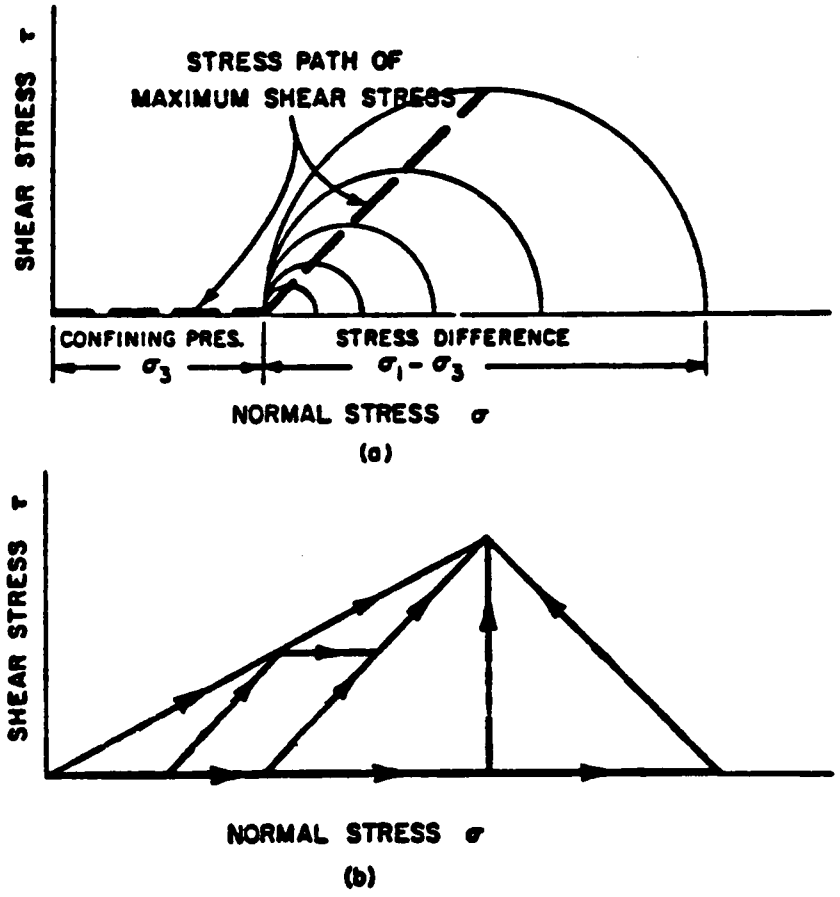

Figure 10: Various loading paths available using triaxial compaction. (R. M. Koerner, "Triaxial Stress State Compaction of Powders," Powder Metallurgy Processing - New Techniques and Analysis, eds. H. A. Kuhn and A. Lawley, Academic Press, New York (1978) 33)

of the major and minor principal stresses and is easily determined through Mohr's circle, i.e.,

$$s_1 - s_3 = 2t$$

where s_1 = largest principal stress

s_3 = smallest principal stress

t = maximum shear stress

The shear stress is limited by the onset of shear failure since the confining mold is flexible.

Density distribution is found to be more homogeneous than in isostatically pressed parts (28). The strength at equal density is higher for triaxially compacted powders compared to isostatically pressed powders. Powders compacted under the highest shear stress give the highest strength at equal density (28). Density versus shear stress curves for various confining pressures are shown in Figure 11 (28). The maximum achievable density by triaxial compaction is found at the termination of the linear portion of the curves, beyond which the deformation becomes localized (28). Figure 12 (28) shows the strength developed by various methods at comparable densities for iron powders; mechanical property data for aluminum are not available. Triaxial compaction allows low cycle times and high producton rates (28). Triaxial compaction of aluminum

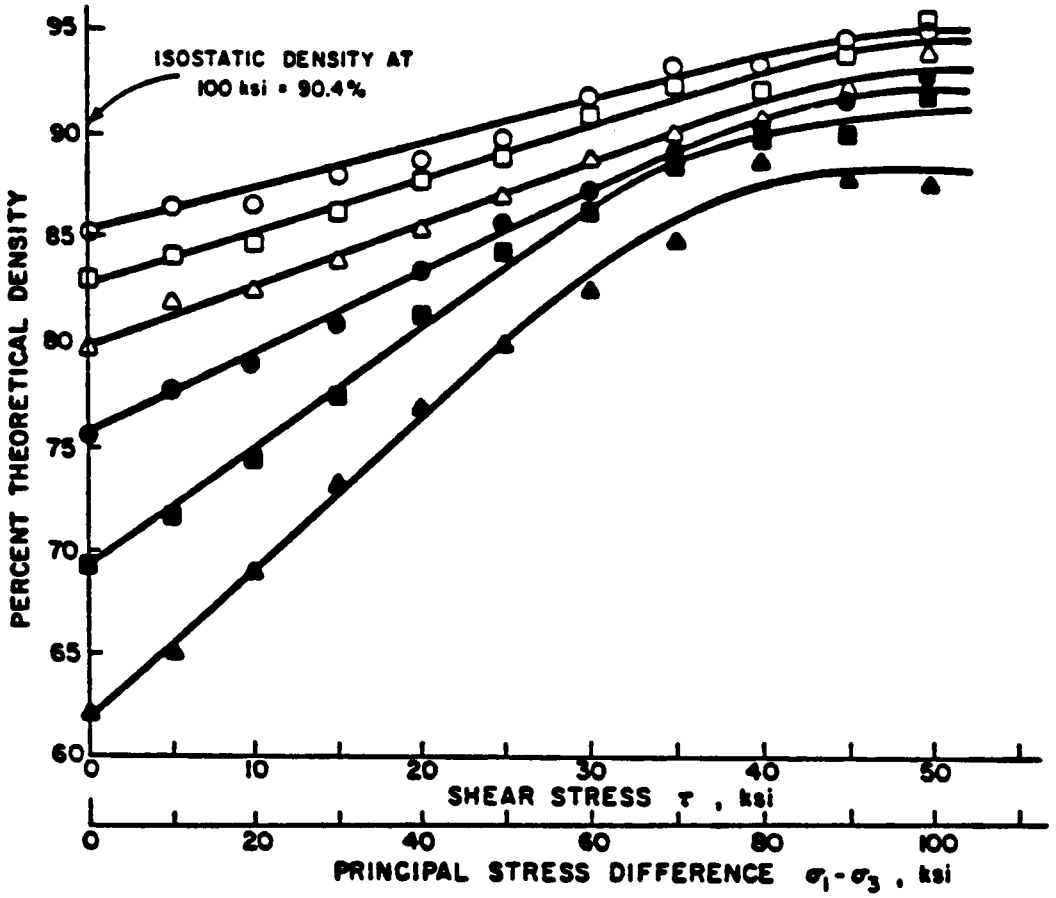

Figure 11: Response of iron powder to triaxial compaction at confining pressures of: ○ 60, □ 50, △ 40, ● 30, ■ 20, ▲ 12 (ksi) (1 ksi = 6.9 MPa) Shear failure occurs when the curves become horizontal. The maximum density is achieved at the termination of the linear portion of the curve. (R. M. Koerner, "Triaxial Stress State Compaction of Powders," Powder Metallurgy Processing - New Techniques and Analysis, eds. H. A. Kuhn and A. Lawley, Academic Press, New York (1978) 33)

(a) CELL PRESSURE COMPARISON			
COMPACTION METHOD	DIE	ISOSTATIC	TRIAXIAL
PRESSURES (ksi)	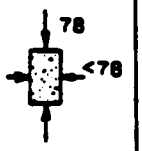	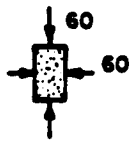	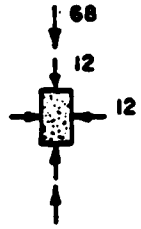
THEO. DENSITY	85 %	85 %	85 %
STRENGTH	20 ksi	25 ksi	55 ksi
(b) GREEN DENSITY COMPARISON			
COMPACTION METHOD	DIE	ISOSTATIC	TRIAXIAL
PRESSURES (ksi)	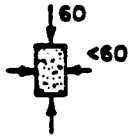	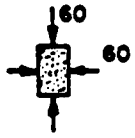	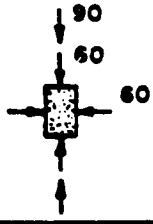
THEO. DENSITY	78 %	85 %	94 %
STRENGTH	15 ksi	25 ksi	73 ksi

[a]1 ksi = 6.9 MPa.

Figure 12: Green density and transverse rupture strength for iron powder compacts formed by various methods. (R. M. Koerner, "Triaxial Stress State Compaction of Powders," Powder Metallurgy Processing - New Techniques and Analysis, eds. H. A. Kuhn and A. Lawley, Academic Press, New York (1978) 33)

is not common commercially, but the pressures are indicated roughly in the literature and range from 0 to 50 ksi for both the background and axial components. The temperatures used are assumed to be comparable to isostatic pressing; they are not given in the literature.

PRESSURE-DENSITY RELATIONSHIPS

The earliest attempts to mathematically model pressure-density relationships were strictly empirical, i.e., based upon curve fitting to the data. Analysis of data, obtained from a multitude of uniaxial pressings in rigid dies, produced equations relating press conditions to density or strength achieved for various powders. The resulting density is commonly reported as a fraction of the theoretical density of the particular material.

A review of the literature on pressure-density relationships for rigid-die, uniaxial compaction was compiled in 1965 by Bockstiegel and Hewing (29).

One of the more widely used relationships was developed by Balshin (30) in 1938. It is only valid for certain powders and only within a narrow range of pressure. Balshin's equation states that,

$$\ln P = -AV + B$$

where P is the applied pressure, V is the relative powder volume (compact/solid of equal mass), and A and B are constants. At high pressures Balshin's relationship predicts the relative powder volume to be less than one, and at low pressures it approaches infinity.

Torre (31) was the first to develop a relationship based on theory. This model made use of an equation for the collapse of a hollow sphere under hydrostatic compression.

$$p = 2\,\sigma_o \ln(r_o/r_i)$$

where σ_o is the yield stress, r_o is the outer radius, r_i is the inner radius, and p is the required pressure.

Konopicky and Shapiro (32) developed the equation,

$$\ln[1/(1-D)] = kP + A$$

where D is the relative density with k and A being constants. The constant, k, is inversely proportional to strain hardening.

Later, Heckel (33) developed Torre's model further and obtained the equation:

$$p = 1/k(\ln(1/1-D)+B)$$

where D is the relative density, defined as the density of the powder divided by the theoretical density, and k and B are constants. This equation is applicable for pressures ranging from 20 to 100 ksi, again for rigid die uniaxial compaction of various powders. The examples given in the literature include Fe, Ni, Cu, and W powders.

In 1977, James (34) developed linear relationships for isostatically pressed powders. One equation is for low pressure and a separate equation is for high pressure ranges. The transition point from one range to the other depends upon the material and differs only by the slope factor. The equation is,

$$\ln[1/(1-D)] = kP + A$$

where D is relative density, P is the isostatic pressure and A is constant. It appears that the Konopicky and Shapiro equation serves as the basis for the equations of Heckel and James.

It should be noted that although the basis for Heckel's and James' relationships is theoretical, the constants are independent of the material. Hence, it has been argued that they, too, are empirical (29). A truly theoretical model depends only upon material constants with no additional constants determined by curve fitting to fit the experimental results.

CONSOLIDATION MECHANISMS

INTRODUCTION

As the complexities of powder consolidation were discovered, researchers began to realize that pressure versus density relationships are not sufficient to conclusively describe the consolidation process. Complications such as die wall interaction and the distinction between average stress, shear stress, and effective stress require a more complex approach to adequately model the system (11). The deformation of each pore is a function of its neighbors. Accurate predictions of actual pore closure on a microscale can not be derived based on single pore models, i.e., Torre's or even models having regular arrays of identical pores (35). Pores with smaller radii in a real system will be subject to higher stress concentration causing them to yield first (35). The interaction of randomly sized pores increases the compexity. Hydrostatic constraint can raise the load required for plastic flow upto three times over that for small particles (35).

STAGES OF CONSOLIDATION

Further consideration leads to more complex models. The next logical step is to break the consolidation process into stages, each dominated by a particular characteristic. Seelig and Wulff (36) divided the process into three stages. Stage 1 involves particle rearrangement, or sliding, whereby bridging, which is inherent in randomly packed particles, is eliminated. Fine powders of -325 mesh, 44 um or smaller, generally do not flow and exhibit a low apparent density (12). Apparent density is the mass divided by the volume of loose powder as when poured into a mold without pressing or vibrating. In stage 2, further densification is achieved by elastic and plastic deformation. During stage 3, brittle and severely work hardened components are fractured, forming finer particles which can fill interstices between larger particles. Naturally, these 3 stages must overlap to some extent. In fact, Fischmeister, Arzt, and Olsson (37) determined by quantitative metallography that deformation and sliding occur simultaneously from the start. Many authors have proposed multistaged mechanisms; most have three stages. Most agree with Seelig and Wulff's definition of Stage 1. Stage 2 generally involves plastic deformation; some specify the deformation to be homogeneous (38). Stage 3 differs in

definition and usually incorporates the fracture of brittle phases, such as the oxide layer on aluminum powder.

A notable exception to the three stage consolidation model is the description by James (34). This description includes six stages. All of the stages over lap and are influenced by the material, particle size, morphology, size distribution, lubrication, the tooling used, and the method of compaction (34). The first stage involves transitional restacking, defined as slipage with out excessive deformation. The second stage is defined as elastic compression at interparticle contact points. In the third stage, plastic deformation expands the contact points into contact areas. The fourth stage includes growth of these areas via further plastic deformation and fragmentation. During the fifth stage, gradual involvement of the whole particle occurs as forces large enough to cause massive deformation are developed. Eventually, the particulate nature of the compact is entirely lost. Finally, elastic compression of the mass as a whole ensues, the sixth stage. It is a matter of convenience to separate the consolidation process into stages, but the actual continuity must be realized in subsequent discussion.

PORE CLOSURE

Another approach is to consider the densification process from the perspective of the powder. The mode of pore closure is determined by the powder's reaction to the applied stress field. The brief descriptions of the current consolidation methods and the following discussion of the resulting mode of pore closure is helpful in discussing the actual mechanisms.

> "While all porosity must be eliminated, this is not a sufficient criterion to guarantee optimal resistance to crack propagation in impact or cyclic loading. Rather, the mode of densification is a further critical factor (21)."

The density of a compact is the most common point of reference, but the size and shape of the individual voids also influence the mechanical properties of the compact (19). The morphology of the residual pores is strongly dependent upon the mode of pore closure and is the major source of anisotropy.

Initially, the loose powder must be considered as individual particles. Once some degree of green strength is developed, the powder begins to behave more like a solid. Hence, most of the work reviewed hereafter considers the consolidation process from these two perspectives: 1) the interaction of individual particles and 2) deformation of a solid containing a distribution of pores or voids.

STATE OF STRESS

The response of a loose powder to applied shear forces depends upon the entire state of stress. In all consolidation processes, densification and deformation of the powder occur simultaneously and both are determined by the state of applied stress. Under purely isostatic conditions, only densification occurs on a macroscopic scale. Locally, the individual powder particles must deform in order to fill the voids. Under pure shear loading, only a shape change occurs (19). Thus, an isostatic component in the state of stress is necessary to produce densification. In soil mechanics, shear forces are considered as a possible source of expansion forces (39). These forces tend to dilate the packed particles in the direction normal to the shear force. Dilation refers to a change in volume which in this case is positive or expansive. This is due to the reaction forces across interparticle contact points. If the hydrostatic, constraining force is greater than the dilation forces generated by the applied shear force, then compaction occurs (39).

During consolidation of a powder, the stress-strain curve obtained experimentally shows, by its shape, a great deal of apparent work hardening. While some actual work hardening may occur, depending on the material and pressing temperature, a major contributor to the shape of the stress-

strain curve is called geometric hardening (20). This effect is simple to explain qualitatively, by introducing the concept of effective stress (40). The initial contacts between adjacent particles are merely points. The applied load must be transferred throughout the powder charge via these point contacts. Thus, the area supporting the applied load is very small, producing a very high effective stress as seen by the individual particle at each point of contact. As deformation of an individual particle occurs, the initial point contact becomes a contact area which increases in size as the load is increased. The effect of increasing the contact area is to decrease the effective stress for a constant load. Thus, the relationship between applied load and resultant strain resembles work hardening. An ever increasing increment in applied load is required to produce a given increment in strain.

Modes Of Pore Closure

The three modes of pore closure lend themselves to the porous solid perspective and are especially useful in understanding the effects of the applied state of stress. The mode of pore closure depends upon the conditions imposed on the compact and the dominant mode influences which mechanism will be active. Associated with each

consolidation method is a unique deformation path to full density. Each path involves at least one mode of pore closure. Figure 13 illustrates the three modes which describe most powder pressing operations: isostatic, repressing and upsetting.

Although repressing and upsetting were introduced in the forging section, a more detailed description will be given here for clarity. Isostatic pressure produces a radially symmetric reduction in the pore size; a spherical void retains its shape as the radius decreases and densification progresses. Repressing is defined as uniaxial compression in a rigid die, where the die is completely filled from the begining, as would be the case for loose powder. Repressing tends to flatten the void but the die walls prevent strain in the lateral direction. Thus, a spherical void becomes a disc with a diameter very near that of the original sphere. Upsetting can be defined as uniaxial compression without the constraining die walls. Upsetting allows unconstrained lateral flow. Under these conditions, a spherical void flattens and extends laterally with the flowing material. It is widely accepted that this lateral flow, or shear deformation, improves the integrity of the interparticle bond (1,2,19,20,21,22,22,27).

Net shape forging combines the upsetting and repressing modes of pore closure. As the preform fills the die, pore closure occurs via the upsetting mode. Once the die is

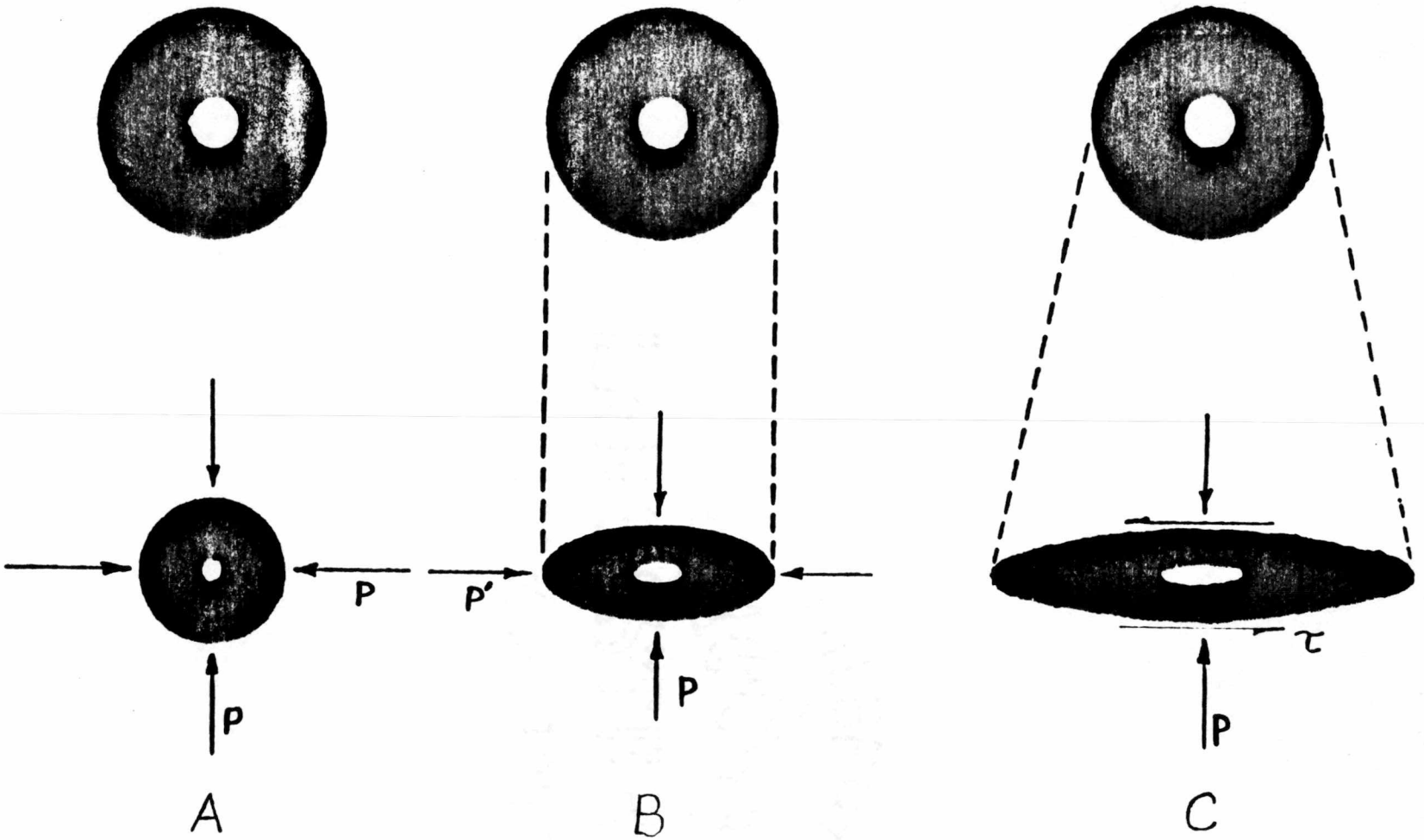

Figure 13: The three modes of pore closure: a) isostatic, b) repressing, and c) upsetting.

filled, the repressing mode dominates. Eventually, the state of stress approaches isostatic conditions and pore closure occurs via the isostatic mode. It is at this point, where the residual pores are smallest, that the isostatic mode is the least effective of the three modes. In extrusion, the repressing and isostatic modes dominate the powder charge up to the throat of the die, where a variation of the upsetting mode determines the subsequent pore geometry.

Lubrication is a very important consideration in repressing and upsetting operations. Insufficient lubrication can prohibit the development of full density and reduce the homogeneity of the microstructure. The particular effects of lubrication and friction are best explained in the context of the specific consolidation technique.

Each mode of densification will be considered separately. There must, however, be some common ground between the three modes since during consolidation the transition from one mode to another is continuous. It is best to consider the active mode as dominating, but implying that other modes may also be active though negligible in their contibution to densification under the given conditions.

Repressing

In a repressed compact, a low preform density, or tap density, will result in more local flow and therefore a greater degree of anisotropy than for preforms of higher initial density (1,21). Tap density refers to the density of a loose powder when poured into a die and subsequently tapped or vibrated. However, at a given repressed density, the tensile strength is higher for specimens with lower initial density (21).

Under repressing conditions, the powder particles move essentially along one axis, that of the applied force. There is little lateral movement of the powder due to the constraint of the die walls. Stage 1 under repressing conditions, i.e., particle sliding, occurs up to a pressure at which the original porosity is approximately halved, ending with a residual porosity of approximately 20% (37). During consolidation, there is a continuous increase in coordination number of the powder particles. The dependence of the coordination number on the applied pressure is very nearly linear (37). Repressing generates more sliding and correspondingly less particle deformation to full density than isostatic compaction. This is explained by the lower stability of particle configurations surrounding voids with respect to the repressing state of stress. Thus, uniaxial compression may produce better packing before the particles

are locked into place around a residual void (37). An individual particle in a randomly packed powder with a given initial density has a resistance to non-radial motion, i.e., sliding, which depends upon the interparticle effective stress. This is because interparticle sliding is a frictional process (39).

As the density increases, the reaction forces increase, acting perpendicular to the applied force. Poisson's ratio for porous material is a function of the pore volume fraction and is less than one half (20). Plastic deformation of incompressible solids requires Poisson's ratio to be 0.5; this limit is approached as a powdered material consolidates (22). Generally, the relation follows the equation:

$$v = 0.5\ p^{\infty}$$

where v is Poisson's ratio and p is the instantaneous relative density (22). As Poisson's ratio increases, the reaction forces normal to the applied force increase accordingly. These reaction forces act on the die wall. Since the friction between the powder and the die wall is a function of the force normal to their interface, the interface can support more load as densification progresses. There are two points to consider: first, the increase in applied force will directly increase the reaction forces, and second, as the applied load increases, the density increases. However, an increase in density also increases

Poisson's ratio towards the 0.5 limit. This second effect adds to the increase in the reaction forces at the die wall.

The initial contacts between adjacent particles are points having little or essentially no area. As consolidation progresses these contact points become contact areas. As the contact area between particles increase, the ability of powder to support both normal and shear stress increases proportionally. The increasing individual contact area and number of particles contacting the die wall both serve to increase the effect of die wall friction (4). The effect of friction at the die wall is therefore a major consideration in repressing. In consideration of this point, Kamm, Steinberg and Wulff (7) have shown interparticle lubrication to be relatively unimportant. Studies indicate that when the ratio of the die wall area to the pressing area is increased, the density decreases (3). As the ratio of diameter to height increases, the die walls play a lesser role (7).

Many attempts have been made to understand how frictional forces are created and distributed during repressing of a powder compact. Whenever friction is present, the density distribution within the compact is disrupted. Using a double action uniaxial press, Shank and Wulff (4) applied strain guages to the exterior of the cylindrical die to determine the tangential strain and hence the radial stress exerted on the die by the powder. They

found that the radial stress is greater at the center of the compact than at the ends. The greater radial stress creates greater friction, manifesting itself as lower density in the powder.

Duwez and Zwell (5) used a pressure sensing device mounted in the wall of a cylindrical die. The device consisted of a cylinder which makes contact with the powder and subsequently transfers the force to a dynamometer assembly to obtain a pressure. The results obtained by this method are "at complete variance with the findings of" Shank and Wulff (4). Shank and Wulff argue that a piston type device in the die wall would change the force it was designed to measure. Thus, the measured pressure will not be the radial pressure, but an indication of the powder's ability to support shear. The powder must flow into the gap created as the piston moves radially outward, which requires deformation by shear.

Uniaxial pressing serves as the basis for most of these friction studies. Not all of the results agree; leaving the true effects of friction on consolidation open for discussion. All of the results acknowledge friction as the major source of disruption to uniform pressure propagation.

Upsetting

Consolidation of a powder by the upsetting mode is generally considered to give the best dynamic properties. The absence of die wall constraint allows more deformation by shear. Under the combined action of compressive and shear deformation, total pore closure is possible (19). The absence of die wall friction improves the homogeneity of the final density. Friction at the platen-powder interface, however, disturbs the state of applied stress and limits the maximum strain to failure of the preform.

A coherent powder billet will show very little lateral expansion initially (37). At high levels of porosity, the Poisson's ratio is very low. Thus, lateral forces generated by the applied load will be very small, generating very little flow. Once the density has increased sufficiently, the increased Poisson's ratio will cause lateral flow to commence. Concurrently, friction begins to have a retarding effect on the lateral flow of material near the interface. This frictional effect causes barreling of the preform billet. As the radius of curvature of the free surface decreases, the tensile hoop stress increases. The height-to-diameter ratio, as mentioned previously, causes a similar effect; increasing the ratio decreases the radius of curvature (20).

Without the die walls to support the powder, formability, or the ability to deform without failure, becomes an important factor. A formability limit may be defined as the strain to failure. The formability of a powder preform is much lower than for the fully dense material because the hot ductility is lower for a powder preform (19). Tensile ductility, however, is an unreliable indicator of the preform's ability to be deformed (20). The upset test is the most common method of estimating the formability limits. There is an apparent anomaly in the deformation behavior of the right circular cylinder used in the upset test. The fact that the formability of a green powder is low would seem to predict a low deformation to fracture. However, it is essentially independent of the initial void content (20). The anomaly is explained by considering that there are two opposing effects. As the initial pore volume fraction increases, the ability to withstand tensile stress decreases. Concurrently, an increase in pore volume fraction causes a decrease in Poisson's ratio and therefore a decrease in the lateral spread, or bulging, of the preform. Less bulge corresponds to a lower tensile stress at the surface of the preform. Thus, the initial porosity of the preform does not effect the compressive strain to failure.

As the axial strain under upset conditions increases, a shear cross may be developed. A shear cross in upset

forging is a region of very high shear deformation which occurs at approximately 45 degrees to the load axis when lubrication at the platen-powder interface is insufficient. Greater friction gives rise to a more pronounced shear cross. Figure 14 indicates the relative positions of the three zones associated with this effect (20). The tensile stresses found in Zone 3 can increase the void size over that of the initial preform. Hydrostatic stress found in Zone 1, the dead metal zone, causes a uniform decrease in void size, though not as effective as the shear stress found in Zone 2. In Zone 2, the shear stress flattens and elongates the voids resulting in high density and maximum strain. The strain concentration in Zone 2 can cause premature failure. The best defense against the heterogeneous microstructure and possible failure associated with the shear cross is sufficient lubrication at the platen-preform interface.

The important differences between repressing and upsetting are the relative motion between adjacent powder particles and the shear stress developed in the upsetting technique. Both of these contribute to the mechanical rupturing and dispersing of the oxide layer which covers each powder particle (21). As a consequence of the lateral flow which occurs during upsetting, inclusions and any residual porosity will be preferentially oriented perpendiclular to the applied compressive load. The

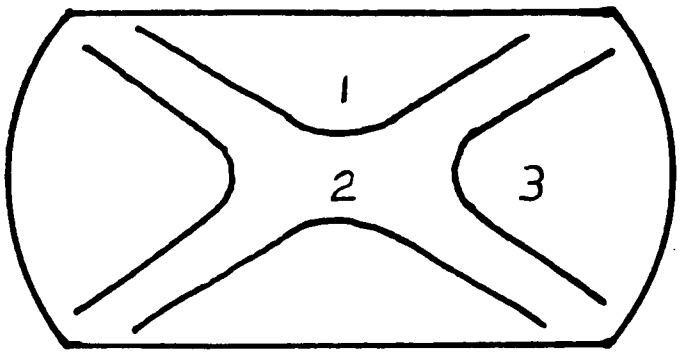

Figure 14: Location of the shear cross found in upset forging when lubrication at the platen-specimen interface is insufficient. The characteristics of the zones are: Zone 1-isostatic stress (the dead metal zone), Zone 2-high shear stress, and Zone 3-tensile hoop stress.

inclusions and residual porosity will also show the same elongation as the matrix material. Thus, anisotropy may develop in the final compact. The magnitude of the anisotropy depends upon the initial packing and overall axial strain of the preform (21). The anisotropy developed by upset forging is more pronounced than it would be for repressed billets of equal height strain.

The benefits of the shearing action include improvements in toughness and fatigue properties, better dispersion of the oxide layers, and relative ease in which total pore closure is achieved. Although chemical bonding can occur across a static interface by diffusion (1), static contact between adjacent powder particles does not ensure acceptable dynamic properties. Dynamic properties are extremely sensitive to the integrity of interparticle bonding.

> "To equal or exceed the dynamic properties of wrought and cast materials, it is essential that extensive particle shearing and lateral flow accompany densification (1)."

On the other hand, the tensile strength and tensile ductility are comparable for repressed and upset forged preforms at full density and are equal to or higher than those of wrought or cast counterparts (1).

In some forging operations, the initial mode of void closure is upsetting, then contact is made with the die wall and the repress mode becomes dominant. Under these conditions, the Zone 3 voids which may have been enlarged by

the associated tensile stress can be difficult to enliminate, especially if the die wall is cold. The reduction in temperature raises the yield strength, preventing further deformation. Hence, the voids will remain and may require further processing such as machining or reheating and pressing if full density is essential. These voids are positioned in the area of greatest tensile stress under a bending load, which may prohibit the use of such a part in many service applications.

Isostatic

Isostatic conditions can be generated in many ways. In isostatic pressing, the condition is intentionally applied from the start. In repressing, the condition can be approached as the powder, confined on all sides by the dies and rams, becomes fully dense. If lubrication is not sufficient, an isostatic state of stress is developed in Zone 1 during upset forging as previously described.

The yield strength of the powder decreases as the temperature is increased for most materials. On an appropriate scale, the stress is not truly isostatic, i.e., since it initially acts across a network of point contacts. It is conceivable that the initial deformation of an individual particle ressembles the flattening of a sphere by uniaxial compression. Within the packed powder several

points of contact are associated with each particle, i.e., a coordination number. As mentioned previously, the coordination number increases as densification progresses. With the reduction in yield strength at elevated temperature and the network of point contacts acting as stress concentrators, plastic deformation of the powder particles is appreciable. However, as the contact points expand into contact areas, the effective stress decreases. In addition to this, entrapped gas in subsurface voids begins to build pressure. There is therefore a limiting density, less than 100% of the theoretical value, beyond which creep or other densification modes must dominate (1). Fischmeister, Arzt, and Olsson (37) have shown, through quantitative metallography, that interparticle contacts formed in die pressing are more numerous and therefore smaller than in isostatic compacts. This supports the idea, previously stated, that isostatic compaction involves less sliding than in repress or upset forging. For this reason, isostatic compaction is not as effective in breaking up the oxide layer on the powder surface (8). Practically no quantitative data exist concerning the pore-welding mechanism. However, it is generally accepted that if shear forces are strong enough to rupture the residual oxide film, highly effective interparticle bonding occurs (19).

Stromgren, Astrom and Easterling (41) have proposed that interparticle sliding, which does not increase the density

but makes further plastic deformation easier, occurs during isostatic compaction. Powder morphology and work hardening determine the extent to which this occurs. Their experimental evidence shows that the mean strength of the compact is reduced at intermediate densities prior to increasing at higher densities. The decrease in strength is a result of shear failure between particles during the proposed rearrangement by sliding.

PHYSICAL MECHANISMS

INTRODUCTION

To develop models with a physical base, the actual mechanism by which densification occurs must be identified and analyzed. While the number of known mechanisms is not overwhelming, the analysis of how they interact, which of them are dominant under a given set of conditions, and their kinetics remains a complex issue which is not fully understood.

There are three general classifications for the physical mechanisms of consolidation: plastic flow, creep, and diffusion. These classifications may be subdivided into specific mechanisms. In most cases, where pressure is the primary variable in the process, initial densification occurs by plastic flow. Once plastic flow has reached its

"limit", the time dependent mechanisms dominate and control the rate of densification. This limit can be increased only by raising the temperature (9). The following review is intended to provide evidence of the importance of extended consolidation via plastic flow to the overall time required to produce a fully dense material. The relative rates are the primary focus. Review of the continuum mechanics approach illustrates the importance of the state of stress to the plastic flow of the material.

TIME INDEPENDENT MECHANISMS

A continuum mechanics approach to powder consolidation has been presented by Sundstrom and Fischmeister (35) and helps to develop a better understanding of the process as a whole. Their model describes compaction as a two stage process. The first stage models the compaction at high porosities by particle deformation. The second stage, at low porosities, is governed by pore closure. The two stage mechanism is based upon two experiments. In the first, randomly stacked cylinders of varying diameters are uniaxially compressed perpendicular to their axes. This arrangement represents a two dimensional powder. A finite element model is used to describe the deformation at the pore boundaries, i.e., between the individual cylinders. In

the second, two holes in a large plate are compressed under plane strain conditions. The smaller hole shows a greater reduction in area than the larger hole; contradicting the accepted ideas at that time. No specific equations are given. However, the approach is common for finite element and continuum mechanical models.

Another continuum mechanical approach uses plasticity theory. The change in Poisson's ratio can be accounted for in this approach. Specifically for warm deformation of aluminum, Kuhn and Downey (42) found:

$$\nu_p = 0.5\ (1-u)^{1.5}$$

where u is the porosity. The major difference between conventional plasticity theory for solid materials and plasticity theory for porous materials is the effect of isostatic pressure. Conventionally, isostatic pressure has no direct effect on the deformation of the material. However, porous materials can be plastically deformed by isostatic stress. The simplest statement of this fact is that constant volume, a corner stone of conventional plasticity theory, does not hold for porous materials.

Naturally, modifications to the known plasticity equations for solid materials serve as the basis for the equations describing porous materials. The equation for plastic yield of a fully dense material is:

$$F = (3J_2')^{0.5}$$

where F is the yield surface and J_2' is the second invariant of the stress deviator, given by:

$$J_2' = [(s_1-s_2)^2 + (s_2-s_3)^2 + (s_3-s_1)^2]/6$$

and s_x, with x = 1, 2, or 3, are the principal stresses (20). One equation for the yield surface of porous materials, as proposed by Prager and Drucker (43), is:

$$F = J_2'^{0.5} + aJ_1$$

where J_1 is the first invariant of the stress tensor, given by:

$$J_1 = s_1 + s_2 + s_3$$

and a is a material constant. The best equation for yield of a porous material is given by Kuhn and Downey (42), since it includes the Poisson's ratio effect:

$$F = [3J_2' - (1-2v)J_2]^{0.5}$$

where $J_2 = J_2' - [(J_1)^2]/3$. This equation reduces to the yield criterion for solid materials as Poisson's ratio

approaches one half. Figure 15 illustrates the relationship between Poisson's ratio and relative density. The need for a pore model is eliminated in this approach (19).

The densification rate, D, is generally considered to be infinite if the state of stress exceeds the yield surface (40). This is a good approximation relative to the densification rates of diffusion controlled mechanisms. The rate is zero if the state of stress is insufficient to cause yield, as it is expected physically.

TIME DEPENDENT MECHANISMS

Dislocation Creep

Of the time-dependent mechanisms, power law creep is fastest with an exponential dependence on time under constant stress. The conditions under which the power law creep contribution to densification may be dominant, in the absence of plastic yield, include intermediate to high stress levels and temperatures above one half of the melting

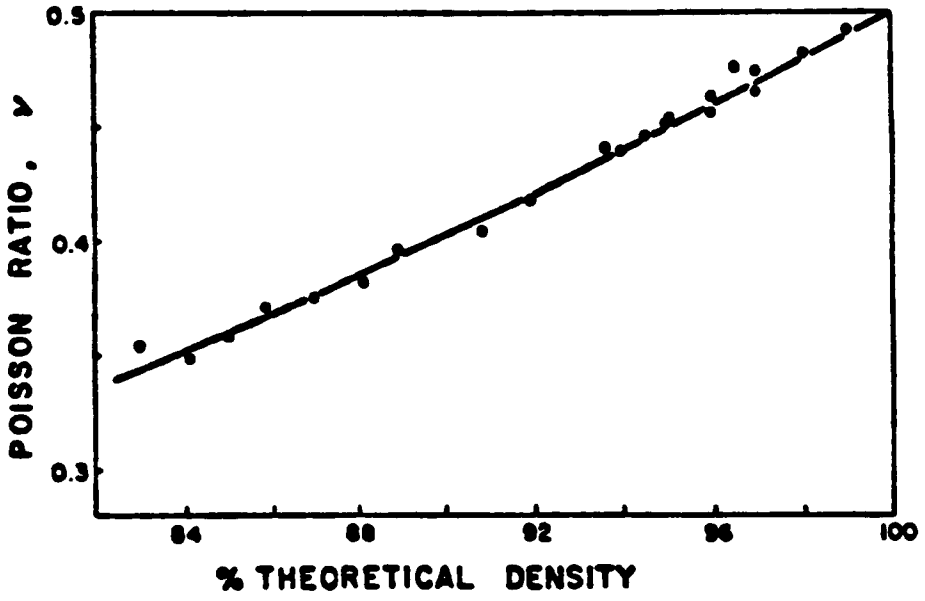

Figure 15: Variation of plastic Poisson ration with increasing density in hot deformation of sintered (700°F) 601AB aluminum alloy compacts. Initial density: ● 81%, ○ 93%. ($v=0.5p^2$) (H. A. Kuhn, "Deformation Processing of Sintered Powder Materials," Powder Metallurgy Processing - New techniques and Analysis, H. A. Kuhn and A. Lawley eds., Academic Press, New York (1978) 99)

point. The creep rate is exponentially proportional to stress (44):

$$\dot{e}_{ss} \propto s^{n}$$

where $\dot{e}_{ss}$ is the steady-state creep rate and s is stress. As densification progresses, the effective pressure on an individual pore decreases; there is more solid material supporting the load. For this reason, Wilkinson and Ashby (45) chose to model power law creep densification based on the steady-state law, where effective pressure is the independent variable. Their results for the spherical-pore densification rate, determined by creep of a thick spherical shell of material surrounding each pore, give the equation (45):

$$\dot{r} = [3A/2] \{[r(r-1) / 1-(1-r)^{1/n}]^{n}\} (3P_{a}/2n)^{n}$$

where r is the instantaneous density, A and n are material constants and P_a is the applied pressure. Under the appropriate loading conditions, the intermediate stages of pore closure via power law creep may be more accurately represented by a cylindrical-pore model than a spherical one. In this case the densification rate is given by (45):

$$\dot{r} = 2A \{[1-r] / [1-(1-r)^{1/n}]^{n}]\} (2P_{a}/n)^{n}$$

In the cylindrical case, the creep rate is approximately three times as fast as for the spherical case. However, all of the pores are eventually represtented best by the spherical-pore model. The contribution from power law creep decreases as the denstiy of the compact increases (45), Finally, any remaining voids are eliminated via diffusion processes which are less sensitve to the applied pressure.

Diffusion Creep Mechanisms

There are a number of diffusion mechanisms by which void elimination occurs. The most detailed studies of this mechanism fall under the context of sintering. Sintering is a consolidation technique that has been rigorously studied. Although, a detailed review of sintering would provide little enlightenment toward the work presented herein, a breif description of each basic diffusion mechanism is usefull.

Coble Creep

Coble creep involves atomic or ionic diffusion along grain boundaries. It is, therefore, very sensitive to particle size and coordination number. The steady-state creep rate is given by (44):

$$e_{ss} = (50\ s\ D_{gb}\ b^4) / (k\ T\ d^3)$$

where s is the applied stress, D_{gb} is the grain boundary diffusivity, b is the Burger's vector, k is the Boltzman constant, T is the absolute temperature, and d is the grain diameter.

Nabarro-Herring Creep

Nabarro-Herring creep is controlled by stress-directed volumetric diffusion. This type of creep can be dominant at low stress levels and high temperatures. The steady-state creep rate is given by (44):

$$e_{ss} = (7\ s\ D_v\ b^3) / (k\ T\ d^2)$$

where D_v is the volumetric diffusivity through the grain interior. Nabarro-Herring creep is not as sensitive to

particle size as Coble creep (44). Both of the rate equations are based on the semi-emperical relation:

$$(\dot{e}_{ss} \; k \; T) \; / \; (D \; G \; b) = a \; (S/G)^{n}$$

where A and n are material constants, D is the diffusivity and G is the shear modulus. The Nabarro-Herring equation results when:

$$A = 7 \; (b/d^{2}) \text{ and } n = 1$$

and the Coble equation results when:

$$A = 50 \; (b/d)^{3} \text{ and } n = 1$$

At high stress levels and temperatures at or above one half of the absolute melting termperature, the controlling mechanism for deformation is believed to be diffusion controlled movement of dislocations (44). Weertman proposed that, under these conditions, the climb of edge dislocations away from dislocation barriers is the rate controlling step. This dislocation creep (power law creep) can be represented by the simi-emperical equation when A is constant and n is approximately five, giving (44):

$$\dot{e}_{ss} = [(A \; D \; G \; b) \; / \; (k \; T)] \; (s/G)^{5}$$

Exponential Creep

It is theorized that at high stress levels, diffusion is accelerated due to the excess vacancy concentration brought about by dislocation-dislocation interactions (44). This theory is the basis for exponential creep:

$$\dot{e}_{ss} = \exp(as)$$

where "a" is a proportionality constant. Easterling and Tholen (46) state that high contact stresses may cause significant diffusion at the interface between powder particles because the chemical potential for vacancy diffusion is proportional to the stress acting perpendicular to the boundary.

Effect Of Consolidation Conditions

Consolidation conditions have an effect on the competition between the individual mechanisms. The morphology of the powder can also affect which mechanism is dominant. A large surface area to volume ratio for a powder significantly affects the relative densification rates between Coble and Nabarro-Herring creep; surface diffusion will play a correspondingly larger role

overall (6). The low temperature and high initial densification rate, for most pressure enhanced processes, allow non-equilibrium defects to contribute to the densification mechanism; in ordinary sintering, these defects would be removed by recrystallization before noticable densification could occur (9).

CHAPTER III

EXPERIMENTAL PROCEDURE

MATERIALS

In order to minimize the effects of possible variations in heat treatment and therefore strength of the raw and compacted powder, a commercially pure aluminum was chosen as the initial material. Alcoa was kind enough to donate an ample supply of Al-123 powder of 90% -325 mesh. This powder is 99.7 wt% aluminum with most of the balance being iron and silicon.

A two-phase approach was taken, in which the first phase provided the basis for the second. In the first phase, a rough approximation of the best consolidation parameters was found. In the second phase, the optimum conditions were used to consolidate specimens for tensile and impact testing.

In order to assess the effect of the bidimensional compression conditions on the consolidation of more structurally significant alloys, the same approach was used for an aluminum alloy MB85, again provided by Alcoa. This powder is also 90% -325 mesh with a composition of 3.7% Cu, 0.2% Mn, 2.0% Mg, 0.7% Zr, and the balance aluminum. The MB85 alloy was developed for composite applications, specifically intended for use with silicon carbide

reinforcement, and may be considered a modified 7050 or 2024 alloy. Thus, a natural extension of this project would be bidimensional compression of aluminum/silicon carbide metal matrix composites.

POWDER HANDLING

The material safety data sheet for aluminum powder clearly states that the potential explosivity of finely divided aluminum is high. There are three conditions required for an explosion. The conditions are, first, a dust cloud containing the powder, second, a source of oxygen, and third, an ignition source. These conditions are easily met if sufficient care is not taken. However, if any one of the conditions is absent, the powder may be considered harmless.

A secondary safety problem is the reaction between powdered aluminum and water. This reaction produces hydrogen gas, which may become highly concentrated, sufficient to present an explosion hazard itself.

The majority of explosions have occurred in an industrial environment. Clean-up of spilled powder may present the most dangerous set of conditions; adequate consideration for safety may not be given to the course of action taken. Sweeping produces a dust cloud in an open air

environment. Electrical switches and motors can arc and ignite the dust cloud. In the atomization process, the powder can build up sufficient static charge to ignite itself, if air is used as the atomizing gas, via the arc generated upon static discharge.

CAN DESIGN

These three conditions were considered in the design of the encapsulating can and handling of the powder required for this project. The initial can design required a glove box, which eliminated the source of oxygen during fabrication of the specimens. The can was fabricated from 6061-T6 aluminum tubing. The end caps were drawn from aluminum sheet to a square-cup shape. The tubing was squared in cross-section using the bidimensional compression apparatus. The bottom end-cap was welded in place with the open end facing out (Figure 16a). This could be done outside the glove box using the TIG welder, but the initial cans were welded in the glove box for extra safety. In the glove box, purged with argon, the cans were loaded with powder in small increments. The cans were tapped on their closed end between each addition of powder, ensuring that the powder was packed as tightly and uniformly as possible (12). The cans were not filled completely, leaving

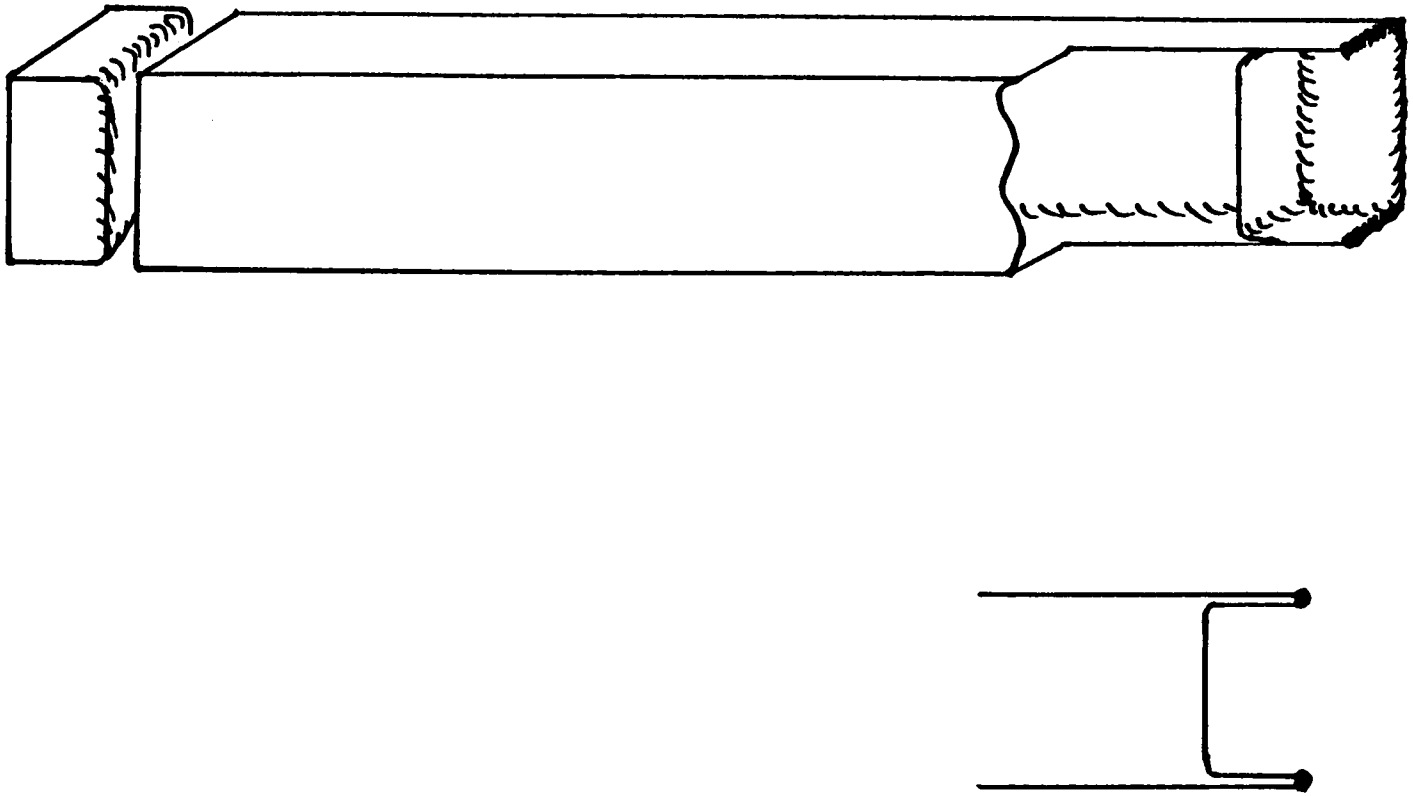

Figure 16: Phase one can design used for consolidation of metallographic specimens.

room for the upper end-caps, which were pressed into place with the open end facing out (Figure 16b). The upper caps were then welded, using TIG, in the argon purged glove box.

For phase two, a different can design was used in order to shorten the specimen fabrication time. The Peerless Tube Company, of Bloomfield, New Jersey, kindly provided 100 aluminum cans. These cans were one inch diameter and with a length of 3.8 inches. The top was curled inside, as on an aerosol can. The can was painted inside and out with a high quality, chemically resistant paint, which had to be burned off. The initial design for these cans is shown in Figure 17.

The can design finally used for the mechanical property specimens did not involve welding. Therefore, in situ outgassing was abandoned, as was vacuum hot pressing. Instead, the powder was outgassed in a separate tube constructed of stainless steel with brass closures. The tube was attached to a mechanical vacuum pump by a quarter-inch diameter copper tube. The copper tube was routed through a bucket of water and then to the rubber hose connection with the vacuum pump, since the thermal conductivity of copper is high. Once the powder was outgassed, the entire stainless steel tube was quenched in water to a temperature cool enough for handling. The powder was then poured in increments into the cans, with ample vibration between additions to ensure optimum packing.

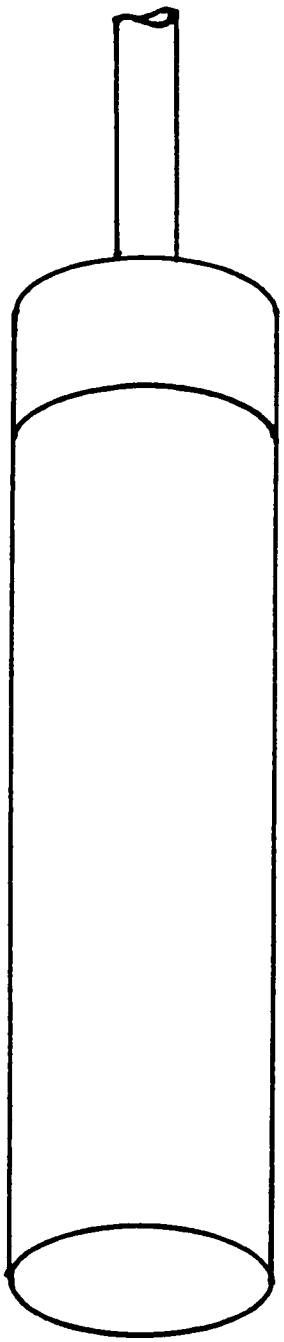

Figure 17: Initial phase two can design with outgassing tube.

These cans had been drawn through a die which squared their cross-section and sized them to fit the specimen chamber in the bidimensional compression apparatus, thus achieving full utilization of the stroke of the apparatus. The flat end of the original can was upset inward during this drawing operation. The end-caps were fabricated from the bottoms taken from half of the original cans. These bottoms were also drawn through a die which sized them to fit the squared cans. Once the powder was loaded, an end-cap was pressed into place and the can was folded inside to mechanically lock the cap in place, as shown in Figure 18.

APPARATUS

The apparatus used to consolidate both microstructural and mechanical porperty specimens is shown in Figure 19. The development of this apparatus is discussed in the results and discussion section. The final aparatus uses an Enerpak electrially powered hydraulic pump with 10 ksi (69 MPa) maximum pressure. The Enerpak hydraulic cylinders produce 50,000 pounds force (222 kN) at full pressure. The hydraulic system is isolated from the heated dies via water jackets surrounding the shafts which transfer the load from the cylinders to the die rests. Triangular braces limit the in plane deflection of these shafts. An electrical contact

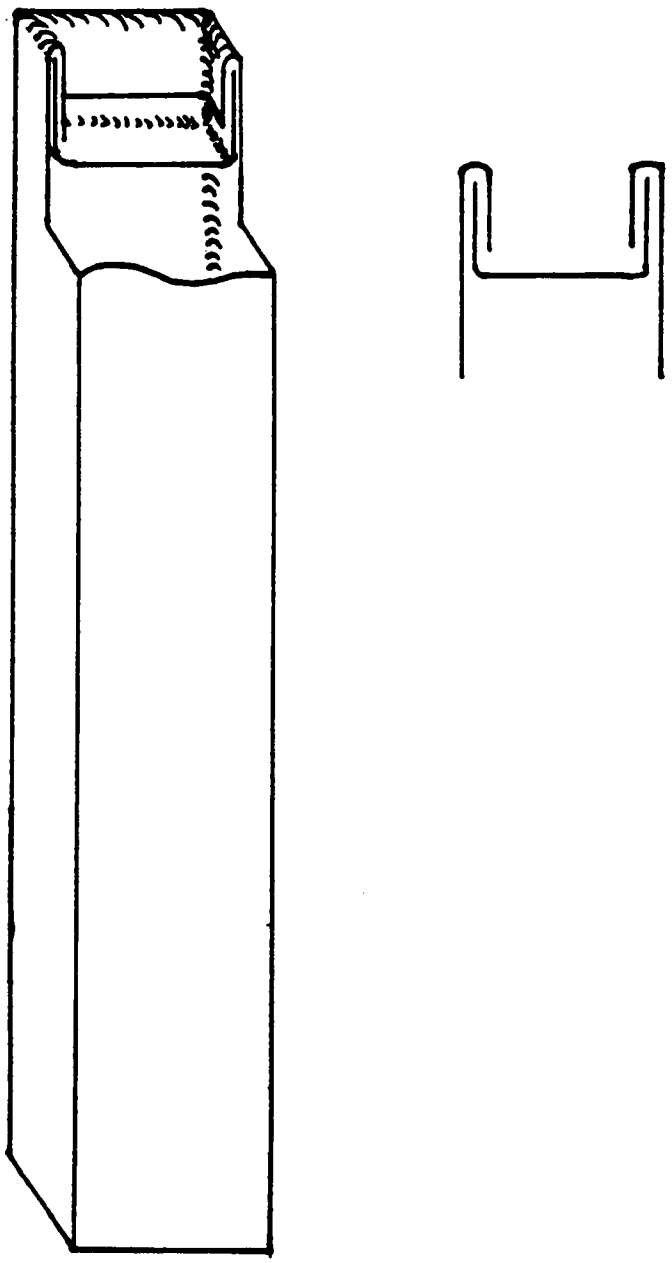

Figure 18: Actual phase two can design used for consolidation of mechanical property specimens. The end cap was mechanically locked in place by folding the can inward over the cap.

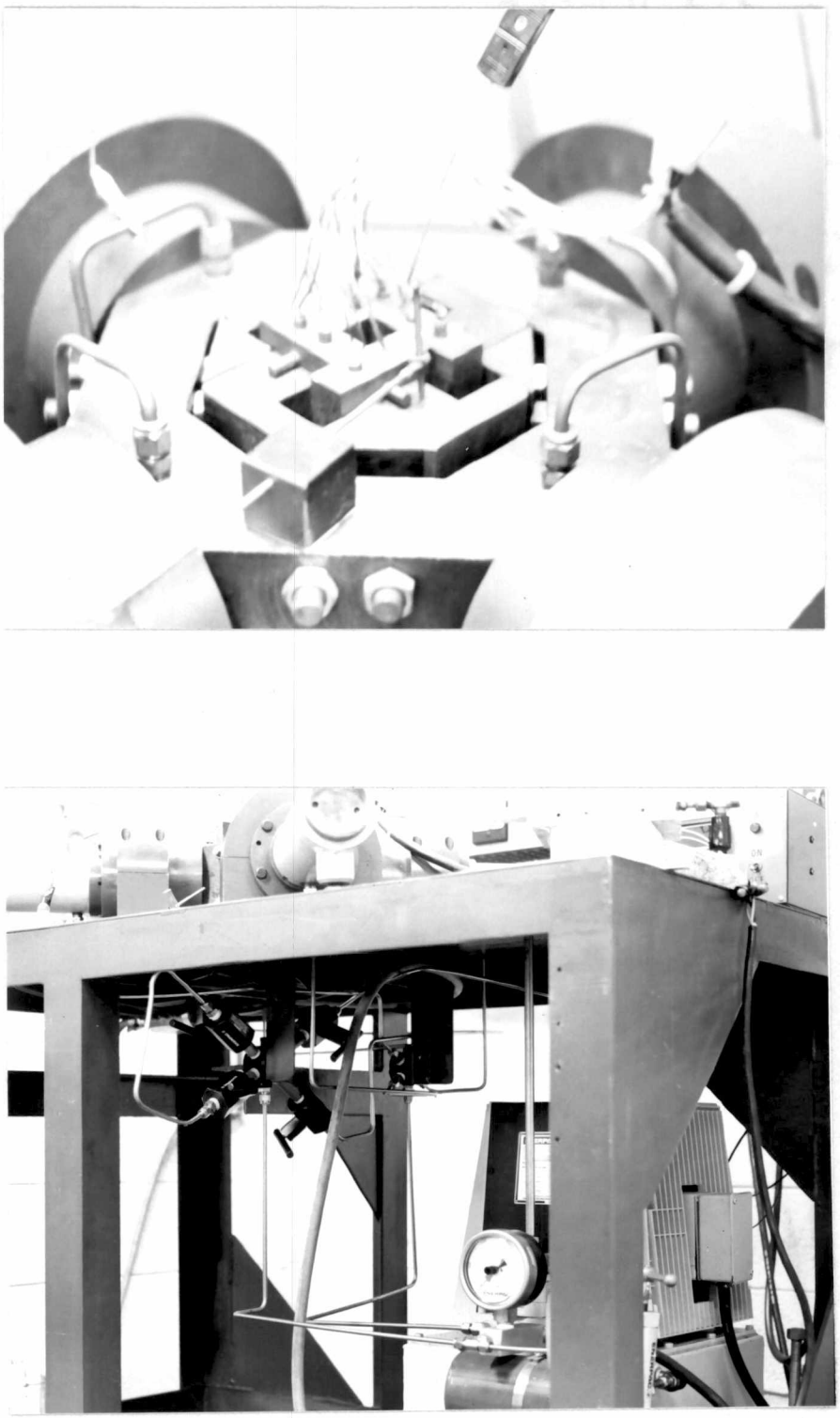

Figure 19: Final apparatus used for both phases.

system warns the operator if the out of plane deflection is too large, whereupon the operator repositions the specimen in the die cavity accordingly. Four throttling valves control the rate of movement for each die individually. These valves are set by trial and error for the current condition of the aparatus.

The flat dies used in the final aparatus were made of H13 hot working tool steel. The dies were machined in the annealed condition and then hardened. The heat treatment of this material was as follows:

1- Wrap the dies in paper individually

2- Cover each wrapped die with cast iron chips

3- Heat to 480°C (900°F)

4- Heat from 480°C to 815°C at <110°C per hour

5- Heat rapidly to 1000°C (1830°F), hold 15 minutes

6- Air cool until able to hold in hand (~60°C, 150°F)

7- Temper <u>immediately</u> at 540°C (1000°F) for 45 min.

8- Air cool to room temperature

9- Repeat 7 and 8

10- Repeat 7 and 8, but temper only 30 minutes

The resulting hardness was 50 HRC. The dies were then ground to produce a low friction, flat surface.

PHASE 1

A matrix of press conditions, see Table 1, was created. Samples of Al-123 and MB85 powder were bidimensionally compacted under these conditions using the initial can design (Figure 16).

The resulting compacts were sectioned, metallographically prepared, and examined. The main point of interest was the resulting density, which was estimated for each specimen from the photomicrographs. Attention was given to pore geometry and distribution.

The procedure used for porosity measurements was simple. A 400X micrograph for each set of condions was taken of a transverse section. At least three measurements were taken per micrograph. For each measurement, a line was randomly drawn across the micrograph. The length of that line spanning the micrograph was measured. The length of each segment spanning a pore was measured and the sum of these lengths calculated. The sum of segments spanning a pore, divided by the total length, gave the fraction of porosity. The average of three measurements gave the porosity. The repeatability of this procedure proved to be very good.

Once the consolidated specimen was cut, using an abrasive cut-off saw, the specimen was mounted in epoxy resin. After hardening, the mount was carefully ground to remove the distorted metal layer which resulted from the

TABLE 1: SPECIMEN NUMBER-VS-PRESS CONDITIONS

TEMP (°C)	HYDRAULIC PRESSURE (ksi)				
	2	4	6	8	10
			Al-123 POWDER		
25	-01	-02	-03	-04	-05
200	-06	-07	-08		
300	-09	-10			
400	-11				
450	-12				
			MB85 POWDER		
25	-501	-502	-503	-504	-505, -513
200	-506	-507	-508		-514
300	-509	-510	-515		
400	-511	-516		-517	
450	-512				

sectioning cut. The use of fresh grinding paper and light pressure was essential, especially for the very soft commercially pure aluminum. The normal sequence of grinding papers was used, i.e., 180, 240, 320, 400, and 600 grit. A copious amount of water was required at each step to prevent the grinding paper from plugging. Once a uniform surface at the 600 grit level was obtained, the specimen was polished using 9.5 micron and 1.0 micron alumina in sequence. The final polish was done on a Syntron vibration polisher using colloidal silica on a nylon cloth. The specimens were thoroughly washed and rinsed after each step to prevent build up of debris in the pores, thus avoiding erroneous porosity data.

Micrographs were initially taken before and after etching. The unetched specimens were expected to reveal porosity more clearly. The etchant used was NaOH (10 % by weight) to show powder particle boundaries. The time required varied depending upon the amount of cold work done on the powder.

PHASE 2

In the second phase, specimens were consolidated under the most promising conditions found in phase one. It was decided that 450°C would produce the best microstructure

using larger specimens. Room temperature specimens were also processed with the hope that the pressure would be adequate to fully consolidate the larger specimens. Complete consolidation at room temperature would be most benificial for rapidly solidified powders. The cans used in Phase 2 were of the design shown in Figure 18. These compacts were machined into Charpy impact and standard tensile specimens. The Charpy test, which measures the energy for fracture was chosen because it is very sensitive to porosity. Dimensions of the Charpy impact specimen are given in Figure 20. The impact specimens complied with ASTM E23. Figure 21 gives the tensile specimen dimensions. The tensile test conditions complied with ASTM B557. A strain rate of 0.1 inches per minute and a gauge length of 1.0 inch was used.

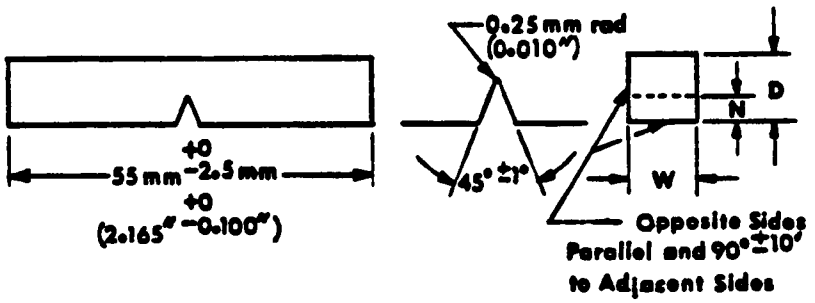

A: W = D = 10 mm (0.394 in.)

N = 2 mm (0.079 in.)

B: W = D = 9 mm (0.354 in.)

N = 1.8 mm (0.071 in.)

Figure 20: Impact specimen dimensions, a) standard size (ASTM E23) and b) actual size used in this work.

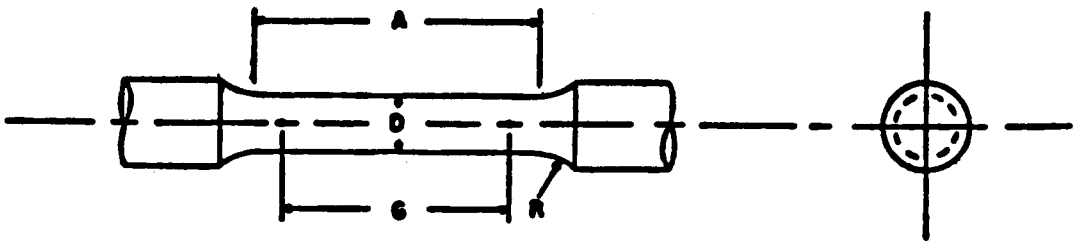

G = 2.54 cm (1.0 in.)

D = 0.635 cm (0.25 in.)

R = 0.478 cm (0.188 in.)

T = 0.953 cm (0.375 in.) dia.
NC16 threads

A = 3.175 cm (1.25 in.)

Figure 21: Tensile specimen dimensions used in this work. Specimens are in compliance with ASTM B557.

CHAPTER IV

RESULTS AND DISCUSSION

PHASE ONE

INTRODUCTION

Phase one of this work involved the development and fabrication of the bidimensional compression apparatus and the microstructural characterization of bidimensionally pressed powders. Both were included as a single phase because the development of a working press design capable of withstanding repeated pressing runs at the stresses developed under application of full hydraulic pressure was necessarily concurrent with attempts to process a sufficient number of specimens for evaluation. With the potential variations in actual specimen load between the various designs, it is necessary to have a sufficient number of specimens consolidated by the same press design. Variations in the data can therefore be attributed to factors other than press design. For clarity, the discussion of the apparatus design will be separate from that of the consolidated powder specimens.

APPARATUS DESIGN

Many modifications to the original bidimensional compression apparatus were required before an adequate system evolved. The current apparatus is the fifth generation. Only the octagonal frame remains from the original apparatus. Each generation involved a complete disassembly of the apparatus along with considerable time in the machine shop. Design and fabrication of the current system spanned more than two years.

The original equipment is illustrated in Figure 22. There were several limitations to this design. Foremost was the hydraulic system, which was designed to provide adequate pressure for fabrication of polymer matrix composites. In such an application, the maximum temperature did not exceed 200°C. However, extended use at that temperature degraded the Viton O-rings rapidly. Consolidation of metal powders required much higher temperatures. These O-rings were a critical component. They were intended to withstand up to 10 ksi pressure. Without sufficient cooling, the heat transfer from the dies imposed a time limit beyond which the equipment could not be used without catastrophic failure of the O-rings.

The pressure control was another limitation of the hydraulic system. Thermal expansion effects caused an increase in pressure as the hydraulic system became hot.

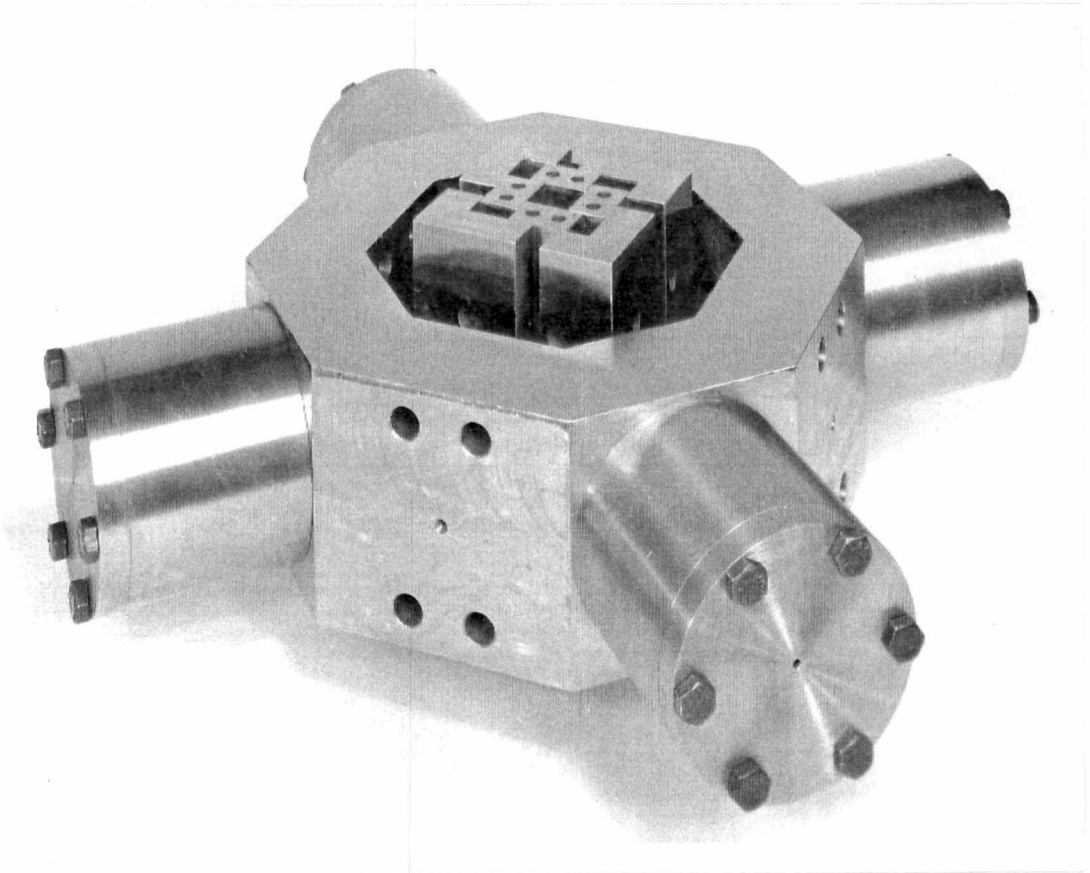

Figure 22: The original rigid die bidimensional compression apparatus.

Thermal expansion of the piston rod and the hydraulic oil both increased the system pressure. The hand pump used presented three potential problems: first, a finite time was required to generate the desired pressure; second, the degradation of the O-rings caused a steady leakage of oil which made application of a constant pressure unobtainable; and third, there was no provision for independently controlling the flow of hydraulic fluid to each cylinder. The third problem combined with the disregard for fit and friction proved to be the worst problem.

Each cylinder had an individual resistance to extension; a different pressure was required to move each piston. As Figure 23 shows, the dies were inter-fitting. They were inherently required to advance at the same rate. Feeding all four cylinders from a single manifold would have, in theory, produced equal pressure and extension in each. However, the unavoidable differences in fit for each cylinder caused sequential movement of each cylinder because of the equal pressure; the cylinder with least resistance would always move first. As a result of the uncoordinated movement of the cylinders, the inter-fitting dies jammed frequently. Each time the dies jammed, the aparatus had to be disassembled, cleaned, and relubricated.

Variation in the fit between the four dies caused them to rotate. The ideal case for the dies would not have permitted this rotation, i.e., perfect fit and perfectly

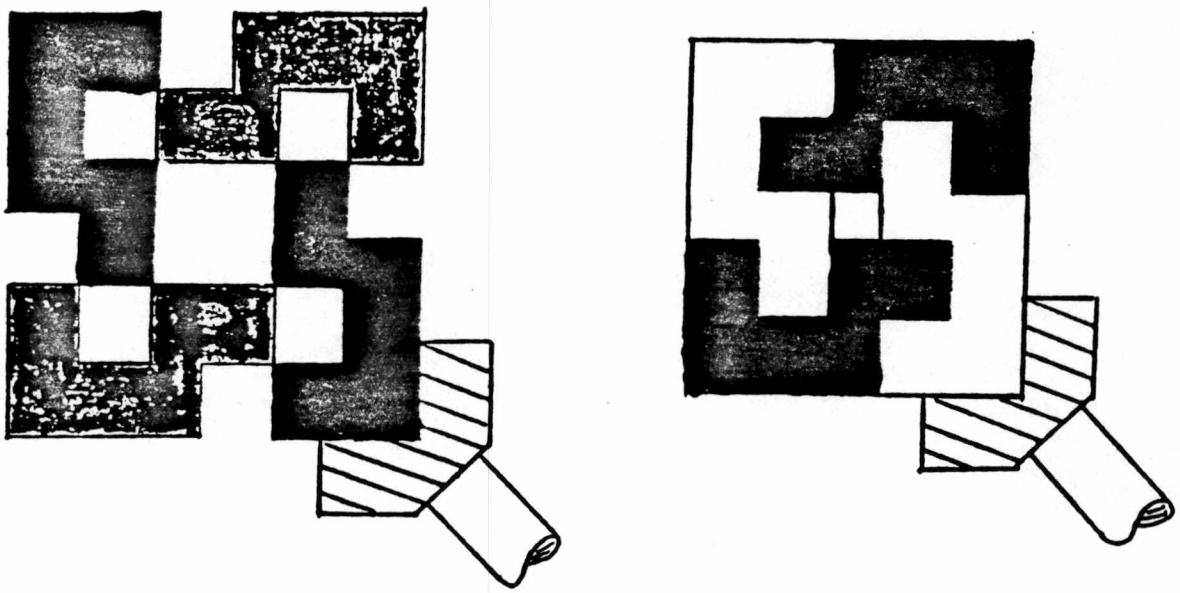

Figure 23: The original dies. The interfitting G-shape design requires that the movement of the dies be perfectly balanced to prevent jamming.

rigid dies. However, the finite fit tolerances and elastic deformation of the dies allowed the rotation. The result of this rotation caused variations in the cross-section of the compressed materials. Figure 24 shows an example. In many cases the elastic deformation of the dies allowed a gap to open at the corners of the die cavity. When the pressure was released, the recovery of the dies pinched the material which had extruded into the gap, thus jamming the dies.

The hydraulic system was capable of both extension and retraction of the dies. Thus, when the dies jammed, they could be forced open. However, the design of the piston rod was insufficient to support the load required to open the dies under adverse conditions. The independent failure of three out of the original four piston rods caused extensive delays for repair.

During the series of piston rod failures, the second generation apparatus was designed. In this design, provisions were made for each of the following: thermal isolation of the hydraulic system from the heat of the dies, an electrically powered hydraulic pump, steady state pressure control, and commercial cylinders to alleviate the O-ring problems. The most extensive machine shop work involved the fabrication of this apparatus.

Although the four commercial cylinders were expected to have more consistent fit among them, the sequential movement of each piston was still a problem. Therefore, the dies

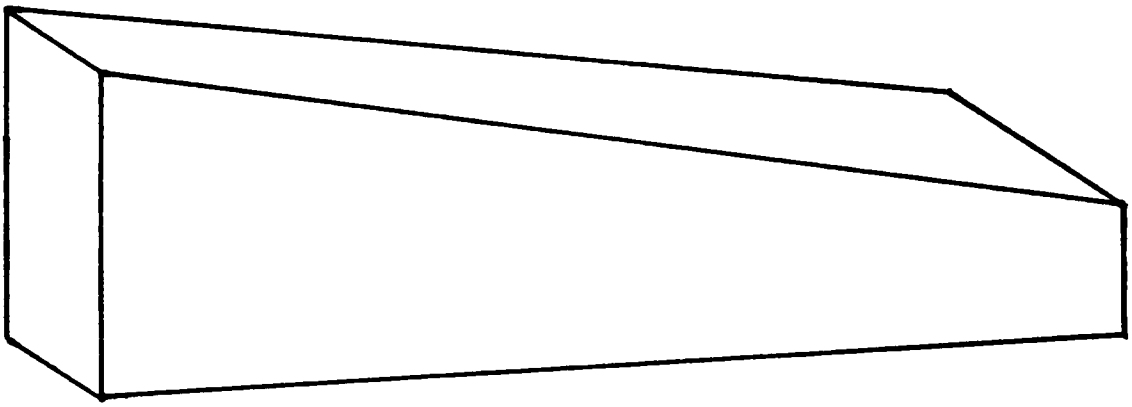

Figure 24: Schematic example of the resulting specimen geometry when the interfitting dies flexed and rotated during the pressing run (exaggerated to illustrate the effect).

continued to jam. With the commercial cylinders, failure of the piston rod was not a problem. However, the unrestricted, instantaneous application of desired pressure, up to 10 ksi, provided quick movement of the pistons. The quick response made the dies more prone to jamming and the jamming potentially more severe. The possibility of separating the dies fully was also much greater. If separation occurred, the dies had to be removed, reassembled, and reinstalled. To prevent this, a ring was machined which limited the travel of the dies. The unbalanced opening, between the x and y axes of Figure 23, caused one set of opposing dies to contact the retaining ring first. It was intended that continued application of pressure would then open the second set of opposing dies to give a uniform die chamber of square cross-section. The third generation apparatus incorporated this ring.

The first attempt to use the ring proved awkward. The ring was laid loosely over the dies in order to avoid drilling mounting holes in the octagonal frame; too many holes would have unacceptably weakened the ring. Since the ring was not rigidly attached to the frame, it did not force the dies to be centered within the frame. This also resulted in binding of the dies. However, several runs were made during which the shafts, which carried the load from the hydraulic cylinder, through the water jacket, and to the dies, became bent and upset at the ends. The deformed

shafts bound in their guides and increased the pressure required to move them. As a result of the increased pressure to initiate movement, the position of the dies was more difficult to control. The resultant binding proved to be more than the inter-fitting dies could withstand. Two of the four die components fractured.

The fracture of the dies was in a brittle mode. These dies were used at a maximum temperature of 400°C. The type of steel used to fabricate these dies was not known; they were machined in Bristol, England long before this research began. Temper embrittlement could not be ruled out. The third generation was therefore the last design to use these dies. A major contributing factor was the lack of fillets in the corners of the dies. Stress concentration was very high at these corners. Both fractures initiated at the same sharp corner. Figure 25 illustrates the fracture of the original dies.

The fourth generation development involved redesigning the die assembly. During the design and fabrication of the new die assembly, the distorted shafts were removed and replaced. The original material was used for the shafts, i.e., 304 stainless steel, since they were continually exposed to water in the cooling jacket. The proposed designs are illustrated in Figure 26. The design used was developed by Bob Hale, a gifted design engineer at the Y-12 plant in Oak Ridge, Tennessee.

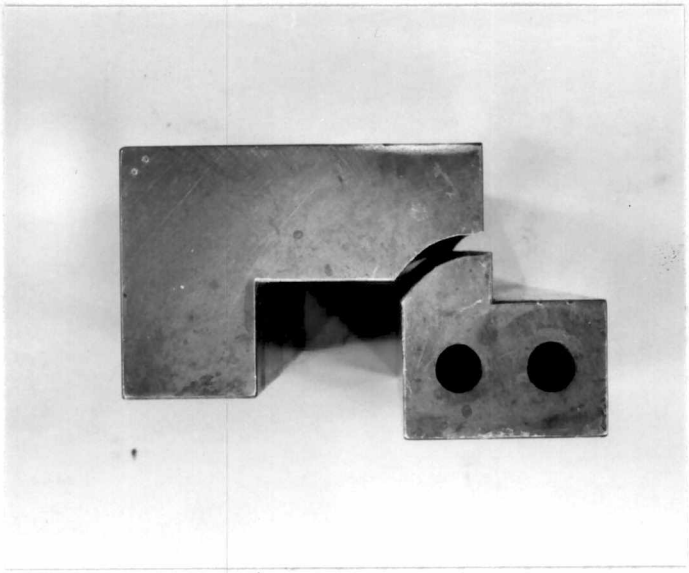

A

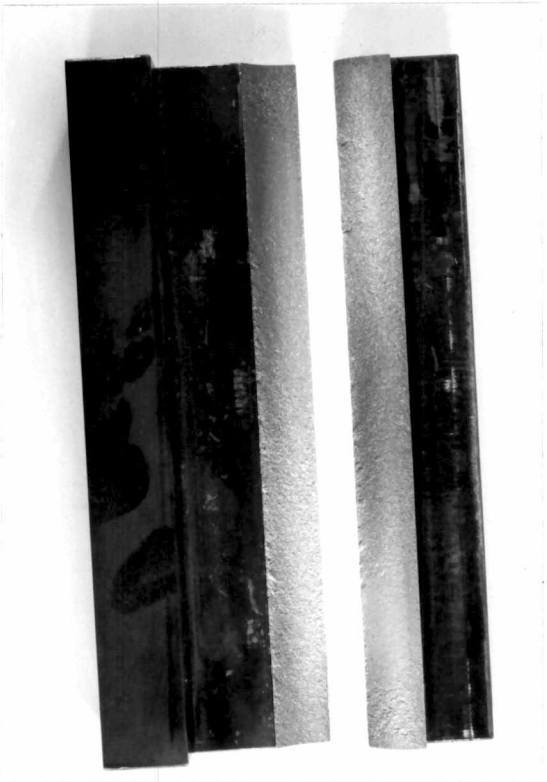

B

Figure 25: Location (a) and fracture surface (b) of the original interfitting, G-shaped dies. The two separate failures originated at the same sharp corner.

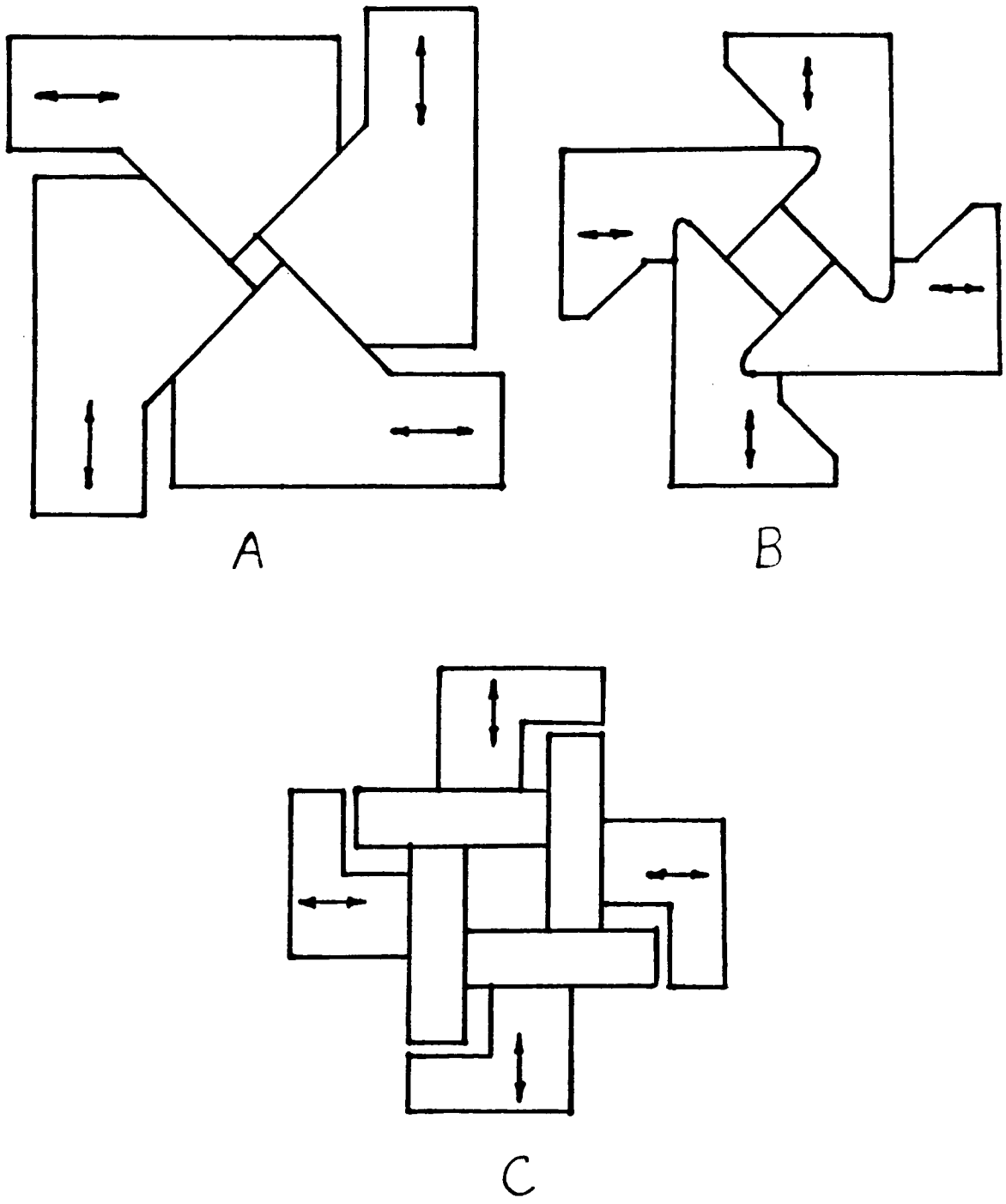

Figure 26: Proposed designs for improved die system, (a) and (b) required offset hydraulic cylinders which could not be accommodated by the existing octagonal frame, and (c) was used in the final apparatus.

There were many considerations in development of the new die assembly. Ease of fabrication, freedom from binding and durability were first priority. Material selection involved a short literature review which led to the choice of H-13 hot working tool steel. This material was readily available in the annealed condition, provided excellent hot hardness, and had excellent stability at the intended service temperatures. The "Heat Treater's Guide" (47) provided the heat treating schedule required for hardening the new dies. After heat treatment, the dies were surface ground to provide a low friction surface.

The major advantage of the new die assembly was the ability to accommodate unbalanced movement of the individual hydraulic pistons. Other advantages included ease of disassembly and cleaning. The dies were not attached to the assembly and, therefore, could not jam the system.

During the initial use of the fourth generation apparatus, the dies performed flawlessly. However, the shafts quickly distorted as before. Again, the movement of the dies became much more difficult to control. Eventually, one piston moved full stroke before the others moved at all.

To aid in positioning the dies for each run, spacers were made to limit the retraction of each piston. These spacers were installed between the octagonal frame and the die rests, as illustrated in Figure 27. They were intended

to serve the same function as the retaining ring did for the original die assembly. The ring would not work for the new dies since they were not attached to the shafts. The spacers worked well until the pressure required to move the shafts became greater than the bolts which mounted the die rests could support. While attempting to fully retract all of the shafts, three of the four bolts attaching the die rests to the shafts failed. These were high strength bolts and failure was catastrophic; they gave no warning prior to failure. Although the broken bolts were removed without disassembly of the apparatus, the need for replacement of the distorted shafts was obvious. Severe galling of the shafts was evident. Continued use in such a condition would jeopardize the bearing surfaces within the octagonal frame, a risk which could not be taken.

In addition to the upsetting of the shaft ends and the galling, the shafts were bent. The bending was a result of two types of loading. First, if the sample was not centered across the plane of the four hydraulic cylinders, an out-of-plane stress resulted, as shown in Figure 28a. Second, the frictional forces caused an in-plane bending as shown in Figure 28b.

The fifth generation apparatus incorporated: a new material for the shafts, supports which limited the in-plane deflection of the shafts, throttling valves to independently control the movement of the dies, and a set of electrical

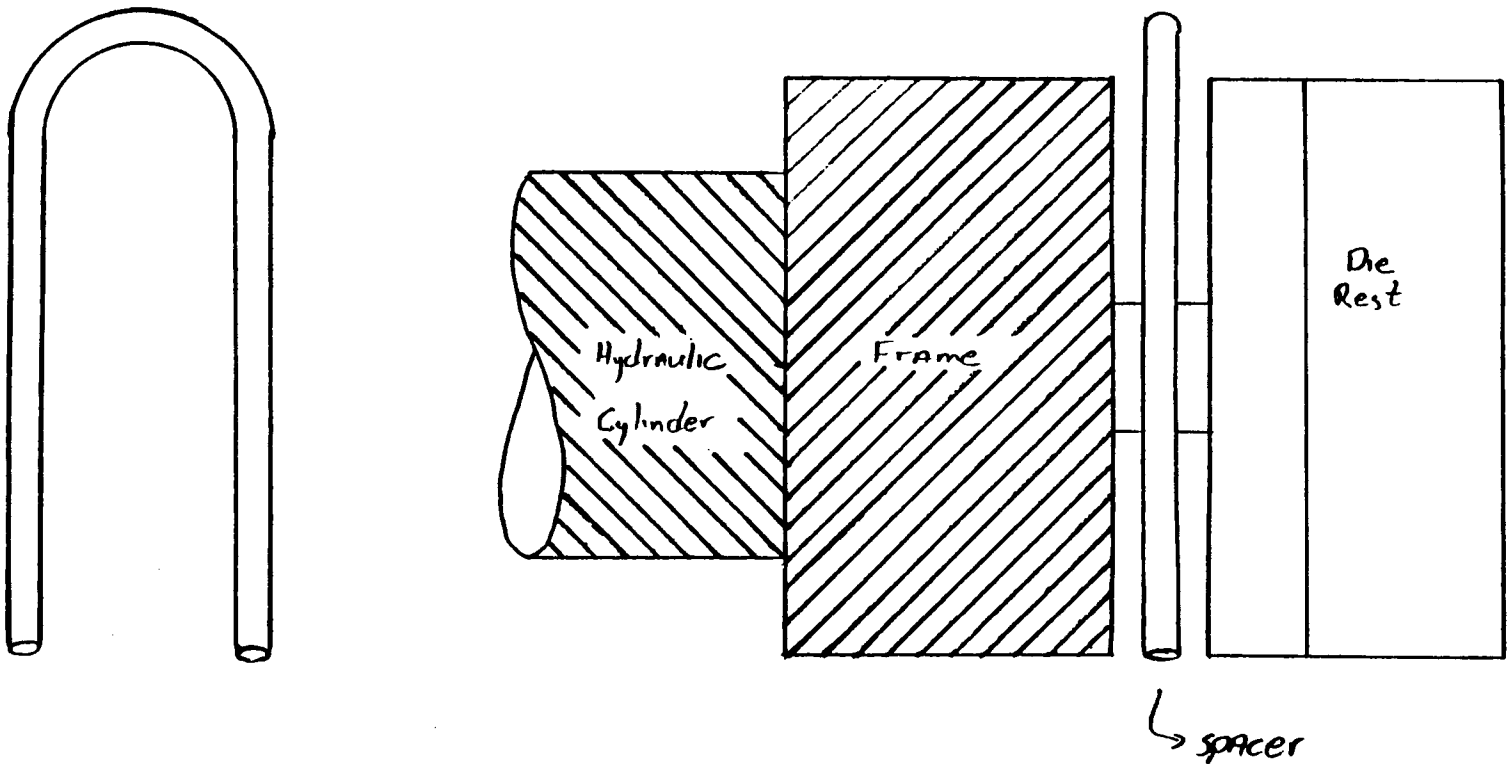

Figure 27: Spacers placed between the die rests and the frame to limit the retraction of the dies.

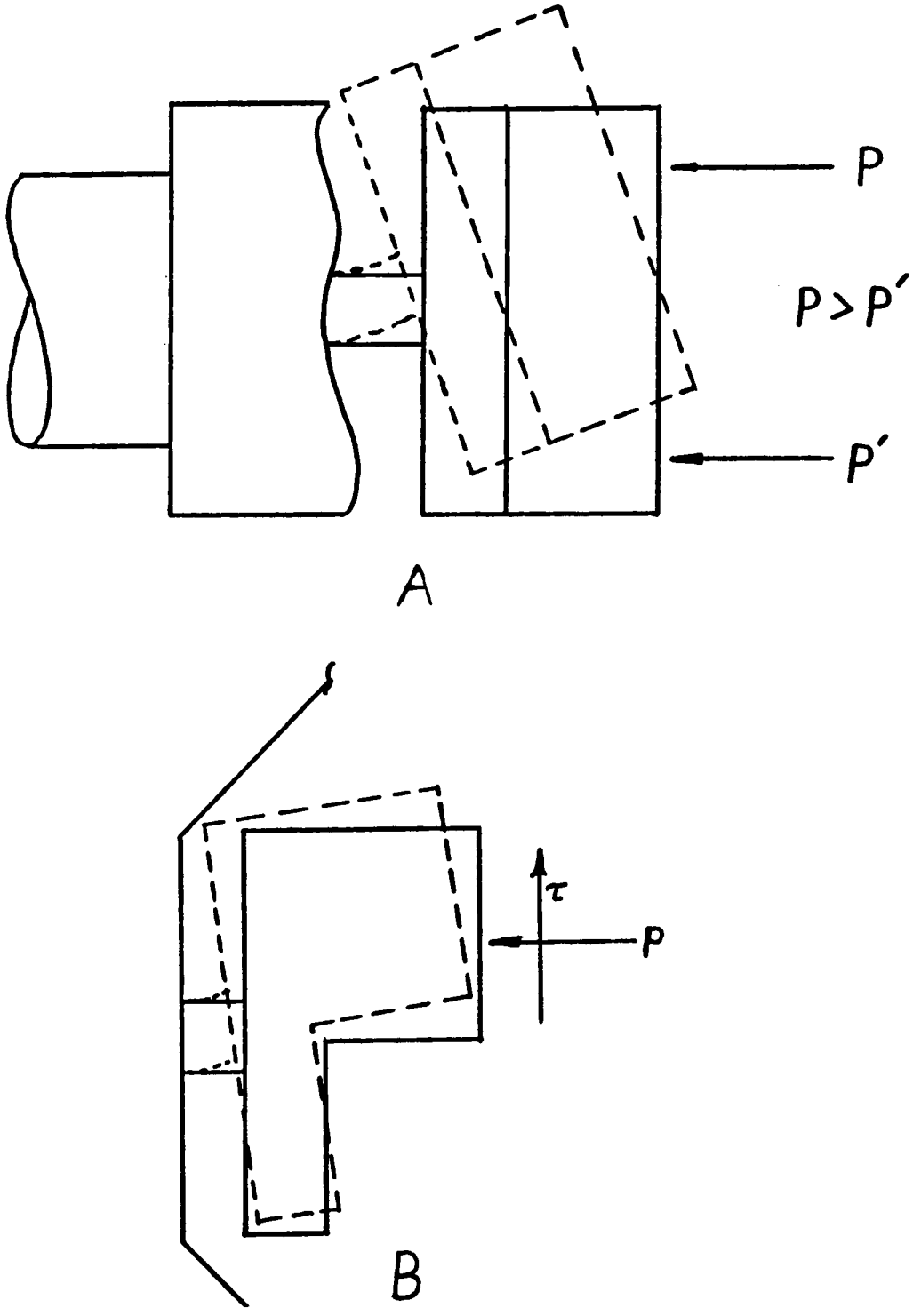

Figure 28: Deflection of the shafts due to loading conditions about the plane of the hydraulic cylinders, a) out-of-plane, and b) in-plane.

contacts which signaled if the out-of-plane deflection was too great. Figure 29 shows the fifth generation apparatus. If the out-of-plane deflection was too great, the sample was repositioned by hand until the deflection was acceptable, taking care to avoid plastic deformation of the shafts. The new material for the shafts was 52100 steel. The higher yield strength increased the load carrying capacity of the shafts. The increased risk of corrosion was considered secondary to the stregnth. The strength of the stainless steel had proven to be unacceptable.

However, all of these modifications cured only symptoms. The cause of each symptom was thought, at each juncture, to be either too expensive or too time consuming to fix. The best cure would have been fabrication of a more substantial frame and active position control for the dies. The larger frame would have allowed larger shafts to carry the loads, but the machine shop lacked the equipment to fabricate a new frame and the active position control was too expensive.

CAN DESIGN

The initial can design was used throughout phase one. A major problem was expansion of the argon trapped in the can. Welding caused some of the aluminum powder to forcefully blow out as the final, closing gap was sealed. This made

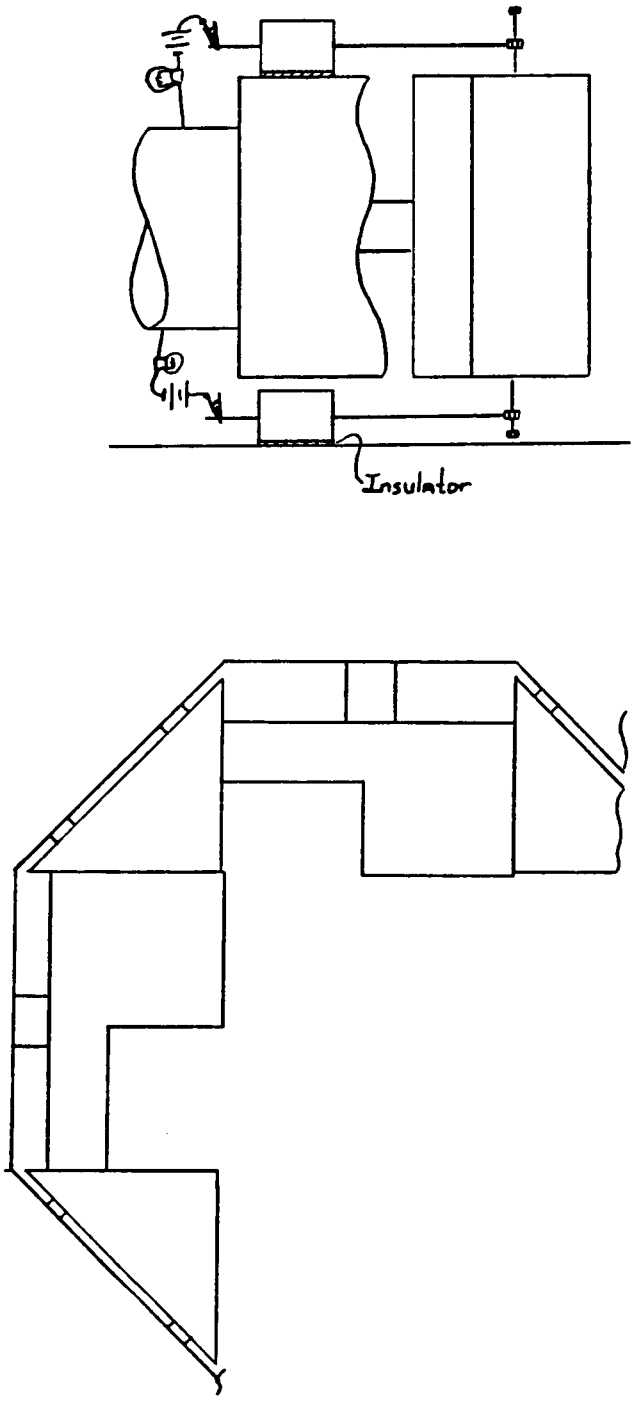

Figure 29: Components intended to prevent the failure of the apparatus due to deflection of the shafts. The triangular braces limit the in-plane deflection. The electrical sensors signal when the out-of-plane deflection is too large.

the welding process difficult and time consuming, since the best way to prevent blow out was to weld in increments small enough to limit the heating of the can and powder. Heating of the powder caused outgassing of adsorbed gasses and was suspected of adding considerably to the blow-out phenomenon.

These cans were adequate for the initial pressure-temperature effect study. However, the time required to fabricate a specimen was long. The cross-sectional area of the specimens was small. It was therefore difficult to size the specimens such that sufficient thickness was obtained after pressing, for fabrication of mechanical property specimens. Therefore, another can was devised which increased the initial cross-sectional dimensions and included a tube for outgassing of the powder in situ. Vacuum hot pressing would have been possible with this design, giving the best possible mechanical properties. This new can design was to be implemented for phase two specimens.

The execution of this design proved to be futile. The Peerless can material was very difficult to weld, even with no powder present in the can. An aluminum solder was tried and was also difficult to use. The solder did not wet the aluminum well and the residual porosity was unacceptable for the intended outgassing of the powder. Loading the can through the outgassing tube also proved to be difficult,

though possible. A vibrating scribe was used to vibrate the can, allowing the powder to flow through the tube, otherwise the powder plugged the tube immediately.

The final can design did not involve welding. The powder was outgassed prior to loading into the cans. The Peerless tubes had been deep drawn so the can was ready after a quick sizing step. This step was necessary since the can diameter was greater than the maximum die cavity opening. Squaring the round cans allowed them to fit into the die cavity and to fill it more completely. The lid was mechanically locked in place by folding the top of the can inward.

EXPERIMENTAL RESULTS

Metallography

The most important experimental consideration in phase one, aside from the design of the bidimensional press, was the preparation of the metallographic specimens. The polishing procedure required absolute consistency in order to achieve repeatability. The procedure was developed using the specimens consolidated during the design of the bidimensional pressing apparatus. Variations in the procedure produced anomalous results during the initial attempts. The cutting procedure produced a shallow layer of

compressed powder due to the concentrated load and localized heating, Figure 30. Careful grinding removed this artificially dense layer. Colloidal silica proved to be the quickest and easiest medium to use for the final polish. Etching was difficult because the time required to reveal the powder boundaries varied with the consolidation conditions. Longer times were required for fully dense specimens; especially for specimens pressed to full density at lower temperatures. The effect of work hardening on the etching rate may account for the latter observation. Long etching times for specimens having less than full density tended to increase the size of the individual pores remaining after consolidation. This effect was considered and kept to a minimum by etching in small increments of time. Scatter in the porosity data may well have been the result of specimen preparation.

When the density is low, it is sometimes difficult to determine if the porosity revealed by the micrograph is genuine or if it was generated by the polishing procedure. If the individual particles are weakly bonded, the nap of the polishing cloth may tear some of them out, giving the appearance of a large pore. The shape of the pore becomes an important consideration in the interpretation of the micrographs. The same phenomenon can occur during etching. If the contact area between particles is small, the etchant may dissolve the interparticle bond allowing the particle

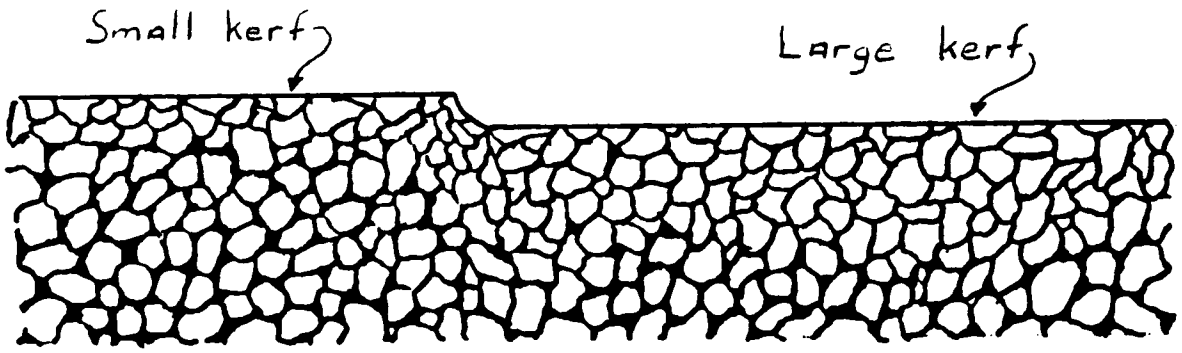

Figure 30: Schematic representation of false density layer produced by sectioning cuts.

to be rinsed away. This is especially true when the specimen is not thoroughly rinsed immediately after etching, because retained etchant continues to attack the particles wherever they are exposed. For this reason, the specimens used to determine the porosity were carefully etched to reveal the particle boundaries.

With the boundaries revealed, the classification of an individual pore was more accurate. Pitting during the 9.5 and 1.0 micron polishing stages was difficult to avoid; when it was unavoidable the shape of the pits distinguished them from porosity. Additionally, the colloidal silica is slightly basic, with a pH greater than seven, which helped to prevent build up of an oxide layer on the specimen. This solution, however, did reveal the structure within the individual powder particles to varying degrees. Precipitates within the powder particles appear black on the micrographs, as does porosity. Knowledge of the particle boundaries prevented confusion between precipitate and porosity. Therefore, all of the micrographs used to interpret the success of consolidation by bidimensional compression were of etched specimens. The etchant seemed to reveal the microstructure by pitting along the particle boundaries. In some cases, the pitting at triple points was severe. When this occured, the triple points were difficult to classify as porosity or etching pits. The shape of the pit was the best indicator.

Porosity

The results of the first phase, concerning the resultant microstructures, are summarized in Table 2. These data define the range of press conditions which produce the best consolidation in terms of residual porosity. Figure 31 shows representative microstructures for the temperature-pressure combinations given in Table 1. The resultant porosities are estimated from similar micrographs taken for each set of conditions.

STATE OF STRESS

The calculated porosity for each specimen is given in Table 2. Figure 32 illustrates the dependence of the porosity on applied bidimensional pressure at various pressing temperatures. As expected, the porosity decreases with increasing pressure. As the porosity of the specimen decreases, the effect of a given increase in pressure also decreases. This is also expected and recognized as geometric work hardening, conventional work hardening, and possibly a friction effect.

This friction effect may alter the specimen's apparent response. An increase in pressure produces an increase in density and therefore higher reaction forces both normal

TABLE 2: RESULTS OF PHASE ONE--POROSITY

SPECIMEN	TEMP. (°C)	HYD. PRESS. (ksi)	ACT. PRESS. (ksi)	POROSITY (%)
		Al-123 POWDER		
-01	25	2	9	17
-02	25	4	17	6
-03	25	6	26	2
-04	25	8	35	0
-05	25	10	43	0
-06	200	2	9	17
-07	200	4	17	6
-08	200	6	29	0
-09	300	2	9	11
-10	300	4	16	0
-11	400	2	9	0
-12	450	2	8	0
		MB85 POWDER		
-501	25	2	9	***
-502	25	4	17	***
-503	25	6	26	17
-504	25	8	35	10
-505	25	10	43	9
-506	200	2	9	***
-507	200	4	17	12
-508	200	6	29	9
-509	300	2	9	9
-510	300	4	16	3
-511	400	2	9	3
-512	450	2	8	2
-513	25	10 (TEFLON)	39	3
-514	200	10	40	3
-515	300	6	25	1
-516	400	4	15	7
-517	400	8	25	1

*** represents insufficient consolidation

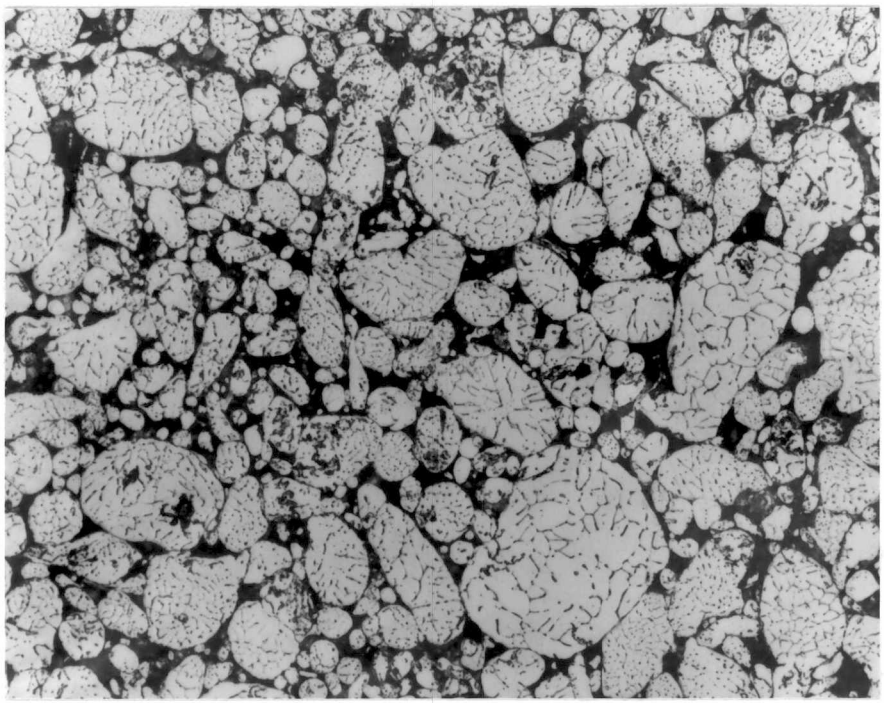

A) Al-123-01, 400X, 25°C, 9 ksi, 17% porosity

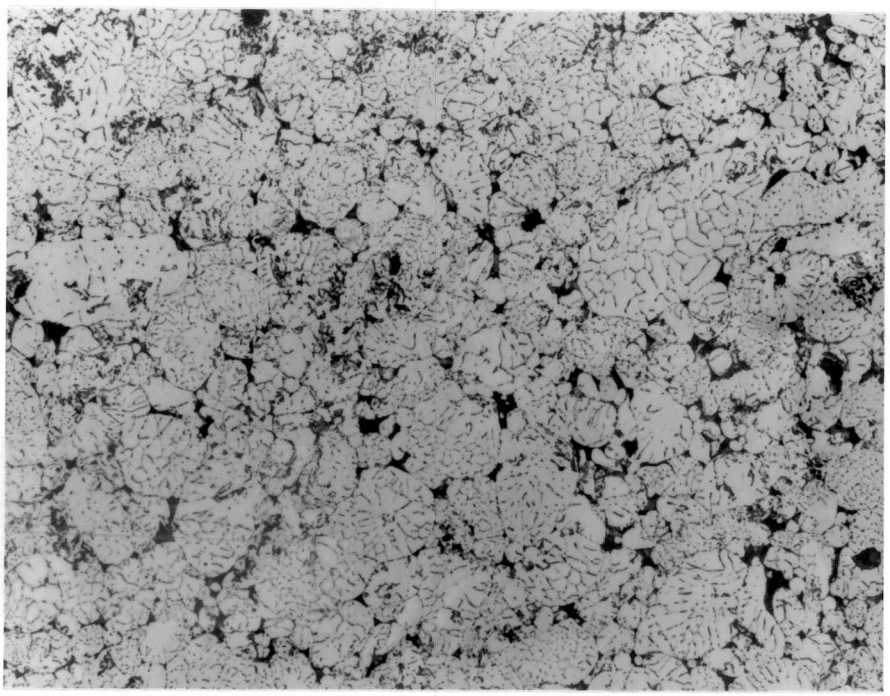

B) Al-123-02, 400X, 25°C, 17ksi, 6% porosity

Figure 31: Phase 1 microstructures (OPT)

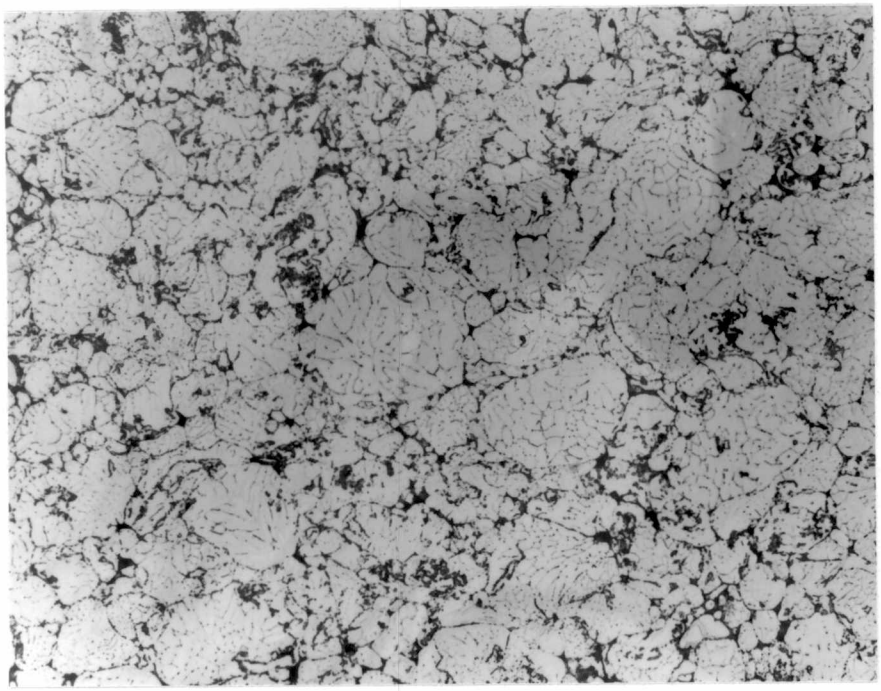

C) Al-123-03, 400X, 25°C, 26 ksi, 4% porosity

Figure 31: Phase 1 microstructures (OPT) cont'd

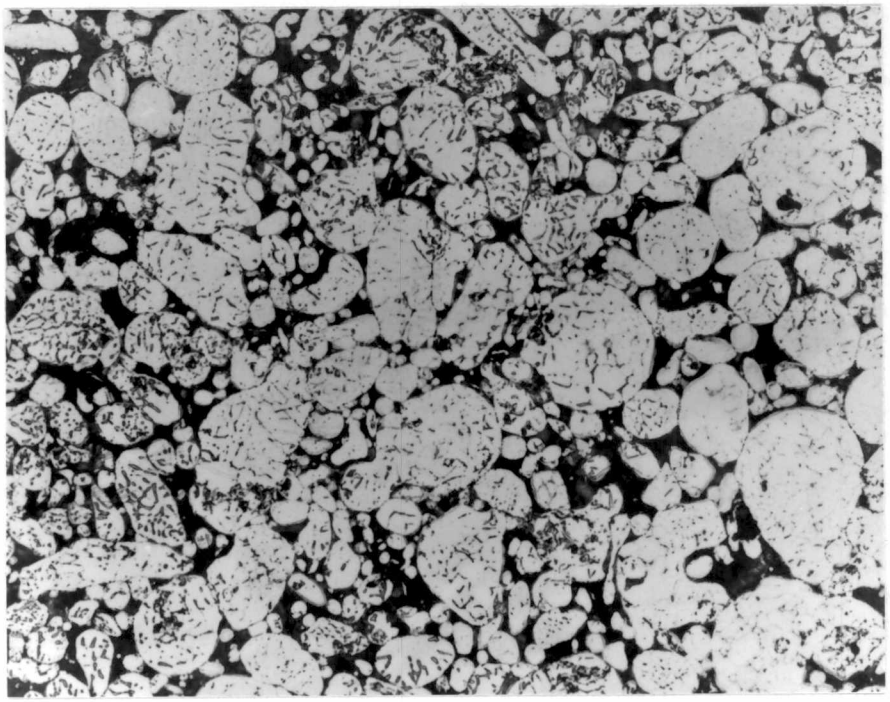

D) Al-123-06, 400X, 200°C, 9ksi, 17% porosity

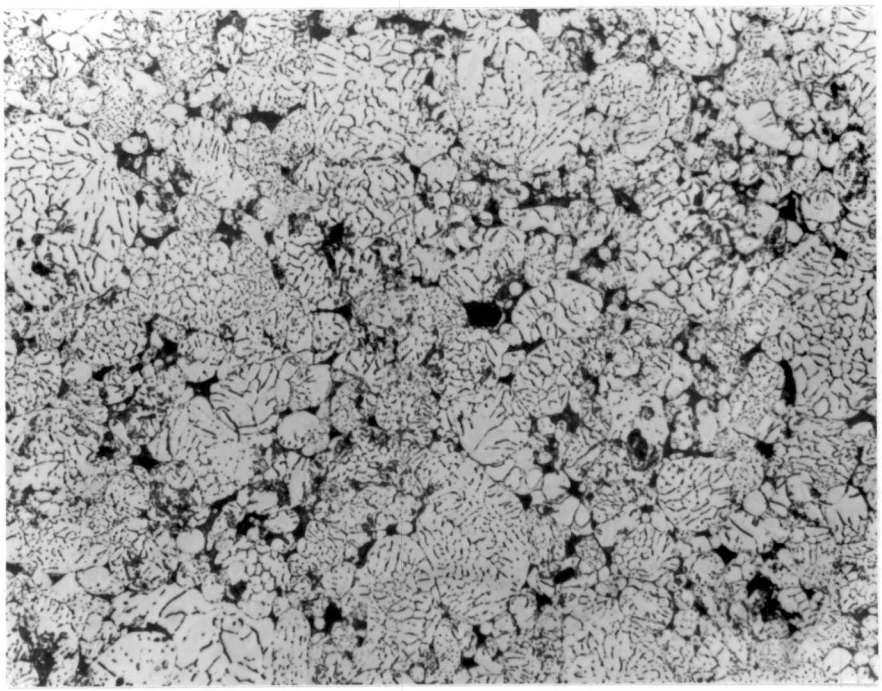

E) Al-123-07, 400X, 200°C, 17ksi, 6% porosity

Figure 31: Phase 1 microstructures (OPT) cont'd

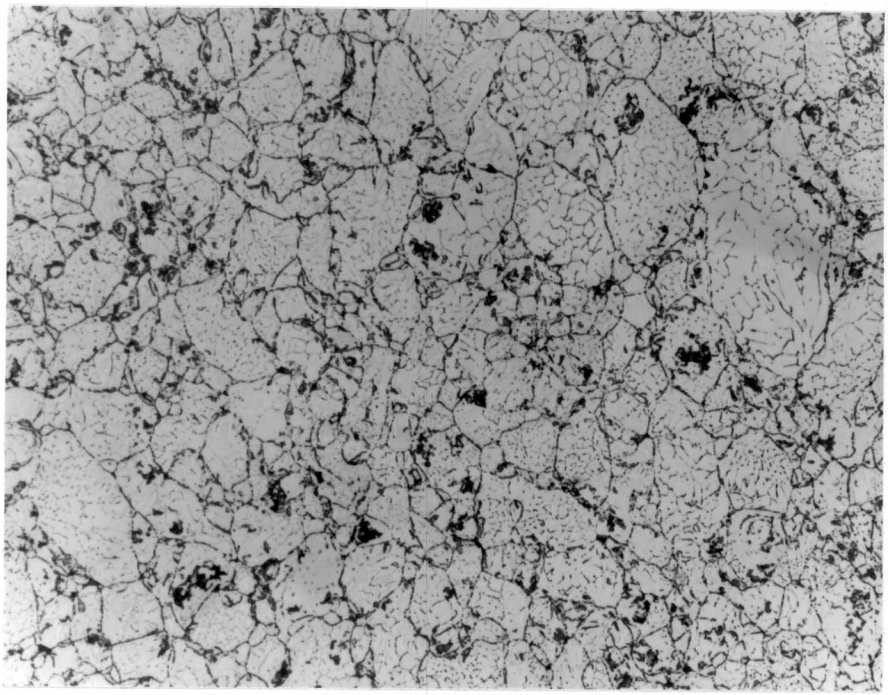

F) Al-123-08, 400X, 200°C, 29ksi, 0% porosity

Figure 31: Phase 1 microstructures (OPT) cont'd

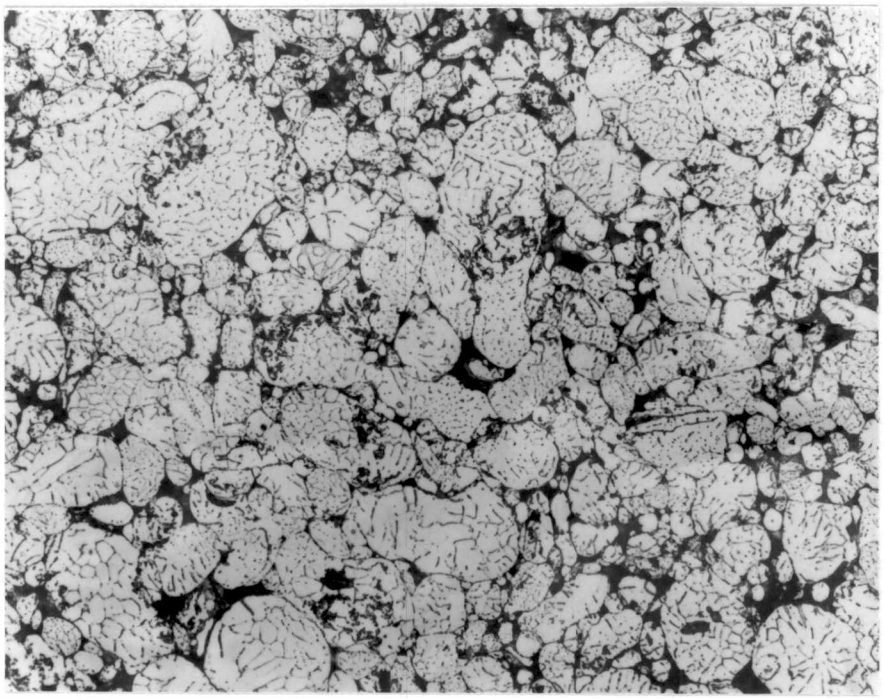

G) Al-123-09, 400X, 300°C, 9ksi, 11% porosity

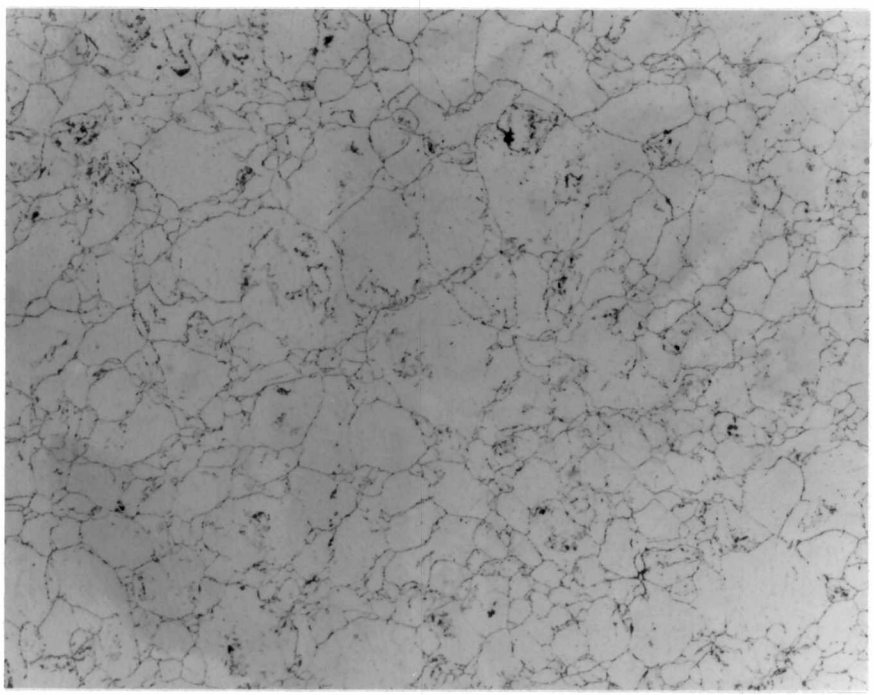

H) Al-123-10, 400X, 300°C, 16ksi, 0% porosity

Figure 31: Phase 1 microstructures (OPT) cont'd

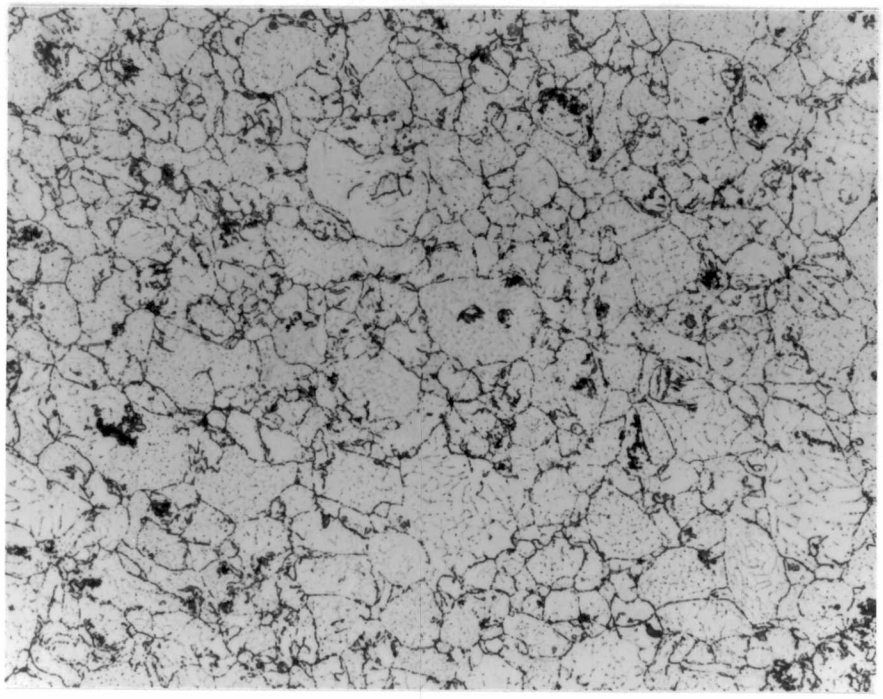

I) Al-123-11, 400X, 400°C,9ksi, 0% porosity

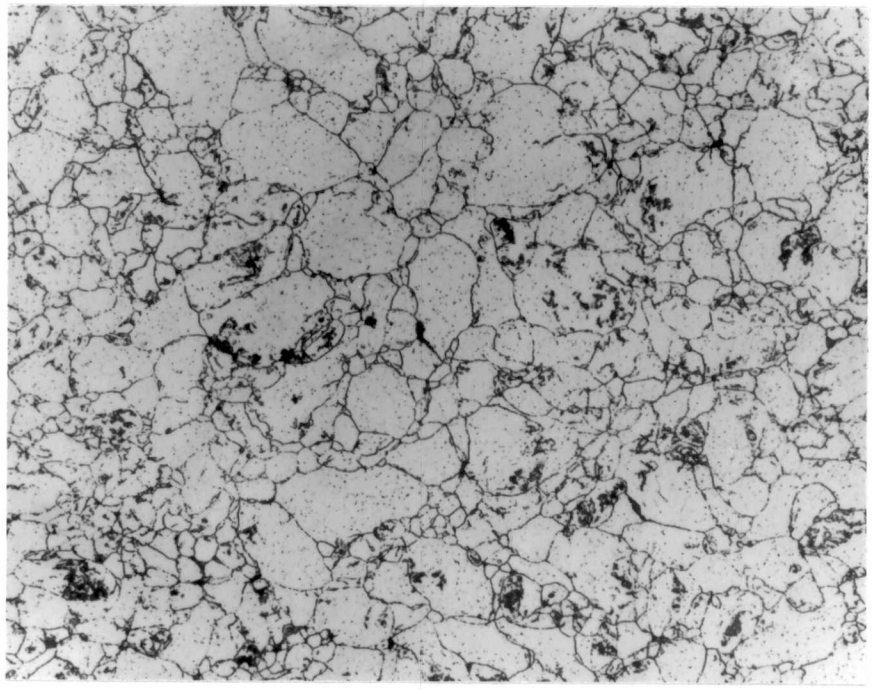

J) Al-123-12, 400X, 450°C,8ksi, 0% porosity

Figure 31: Phase 1 microstructures (OPT) cont'd

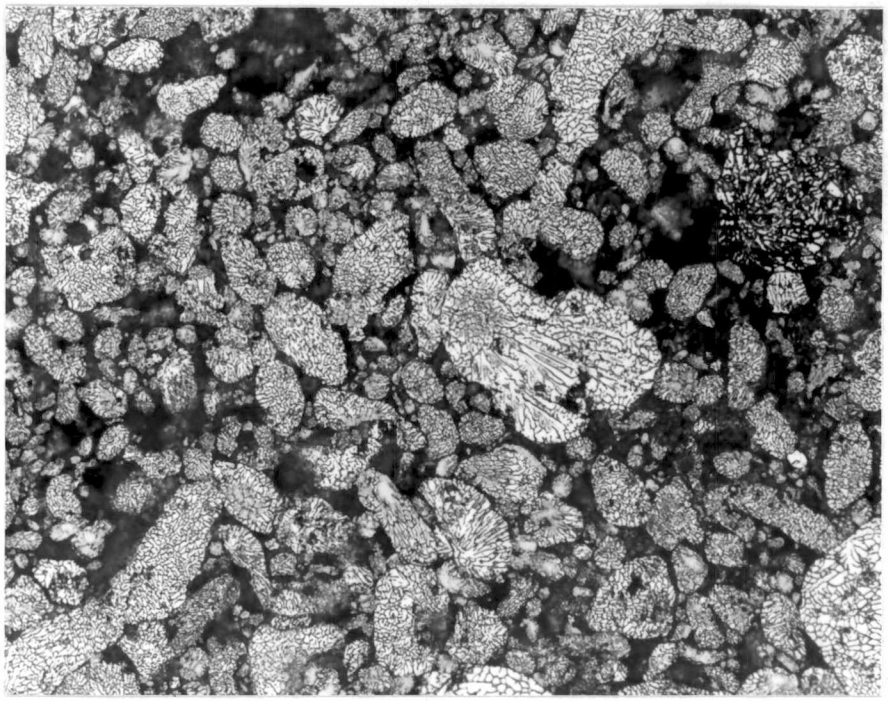

K) MB85-502, 400X, 25°C, 17ksi, 17% porosity

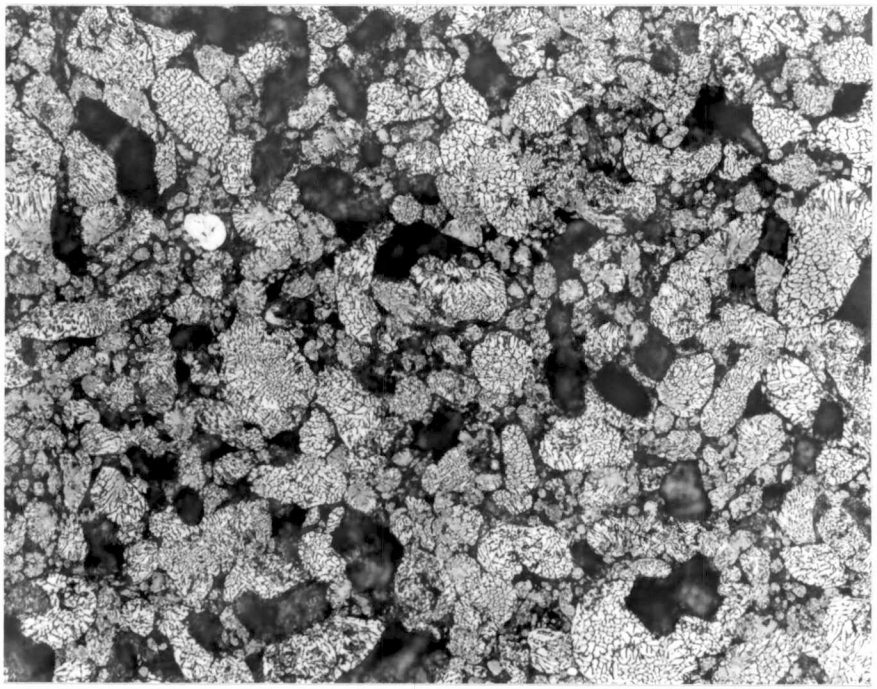

L) MB85-503, 400X, 25°C, 26ksi, 17% posority

Figure 31: Phase 1 microstructures (OPT) cont'd

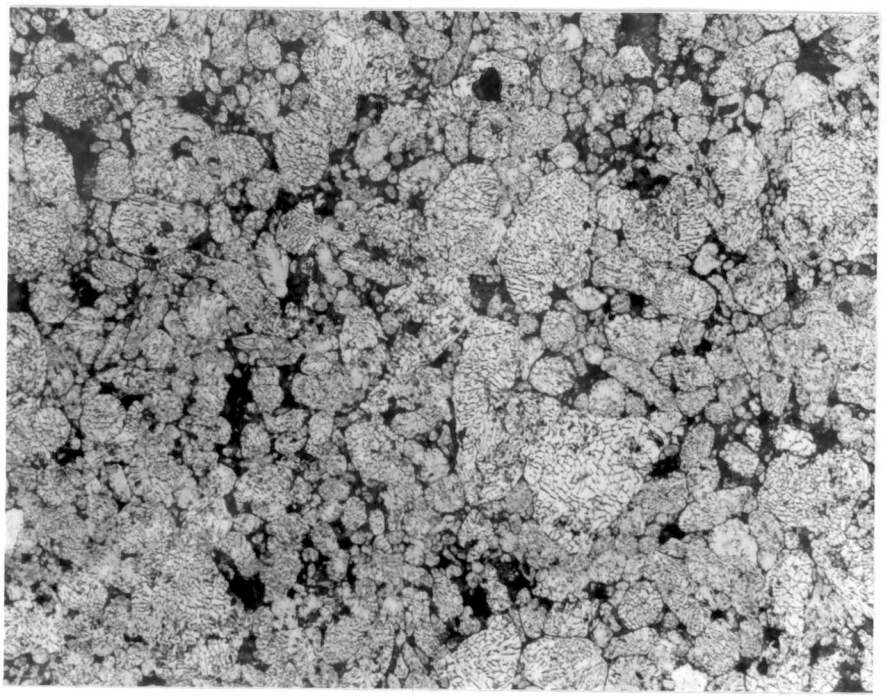

M) MB85-504, 400X, 25°C, 35ksi, 10% porosity

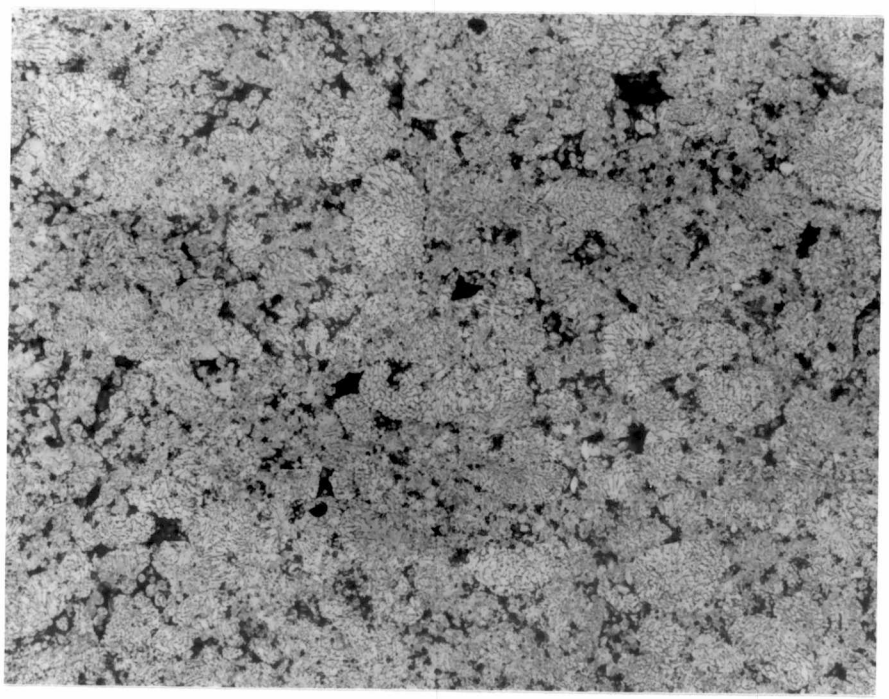

N) MB85-505, 400X, 25°C, 43ksi, 9% porosity

Figure 31: Phase 1 microstructures (OPT) cont'd

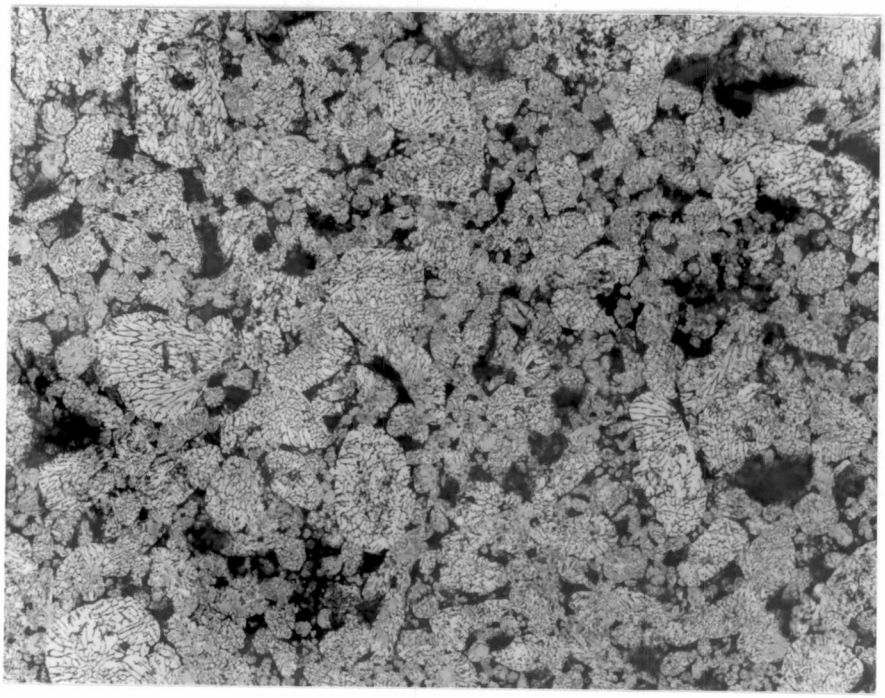

O) MB85-507, 400X, 200°C, 17ksi, % porosity

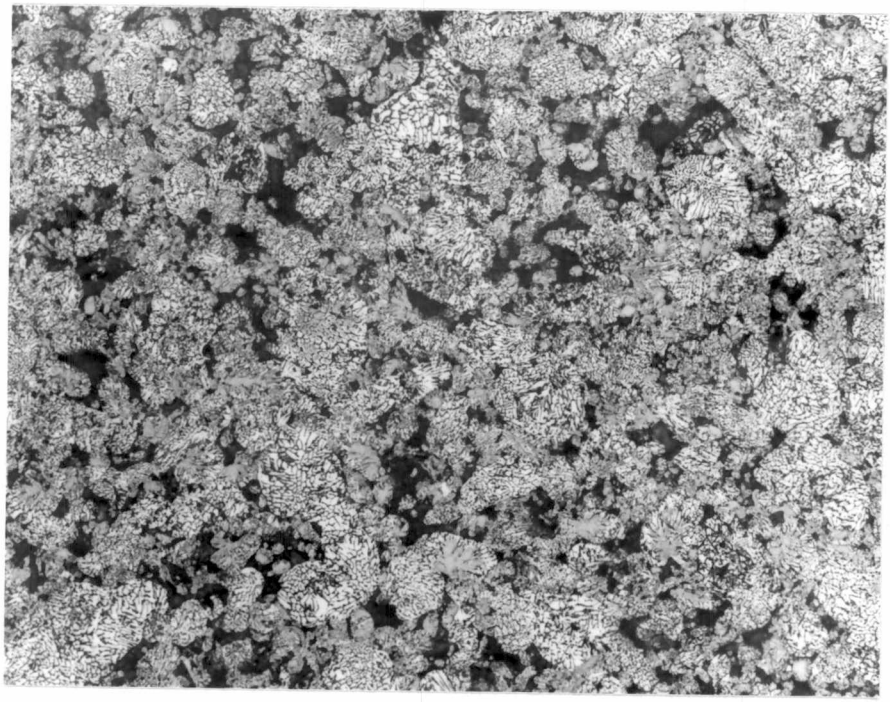

P) MB85-508, 400X, 200°C, 29ksi, 9% porosity

Figure 31: Phase 1 microstructures (OPT) cont'd

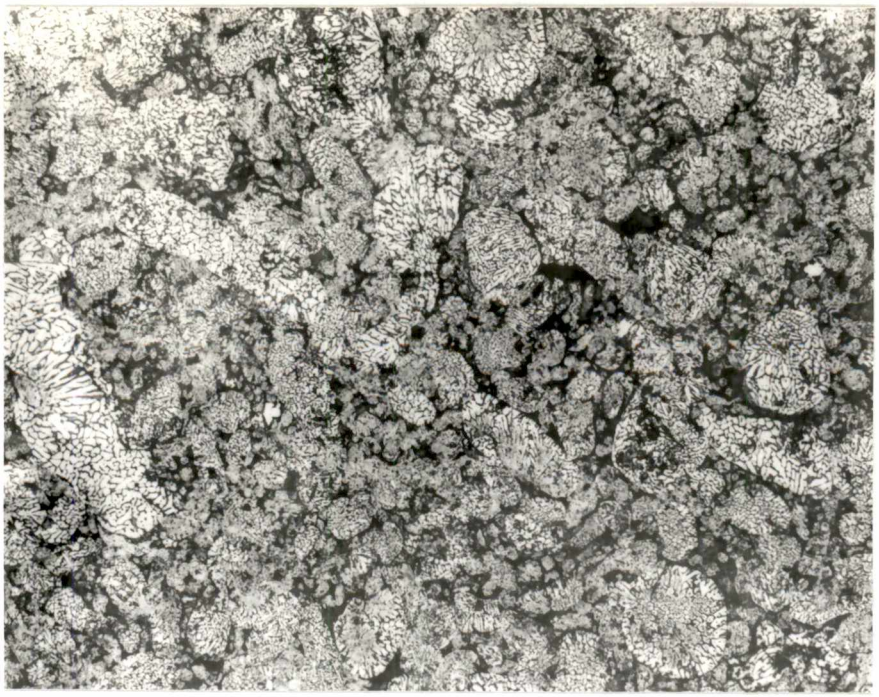

Q) MB85-509, 400X, 300°C, 9ksi, % porosity

R) MB85-510, 400X, 300°C, 16ksi, 3% porosity

Figure 31: Phase 1 microstructures (OPT) cont'd

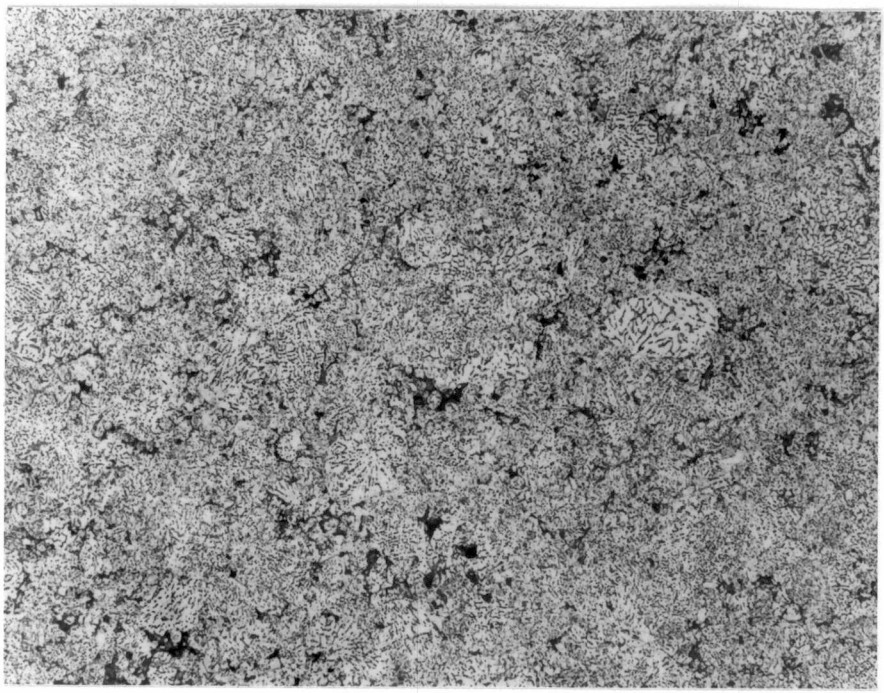

S) MB85-511, 400X, 400°C,9ksi, 3% porosity

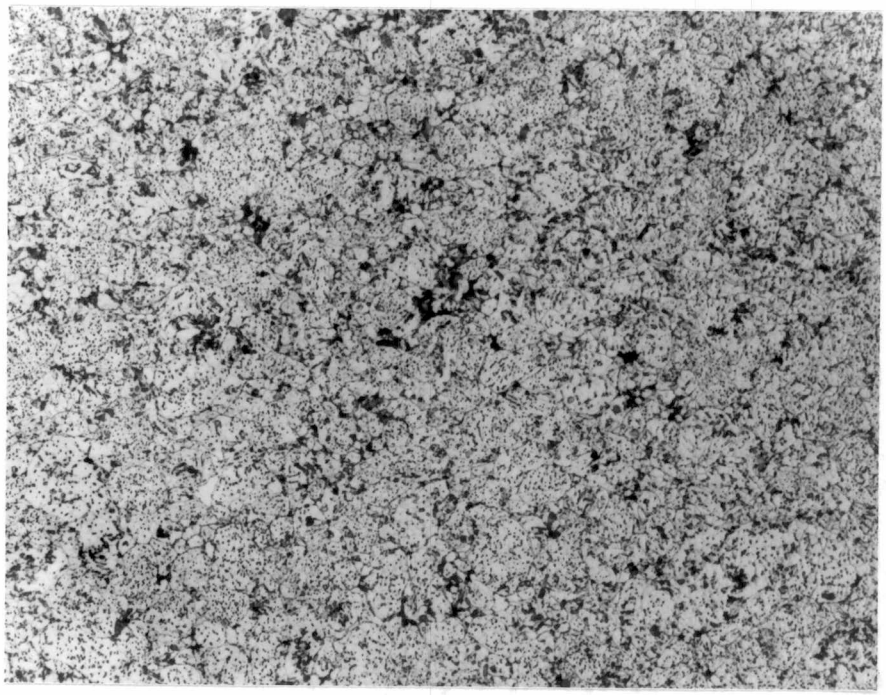

T) MB85-512, 400X, 450°C,8ksi, 2% porosity

Figure 31: Phase 1 microstructures (OPT) cont'd

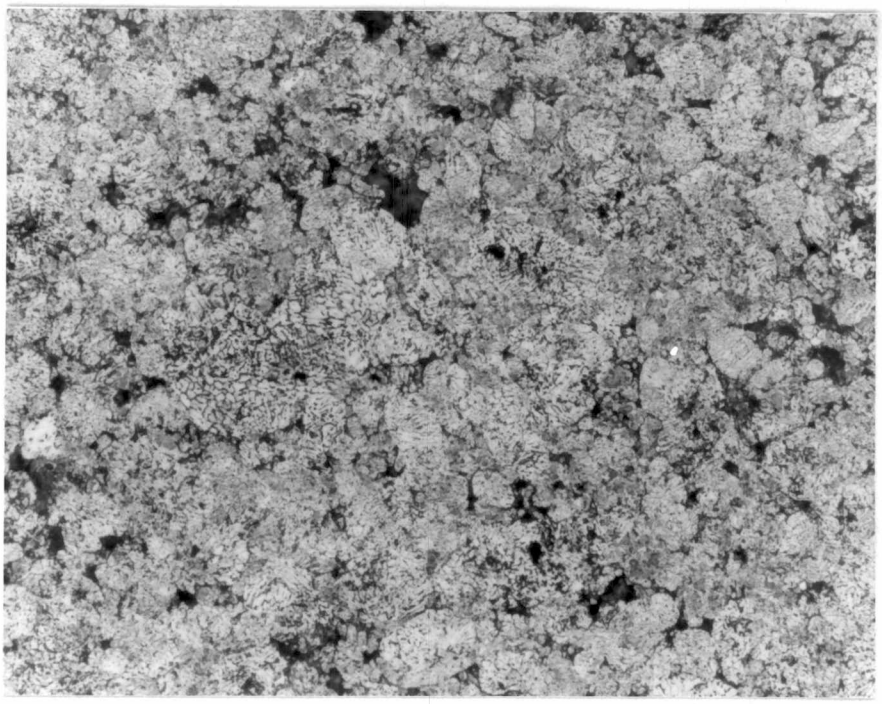

U) MB85-513, 400X, 25°C, 39ksi, 3% porosity

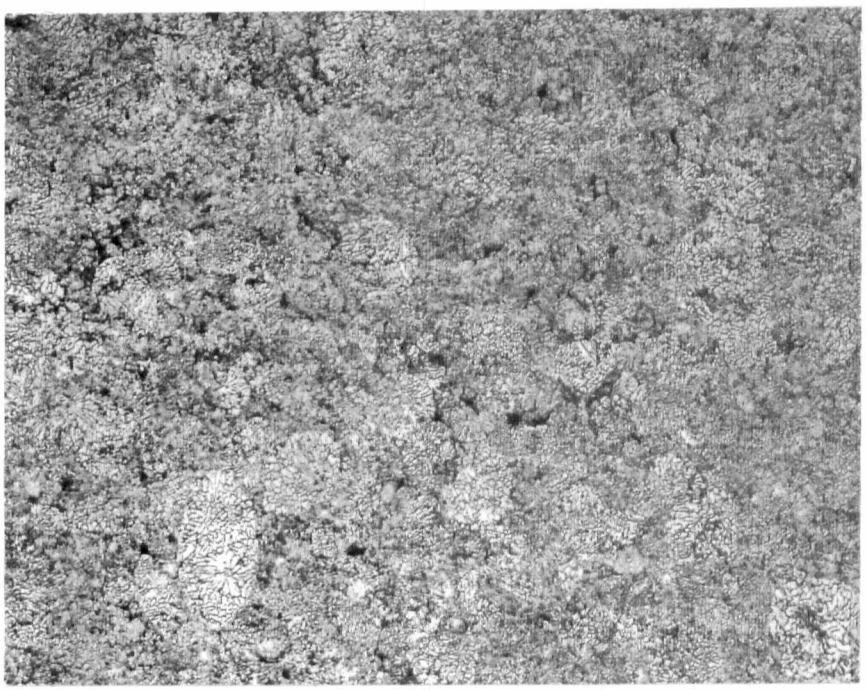

V) MB85-514, 400X, 200°C, 40ksi, 3% porosity

Figure 31: Phase 1 microstructures (OPT) cont'd

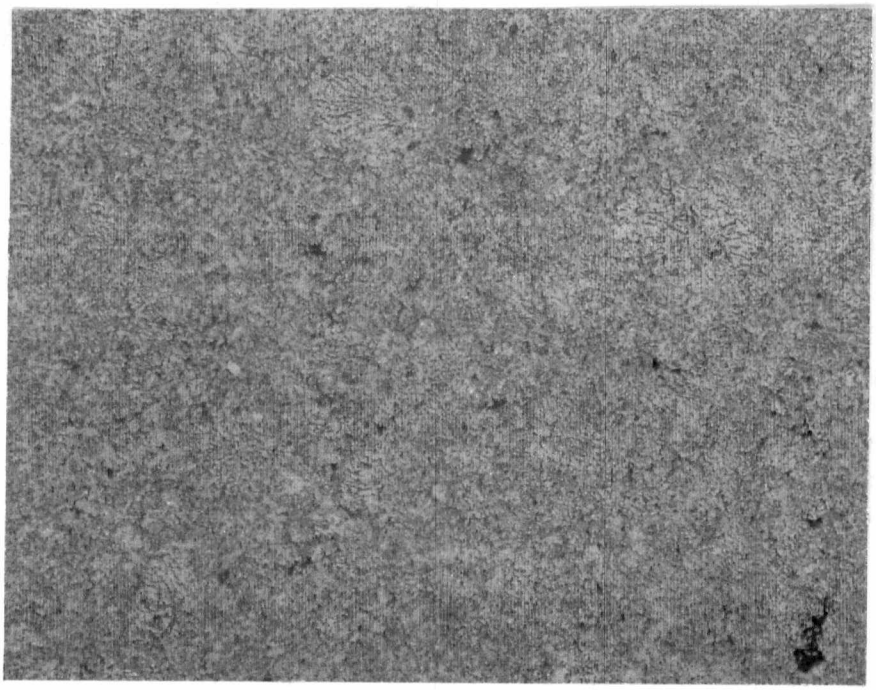

W) MB85-515, 400X, 300°C, 25ksi, 1% porosity

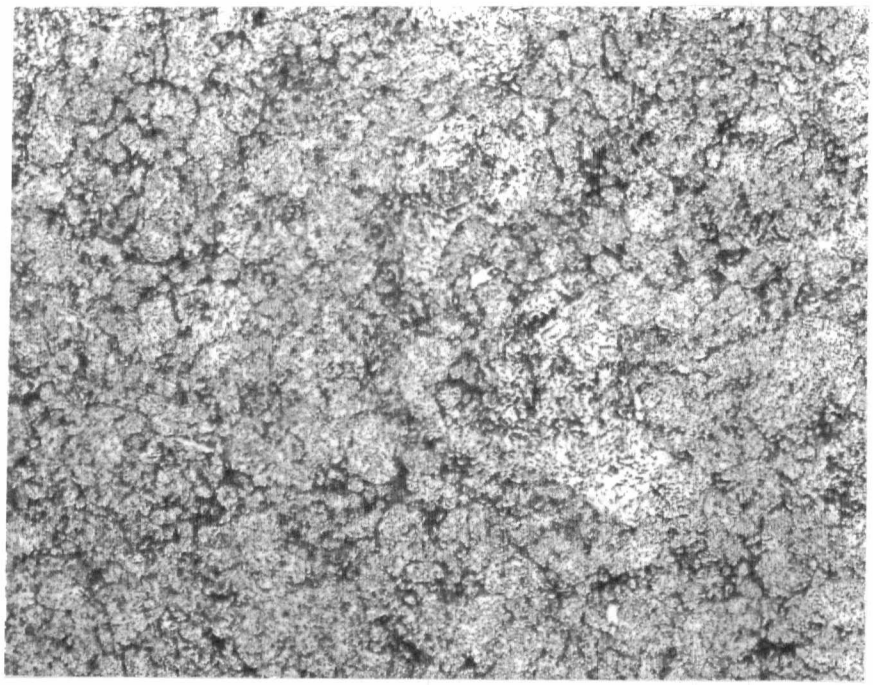

X) MB85-516, 400X, 400°C, 15ksi, 7% porosity

Figure 31: Phase 1 microstructures (OPT) cont'd

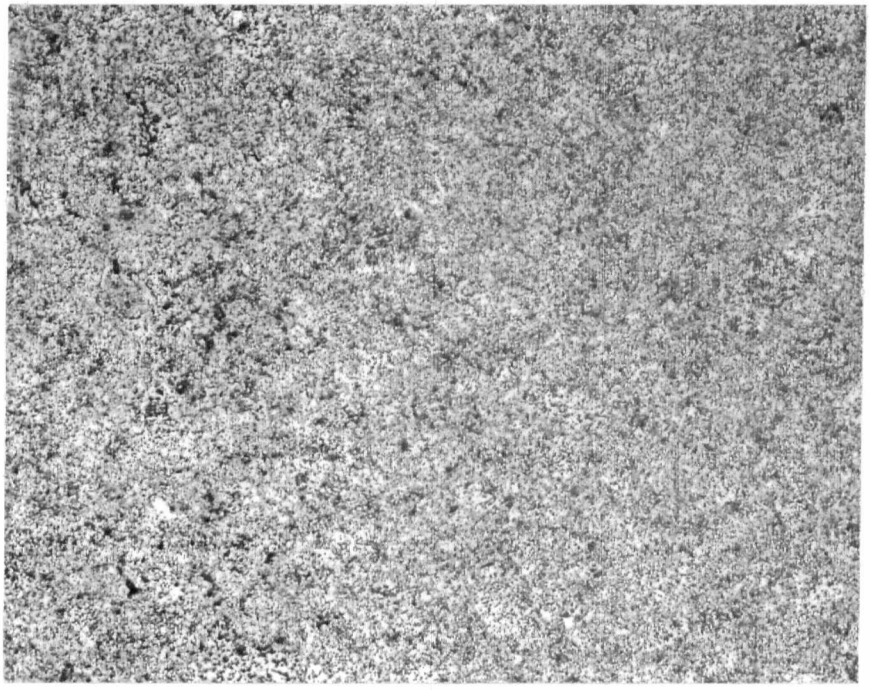

Y) MB85-517, 400X, 400°C, 25ksi, 1% porosity

Figure 31: Phase 1 microstructures (OPT) concluded

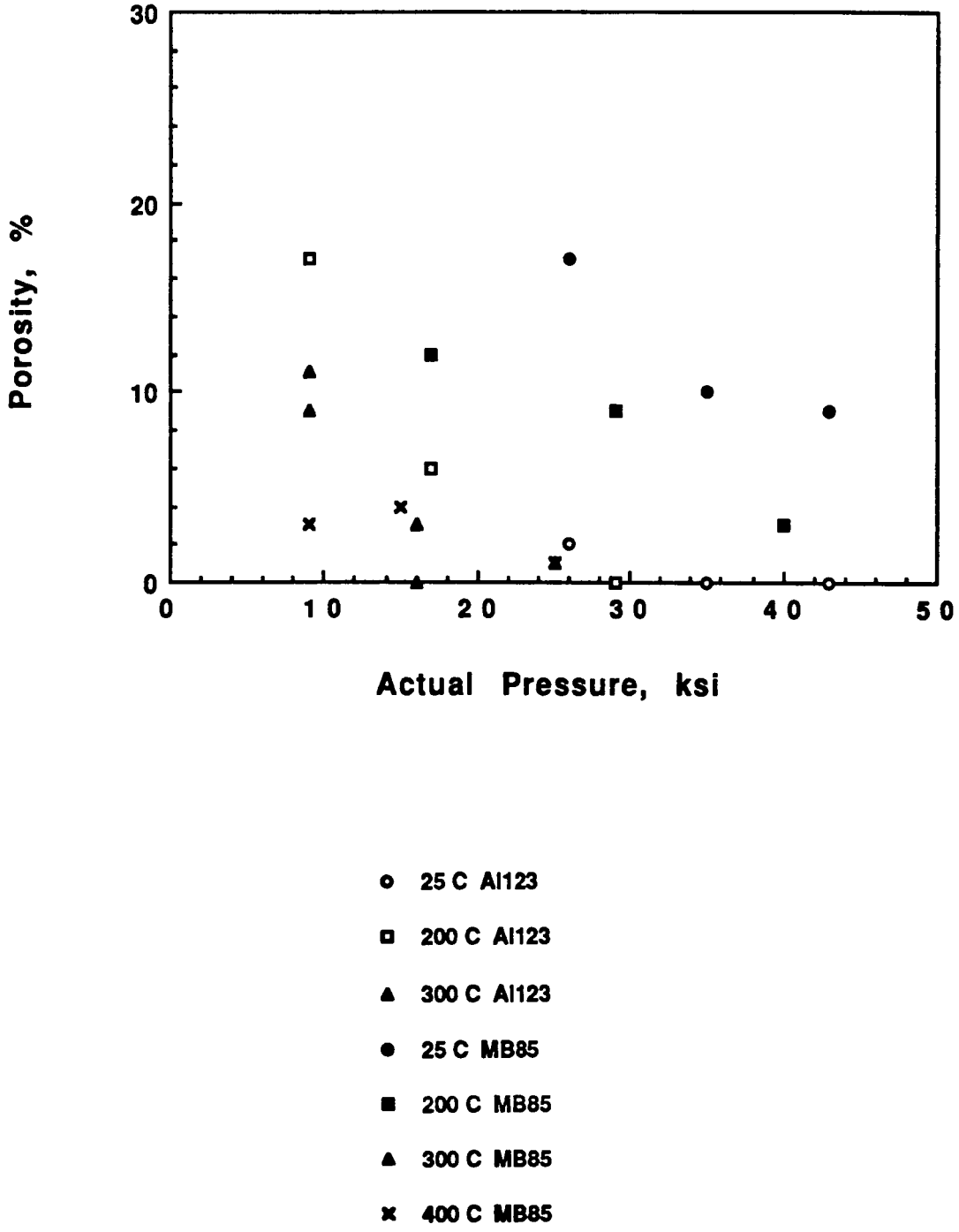

Figure 32: Pressure versus percent porosity curves at constant temperature.

and parallel to the specimen-die interface. How this increase in pressure effects the movement of parts within the bidimensional compression apparatus may very well determine the actual pressure exerted on the specimen.

The actual pressure applied generates reaction forces depending on the response of the powder. If the z-direction is along the length of the die cavity, then the reaction of the powder to pressure applied in the x-direction will act in both the z- and y-directions, as well as in the opposing x-direction. The z-directed reaction force may cause elongation, but the y-directed reaction force adds to the normal force required to advance the dies which move along the y-axis. The magnitude of this force will depend upon the coefficient of friction between the specimen and the die face, especially for the material immediately adjacent to a speicmen-die interface. In the interior of the powder specimen, the effect of friction is not as great; this is one reason for barreling under upset forging conditions with a non-zero coefficient of friction.

The entire state of stress determines the plastic response of the material, but the response of the material also determines the state of stress. The open dimension in the bidimensional apparatus provides a means to not only limit the magnitude of the isostatic stress component, depending again on the coefficient of friction, but also to limit the magnitude of the forces normal to the open

dimension, i.e., within a cross-sectional plane. The latter effect results from the flow of material in the open direction, the z-direction. This limits the stress in the x- and y-directions and depends on Poisson's ratio, which changes during consolidation. The limiting component of stress is the one which first exceeds the critical value for plastic flow. Because any stress in the open direction is generated by reaction to the applied stresses, in the x and y directions, the applied stresses have a maximum which corresponds to the development of a reaction stress in the open direction equal to the critical stress for plastic flow including frictional stresses. A higher coefficient of friction will increase the isostatic component of stress on the powder. It will also decrease the elongation in the z-direction.

The barreling effect for bidimensional compression may cause "capping," where a four-sided pyramid falls out of the ends of the pressed billet. It was for this reason, that the end caps of the cans were designed to collapse inward, providing some isostatic component of stress on the ends of the powder charge. This prevented capping and did not create an open area at the can ends as would have occurred if the ends bulged outward upon compression. Capping was observed when open ended cans and containerless pressing were attempted, indicating that the coefficient of friction

was not zero. Therefore, the actual state of stress was more complex than simple bidimensional compression.

MODELING

Attempts to model the results using the equations found in the literature proved to be futile. Either the scatter in the results or the difference in consolidation technique was responsible for the inability of the models to acceptably represent bidimensional compression. For this reason, the data were plotted as porosity versus pressure at the given temperature. From this plot, Figure 32, some trends were evident. In addition to those trends previously mentioned, it was evident that a limit of approximately one percent porosity existed for the MB85 powder and the decrease in porosity with increasing pressure appeared to be logarithmic. Based on this latter observation, it appeared that scatter in the porosity data may have been the reason for the failure of the models found in the literature to represent consolidation under bidimensional compression; the models predict a logarithmic relationship between pressure and porosity. If development of a model for pressure dependence of bidimensional compression was the goal of this effort, a significantly larger number of specimens would have been required.

TEMPERATURE EFFECTS

Another perspective on the data was the effect of temperature which is illustrated by the temperature versus porosity curve at constant pressure shown in Figure 33. This approach was limited to low temperatures since the low yield stress of aluminum at high temperatures limits the pressure, i.e., the specimen would be squeezed out of the die chamber if much pressure was applied.

An increase in temperature decreased the porosity at a given pressure. This was a yield point effect. There was insufficient data to determine the degree to which work hardening may have effected the response of the powder to bidimensional compression. At a temperature depending upon the material, the effect of work hardening should have disappeared. At this temperature, dynamic recovery would have been sufficiently rapid to prevent dislocation pile-ups.

MATERIAL EFFECTS

A rough characterization of material effects on the response to bidimensional compression could be made based on the porosity data. Comparison between the response of Al-123 and MB85 powder for equivalent press conditions revealed

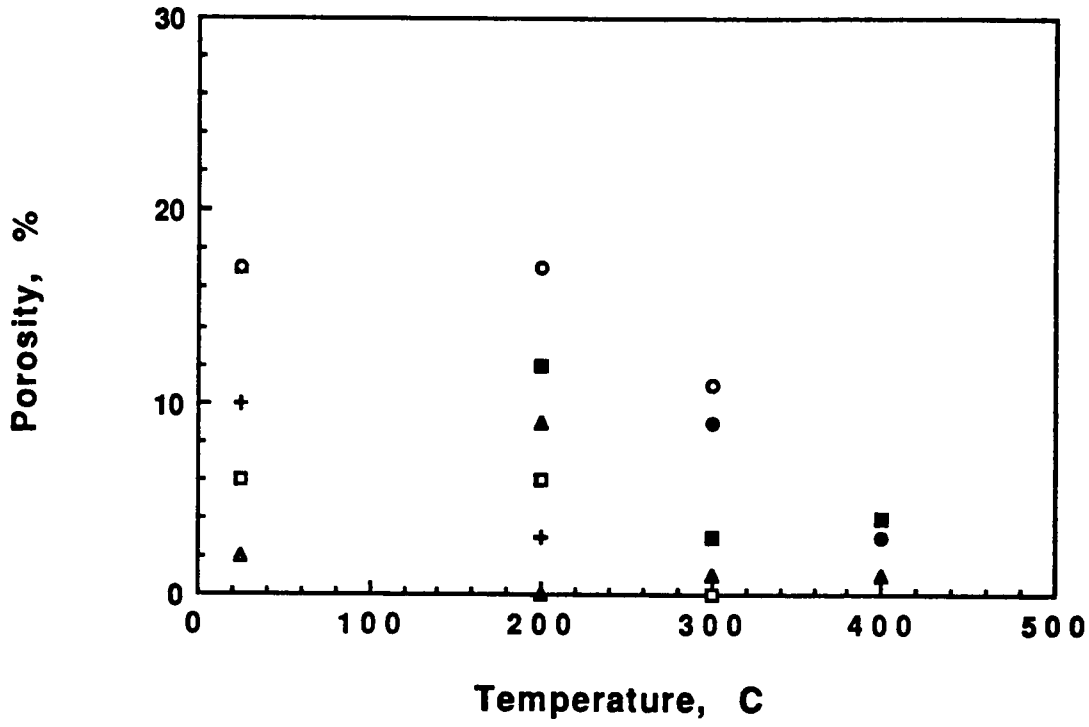

Figure 33: Temperature versus percent porosity at constant pressure.

the qualitative effects of material properties, such as yield strength, work hardening, work hardening rate, and the response of these to temperature. The effect of yield strength was to displace the pressure versus porosity curves as a group. The higher yield strength material was shifted to lower densities for the same applied pressure.

ASPECT RATIO

Further information was contained in the micrographs concerning the mode of pore closure. The aspect ratio of the individual powder particles revealed the state of stress imposed upon the powder during consolidation. The powders used in this study were gas atomized. Figure 34 shows that gas atomized aluminum is irregular and globular. It is expected that an isostatic state of stress will retain the initial morphology of the individual powder particles. A high aspect ratio for all particles in the cross-section would indicate that significantly higher stress acted perpendicular to the major axis of the powder particles. The combination of aspect ratios found in longitudinal and transverse metallographic sections of the same specimen allowed the characterization of the entire state of stress. Obviously, the plane of the micrograph revealed only stresses acting in that plane; an equiaxed particle in a

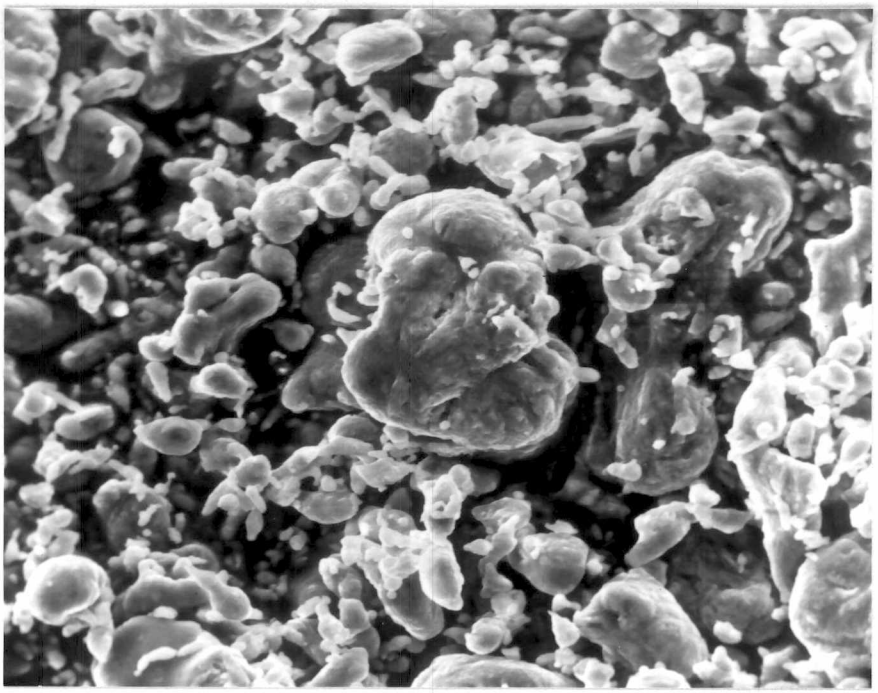

A) MB85, 500X

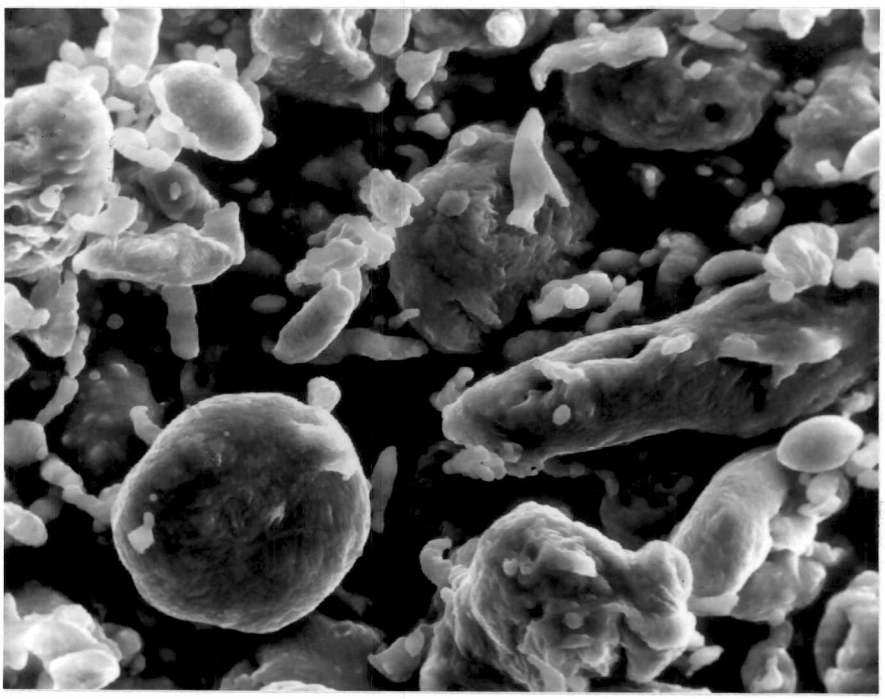

B) MB85, 1000X

Figure 34: Morphology of raw powders (SEM).

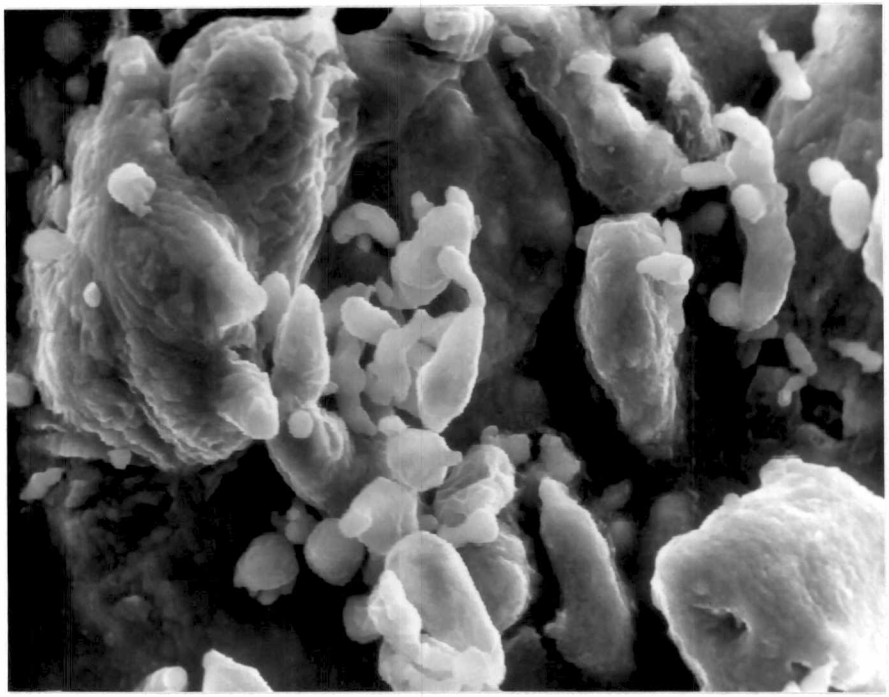

C) MB85, 2000X

Figure 34: Morphology of raw powders (SEM), cont'd.

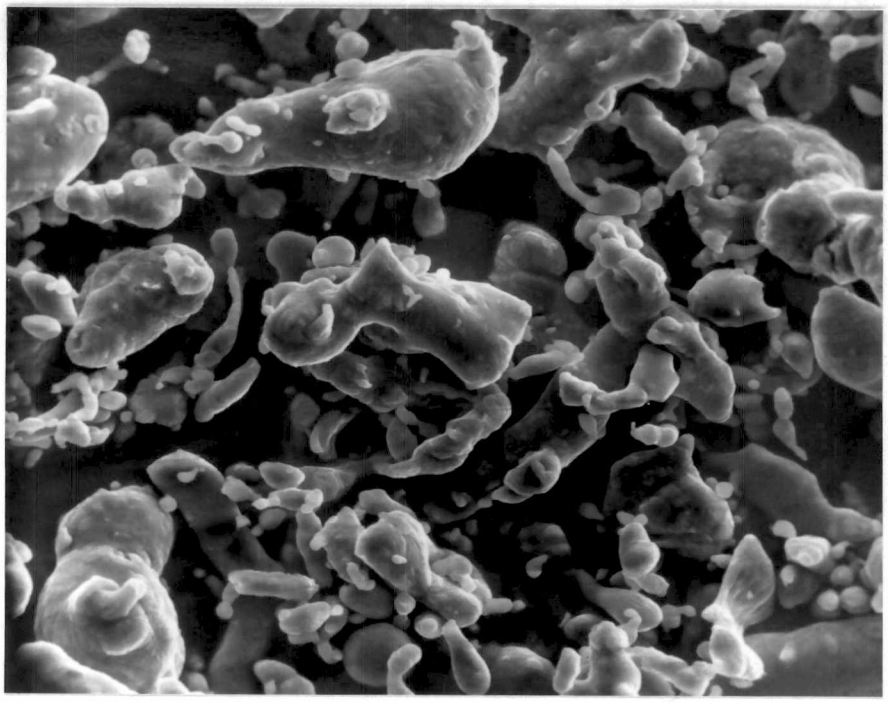

D) Al-123, 500X

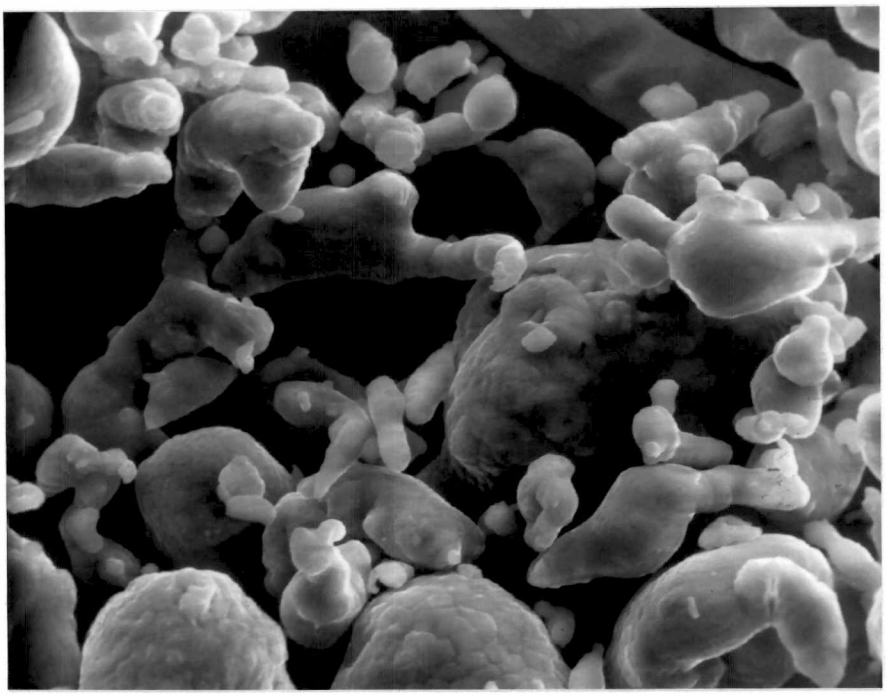

E) Al-123, 1000X

Figure 34: Morphology of raw powders (SEM), cont'd.

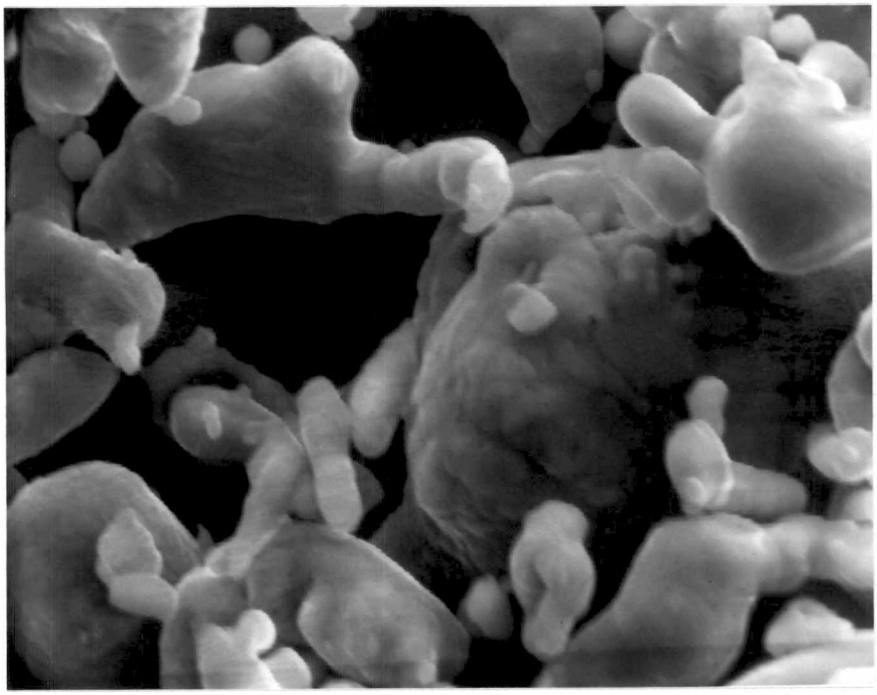

F) A1-123, 2000X

Figure 34: Morphology of raw powders (SEM), concluded.

transverse section indicated balanced forces acting in that plane. The symmetry of the bidimensional stress field applied to the specimens in this study permit the assumption that the two longitudinal orientations are equivalent, reducing the number of specimens required to be polished by one third.

In all of the transverse sections, the particles appeared equiaxed. This supports the assumption that longitudinal orientations are equivalent and that the applied bidimensional stress field was nearly balanced, i.e., s_1 equals s_m. The longitudinal sections varied depending on the press conditions. Higher temperatures generally produced greater elongation of the specimen, resulting in smaller cross-sections, but not necessarily greater aspect ratios.

A possible explanation for this is rearrangement. If a large degree of rearrangement occured, the aspect ratio would have been smaller than anticipated. Rearrangement, if it occurred, did so during the initial stages of compaction at low pressures. Rearrangement is a frictional process. Higher pressure increases the frictional forces and reduces the probability of rearrangement. Such a mechanism would be very beneficial to the consolidation of composite materials when the reinforcement is brittle. Optimum packing would result with less damage to the reinforcement.

FRICTION

Another explanation for low aspect ratios concerns friction at the can-die interface. If the coefficient of friction was high, then the entire cross-section of the specimen may have been contained in the dead metal zone, i.e., zone one in upset forging. In this zone, the state of stress is nearly isostatic. While attempts to minimize friction were made, no attempt was made to determine the coefficient of friction between the die face and the can.

Greater aspect ratios represent a larger degree of deformation in the upset mode. Therefore, the dispersion of the oxide layer is expected to be better as the aspect ratio increases. Metallography does not reveal the distribution of the oxide layer. The impact test is the best simple test to reveal this well established effect. Impact testing is discussed in phase two of this work.

To gain another perspective on the degree of shear strain resulting from bidimensional compression, a sample containing alternate layers of graphite and aluminum powders was pressed. This specimen provides evidence of macroscopic flow. It was assumed that each initial graphite layer was a flat plane. Figure 35a shows the results for an A1-123 specimen pressed at 250°C (480°F) under approximately 138 MPa (20 ksi) actual pressure. The curvature of successive graphite layers revealed that a nearly isostatic

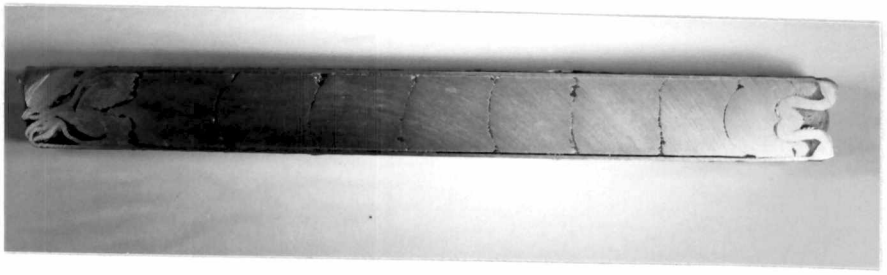

A

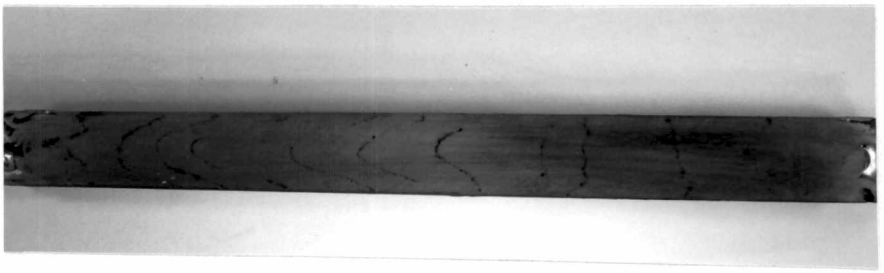

B

Figure 35: Macroscopic flow resulting from bidimensional compression at: a) 250°C, 20 ksi (480°F, 138 MPa) and b) 450°C, 20 ksi (840°F, 138 MPa).

state of stress exists at some point within the specimen, i.e., at the neutral plane in Figure 35a. A second graphite layered specimen was pressed at 450°C (840°F) under approximately 138 MPa (20 ksi) actual pressure. Figure 35b illustrates that the macroscopic flow of the powder under these conditions was in one direction only. It was therefore concluded that the location of the neutral plane varied from specimen to specimen depending upon the frictional stresses, the uniformity of the initial powder packing, and whether or not the faces of the opposing dies were parallel.

It was obvious that friction played an overwhelming role in the response of the powder to the press conditions. Perfect lubrication would have produced an elongated specimen with no curvature of the graphite layers. In such an ideal case, the elongation would have come from elongation and rearrangement of the individual particles uniformly across the specimen. Homogeneous, microscopic flow across the entire section, rather than macroscopic flow varying across the section, would have provided the shear strain.

The point of greatest friction between the can and die face may have determined the location of the neutral plane, since the material would flow to either side of this plane. If the die faces were not parallel, the reaction forces generated would not be balanced along the open axis. A

resultant force directed out from the end with the largest cross-sectional area would be generated; causing macroscopic flow in that direction over the entire length of the specimen. Variation in the inital powder packing may have been minimized by rearrangement. However, if such a variation persisted, the effect would be similar to a point of maximum friction. The higher density would generate higher reaction forces, providing greater friction at that point. The possibility that the end caps caused variations in the neutral plane location may be ruled out for two reasons. First, the yield strength of the can material at 450°C (840°F) is very low. Second, the strength of the billet increases rapidly during consolidation to that of the can (or more); any variations in the can which may have caused a shift in neutral axis position would have been quickly diminished. There was a slight difference between the end closures of each can since one end was an integral part of the can body and the other was not.

PHASE TWO

INTRODUCTION

Phase two of this work involves mechanical property testing. The purpose of the tests performed was to allow comparison between the two alloys consolidated under

bidimensional compression and with literature values for wrought aluminum and conventionally processed P/M aluminum. An extensive study of mechanical properties is not the intent. Rather, the feasability of producing fully dense powder compacts is under investigation. However, a comparison of basic mechanical properties should prove helpful in this evaluation.

IMPACT TESTING

Apparatus

The impact tests were conducted at Oak Ridge National Laboratory. A 1.067 kN (240 ft-lb) Charpy impact tester was used. The testing apparatus also displayed a load versus time plot for each test. The specimen dimensions were slightly undersize compared to standard 10mm x 10mm Charpy bars. Figure 20 illustrates the differences. The specification for impact testing of powder based materials, ASTM E23, states that a notch is not required.

Specimens

Based upon ASTM E23, notch-free specimens were machined with the dimensions shown in Figure 20. The only exception

was specimen number 3-3 which differed in cross-section only and was 5mm square. It was not known how tough or strong these specimens were prior to the initial testing. Accordingly, extreme caution was used during the machining process. Each compact was machined to the specified cross-sectional dimensions and then cut to length. No evidence of failure due to the machining process was evident. However, some variation in the surface appearence between specimens was evident, especially MB85 versus Al-123 specimens and sometimes from end to center of the same specimen. The final specimens were cut from the machined compacts with full attention to the surface variations.

The ends of some compacts had a rough, powdery surface upon machining. In some cases, the size of these areas decreased with each pass of the fly-cutter. When the length of the compact permitted, the powdery ends were discarded. The impact of the pendulum foot was always opposite the best surface area of the compact.

The room temperature compacts proved to be largely incapable of withstanding the machining operations. The length of the compacts prevented sufficient load for consolidation. The actual pressure was only 240 MPa (35 ksi) compared to 297 MPa (43 ksi) for the microstructure specimens evaluated in phase one. The actual pressure was calculated as the force generated by one hydraulic cylinder divided by the surface area of one face of the resulting

specimen. Table 3 lists the results of the impact testing. Only ten specimens were tested. It was intended that three specimens for each set of consolidation conditions be tested. The lack of interparticle bonding for the room temperature specimens excluded most of them completely and uncertainty of the material's response to impact loading eliminated five specimens from direct comparison with the others. The five specimens tested without notching cannot be compared directly with the notched specimens.

This uncertainty manifested itself during the first attempted test of the specimens compacted at 450°C (840°F); the 5 mm square specimen did not fracture upon impact. A "full" size specimen was then tested in the belief that the larger cross-section might provide sufficient constraint to cause fracture. Again, the specimen bent nearly double without cracking. The pendulum did not jam, but the test was meaningless.

With a limited number of samples remaining, it was decided that a notch <u>was</u> required. All of the remaining specimens were notched in order to allow direct comparison between them. The specification for Charpy impact testing, ASTM E23, requires that the notch be 20% of the cross-section dimension. Therefore, the notch depth was 0.18 mm (0.007 in.).

The notch provided sufficient constraint to fracture all of the remaining specimens. The commercially pure, Al-123,

TABLE 3: RESULTS OF PHASE TWO--MECHANICAL PROPERTIES

SPECIMEN	ALLOY	UTS (ksi)	YIELD (ksi)	% el	CVN/A $\left(\frac{\text{ft-lb}}{\text{sq.in.}}\right)$	NOTCH
	25°C, 10 ksi (35 ksi actual)					
1-1	AL123	---	---	---		
1-2	AL123	---	---	---		
1-3	AL123	---	---	---		
1-4	AL123				5.58	NO
1-5	AL123				---	
1-6	AL123				3.98	NO
2-1	MB85	---	---	---		
2-2	MB85	---	---	---		
2-3	MB85	---	---	---		
2-4	MB85				3.98	NO
2-5	MB85				---	
2-6	MB85				---	
	450°C, 10 ksi (20 ksi actual)					
3-1	AL123	16.3	9.2	38.6		
3-2A	AL123				169.68	YES
3-2B	AL123				223.58	YES
3-3	AL123				178.48	NO
3-4	AL123	14.3	9.2	6.7		
3-5	AL123				434.09	NO
3-6	AL123	17.3	9.5	16.2		
4-1	MB85	47.5	31.4	2.0		
4-2	MB85	45.8	32.6	8.6		
4-3	MB85	36.2	31.1	3.7		
4-4	MB85				7.98	YES
4-5	MB85				9.98	YES
4-6	MB85				8.98	YES
	WROUGHT ALUMINUM					
O	1060	10	4	43		
H16	1060	16	15	8		
H18	1060	19	18	6		
O	2024	27	11	20		
T3	2024	70	50	18		
T4	2024	68	47	20		
T736	7050	75	66	11		

specimens did not fracture completely through the cross-section. All of the MB85 specimens fractured completely with negligible energy required--less than one foot-pound.

TENSILE TESTING

Apparatus

The tensile tests were conducted on an Instron screw driven tensile frame. This apparatus is under the care of Dr. Archie Matthews in the Engineering Science and Mechanics Department at the University of Tennessee, Knoxville. The specimen size was chosen based on the consolidated powder specimen dimensions and the grips available.

Specimens

Many specimen configurations were considered, but the special grips used with most of them would have required additional machine shop time. No guarantee could be made that the more complex specimen configurations would provide better results. The specimen configuration is given in Figure 21 of the experimental procedures section. It should be noted that the center of the gauge length section had the smallest cross-sectional area; the root of the threads was

several thousandths larger. The thread size was chosen as large as possible within the range of existing grips. The MB85 specimens were tested in the as pressed condition.

The powdery ends of the room temperature-pressed specimens excluded all of them from testing. To attempt to thread the powdery ends, which would have been required due to their length, was hopeless. The specimens consolidated at 450°C (840°F) had sufficient length and provided ample solid material for the threads. The specimens were machined initially into full length cylinders using a metal lathe. Based upon their appearance, the position of the tensile specimen along the length of the cylinder was chosen to ensure the threads would support the greatest load possible. Once the specimen was cut to length, the ends were threaded. The threads were cut before machining the reduced section to take advantage of the greater strength of the full cross-section. As for the Charpy impact specimens, the strength of the consolidated powder was not known. The first attempt to machine a tensile bar failed during the threading operation, however this trial specimen was less than full density. All of the 450°C (840°F) consolidated specimens were machined without any evidence of failure.

Lubrication during the machining operations proved to be very important. The surface finish of the specimens became very irregular when insufficient lubrication was applied. The best lubricant was a mixture of cutting oil and Jello

pudding (which we called JP-10), discovered accidentally by Larry Smith in the Materials Science and Engineering-Mechanical Systems Laboratory (Machine Shop). When lubrication was insufficient, the chips from the cutter curled back into the specimen, causing the observed irregularities. The surface finish was best when JP-10 was used.

The planned test conditions were used through the yield point for each specimen. However, due to the excessive testing time required at such low cross head speeds, the rate was increased after the load-time curve had sufficiently progressed to allow accurate determination of the yield strength. This procedure is permitted under ASTM B557. The initial cross head speed was 0.01 inches per minute and the faster speed used was 0.2 inches per minute. The full scale load was estimated to be 8.9 kN (2000 pounds) for the size specimens used. This proved to be adequate for the Al-123 specimens, but the MB85 specimens required a full scale load of 22.2 kN (5000 pounds). The same load cell was used throughout, which maintained the calibration and allowed comparison of the results without fear of error due to changes in the apparatus. The first MB85 specimen, #4-1, required the change of full scale load in mid-test. The chart speed was changed from 1.0 inch per minute to 0.2 inches per minute to conserve paper at the same time as the cross head speed was changed in each case.

INTERPRETATION OF RESULTS

The results of the tensile tests are given in Table 3. The Al-123 specimens all exhibited ductile failure. The consistency of the yield strength and ultimate tensile strength is promising. The scatter in the elongation may be due to variations in the powder packing, outgassing, or the macroscopic flow of the powder during consolidation, i.e. the variation in the position of the neutral plane. All of the MB85 speicmens exhibited brittle fracture. However, the elongation is better than expected based on the impact energies, which were obtained prior to tensile testing. Some variation in ultimate tensile strength is evident, but all of the MB85 specimens failed in the threaded section of the bar. As such, variations in the stress concentration at the root of each set of threads may very well account for this scatter. The yield strengths of the MB85 specimens are remarkably consistent. The wide variation in elongation can be related to the scatter in the ultimate tensile strength. Failure occurred when the stress at the root of the threads reached its critical magnitude. The material in the gauge section may have been more consistent than the stress concentrations; premature failure prevented full elongation in the gauge section.

Comparing the results of the impact and tensile tests, the integrity of the interparticle bonding may be better

understood. The tensile elongation may indicate that the material is ductile and that the interparticle bonding is good. However, the impact properties are more sensitive to interparticle bonding than tensile properties. The MB85 specimens show a considerable amount of elongation under tensile test conditions, which is often interpreted as evidence of ductility. The impact test, however, reveals that essentially no energy is required to fracture the specimens under impact loading. The loading conditions for real-world powder parts must be well defined to allow the use of such a material. If the loading conditions are not static, the risk of failure is high. Impact testing is a rough indicator of other dynamic properties, such as fatigue strength. Impact testing is the simplest test to determine the response of powder based materials to dynamic loading.

The difference in elongation and impact energy results indicate that the resistance to crack initiation can be very much different than resistance to crack propagation. The interparticle bond can be strong, providing resistance to crack initiation and good elongation under static loading. However, the strong bond may also be brittle, showing no resistance to crack propagation.

One explaination for the existance of strong, brittle interparticle bonds is oxide-metal bonding. The aluminum oxide coating is very tenacious. It is concievable that bonding between the oxide coating on one particle and the

virgin metal of another particle occurs under the pressure and temperature of consolidation. The oxide boundary provides an easy path for fracture, but its strength may allow the bulk of the particle to deform plastically to give considerable elongation under static loading conditions. Under high loading rates, the observed strength of a material is greater than under static conditions. Therefore, the yield of the powder interior may occur at higher stresses for the impact specimens. The stress required for yield in this case would be higher than the fracture strength of the oxide-metal interface. The metal-metal bonding which occurs in upset mode consolidation, provides the best dynamic properties, as well as excellent tensile strength. The impact test best reveals the degree to which the consolidation occurs under upset mode conditions.

Mode Of Failure

Figure 36 illustrates the difference in the fracture surfaces between representative Al-123 and MB85 impact specimens. Figure 37 illustrates the fracture surfaces for tensile specimens. Comparrison between impact and tensile failure surfaces for the same material illustrates the effect of loading conditions on fracture path.

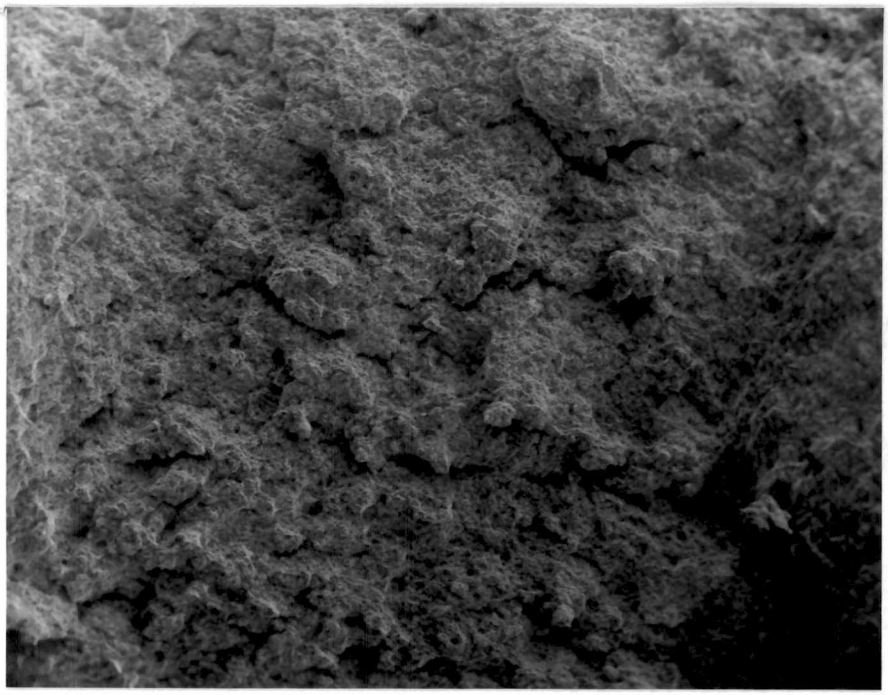

A) Impact, Al-123, #3-2, 20X

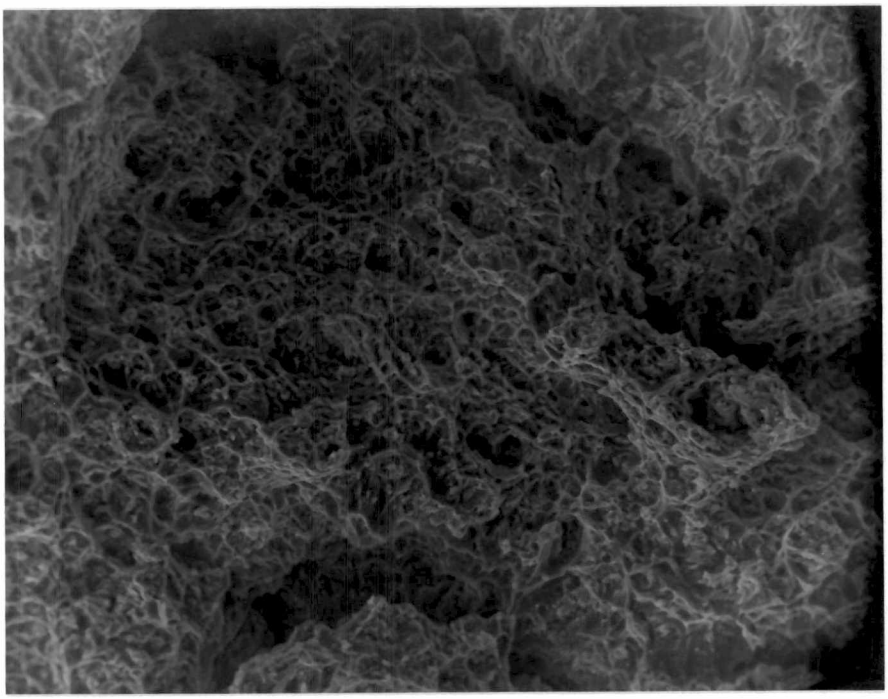

B) Impact, Al-123, #3-2, 200X

Figure 36: Fracture surfaces of Al-123 and MB85 impact specimens (SEM), [400°C, 20 ksi, outgassed 30 min. at 400°C (750°F, 138 MPa, outgassed 30 min. at 750°F)].

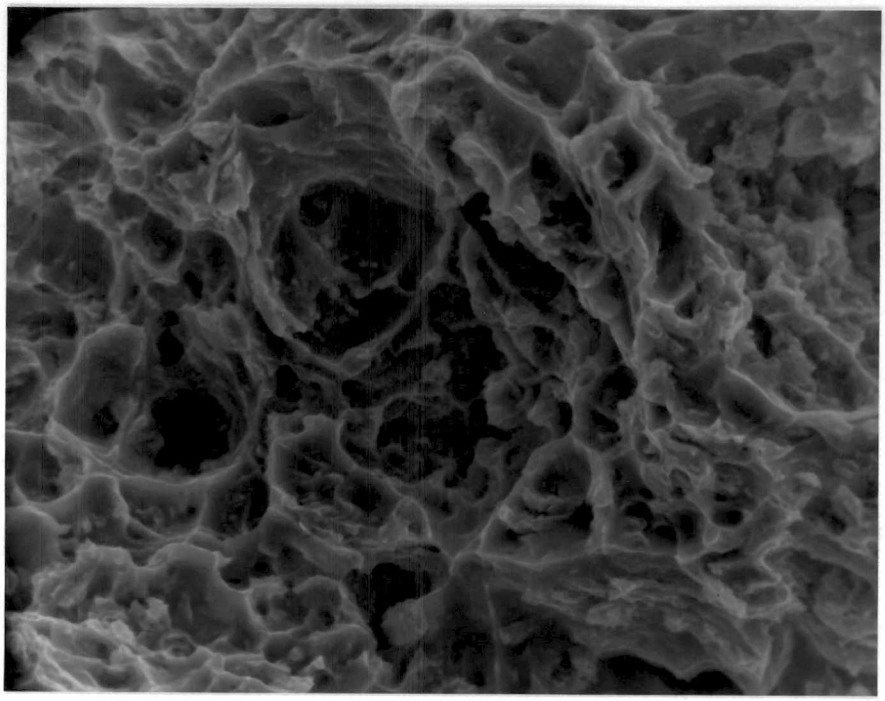

C) Impact, Al-123, #3-2, 1000X

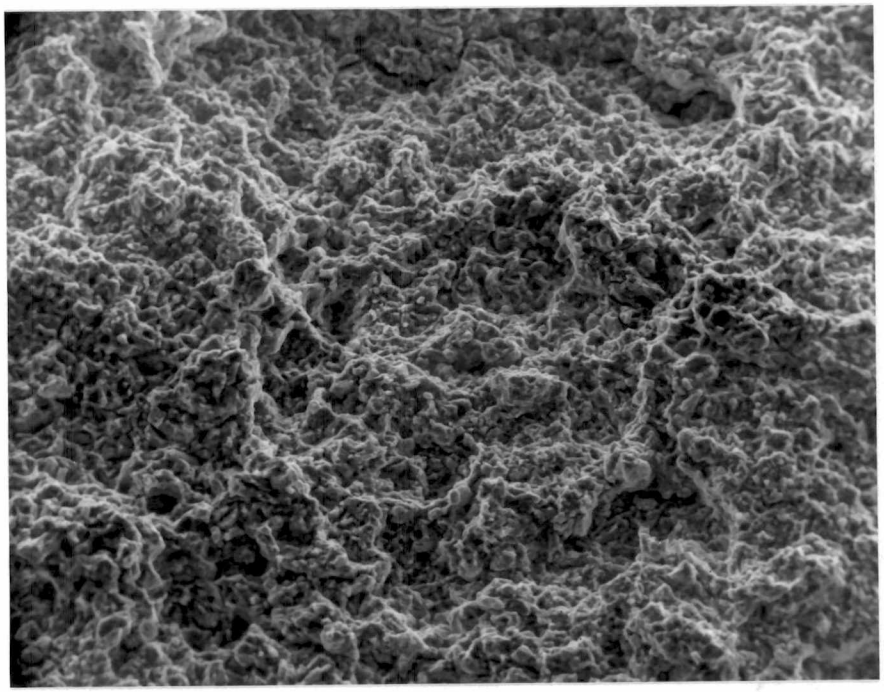

D) Impact, MB85, #4-5, 200X

Figure 36: Fracture surfaces of Al-123 and MB85 impact specimens (SEM), [400°C, 20 ksi, outgassed 30 min. at 400°C (750°F, 138 MPa, outgassed 30 min. at 750°F)] continued.

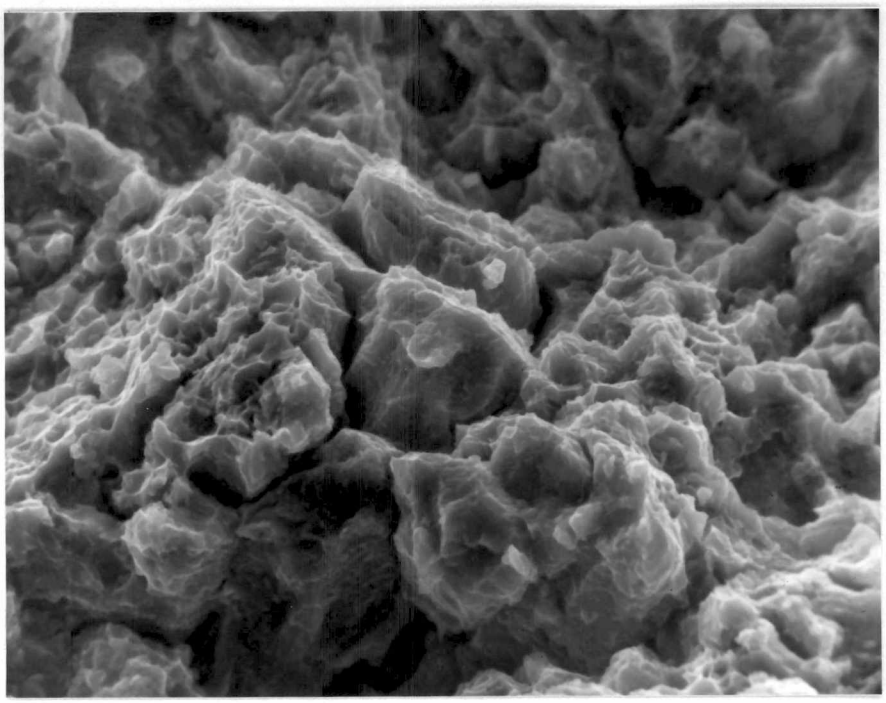

E) Impact, MB85, #4-5, 2000X

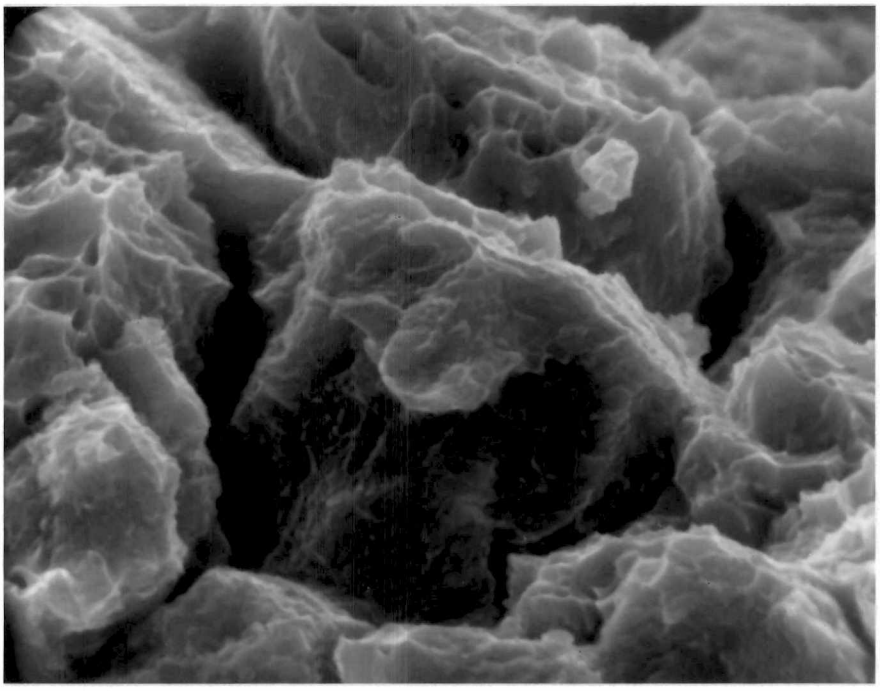

F) Impact, MB85, #4-5, 5000X

Figure 36: Fracture surfaces of Al-123 and MB85 impact specimens (SEM), [400°C, 20 ksi, outgassed 30 min. at 400°C (750°F, 138 MPa, outgassed 30 min. at 750°F)] concluded.

A) Tensile, Al-123, #3-6, 20X

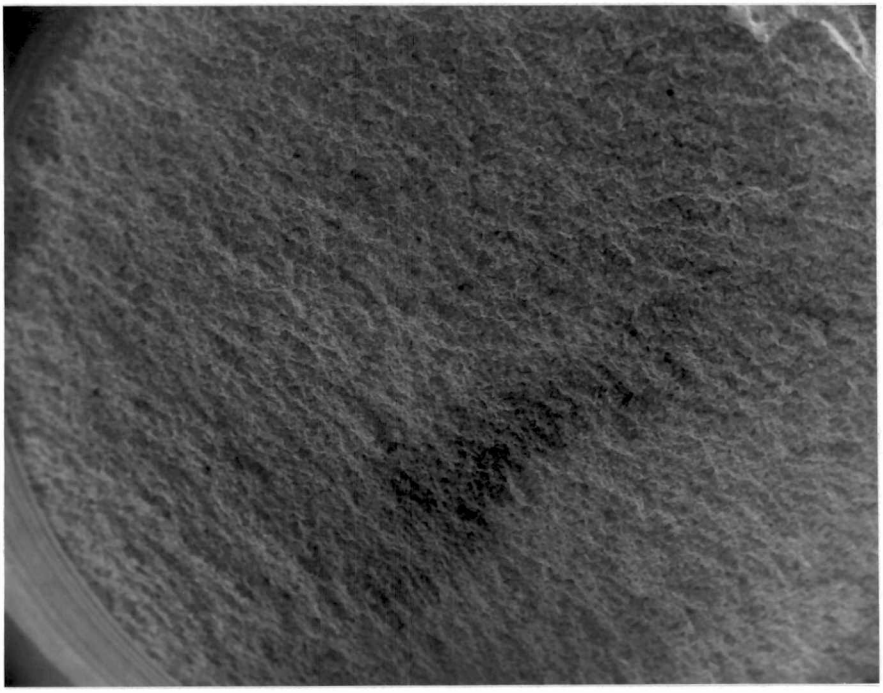

B) Tensile, MB85, #4-1, 20X

Figure 37: Fracture surfaces of Al-123 and MB85 tensile specimens, (SEM) [400°C, 20 ksi, outgassed 30 min. at 400°C (750°F, 138 MPa, outgassed 30 min. at 750°F)].

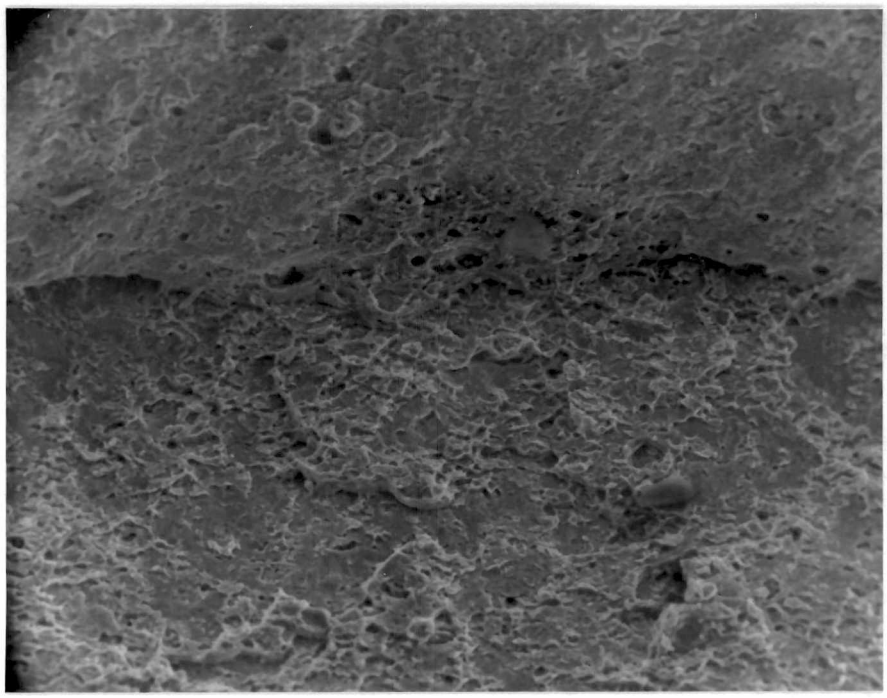

C) Tensile, Al-123, #3-6a, 200X

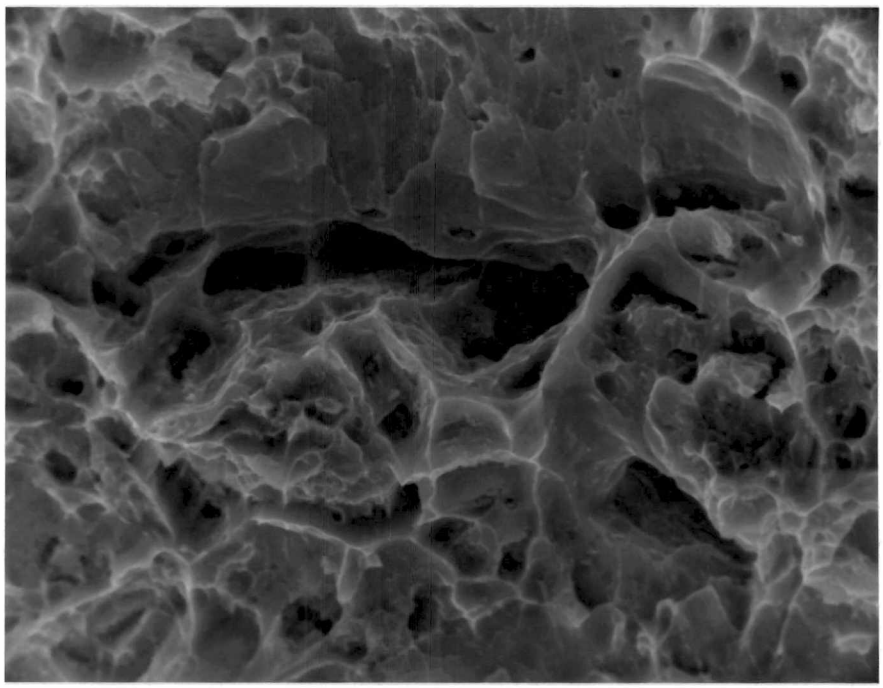

D) Tensile, Al-123, #3-6a, 2000X

Figure 37: Fracture surfaces of Al-123 and MB85 tensile specimens, (SEM) [400°C, 20 ksi, outgassed 30 min. at 400°C (750°F, 138 MPa, outgassed 30 min. at 750°F)] continued.

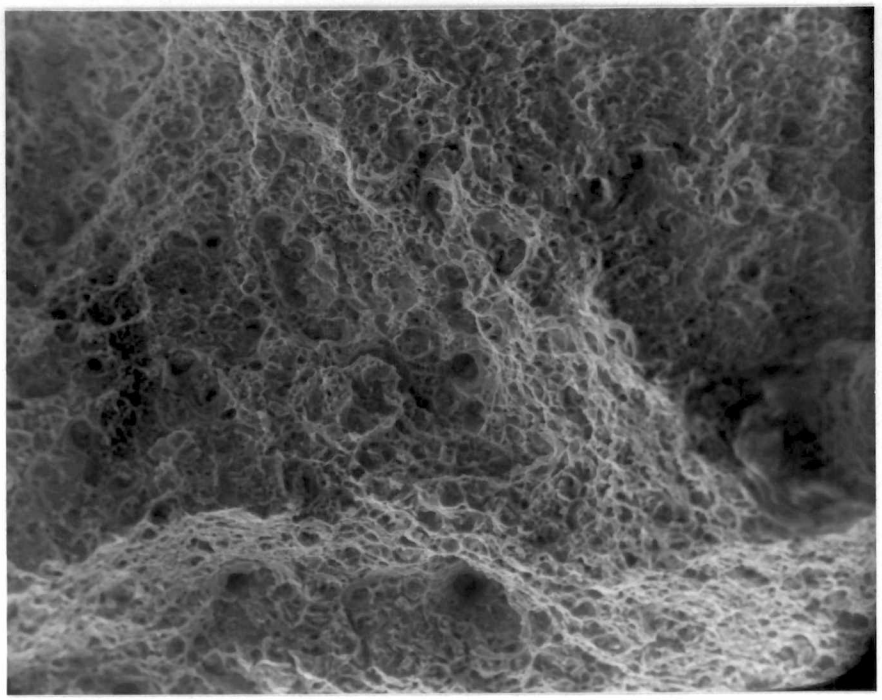

E) Tensile, Al-123, #3-6b, 200X

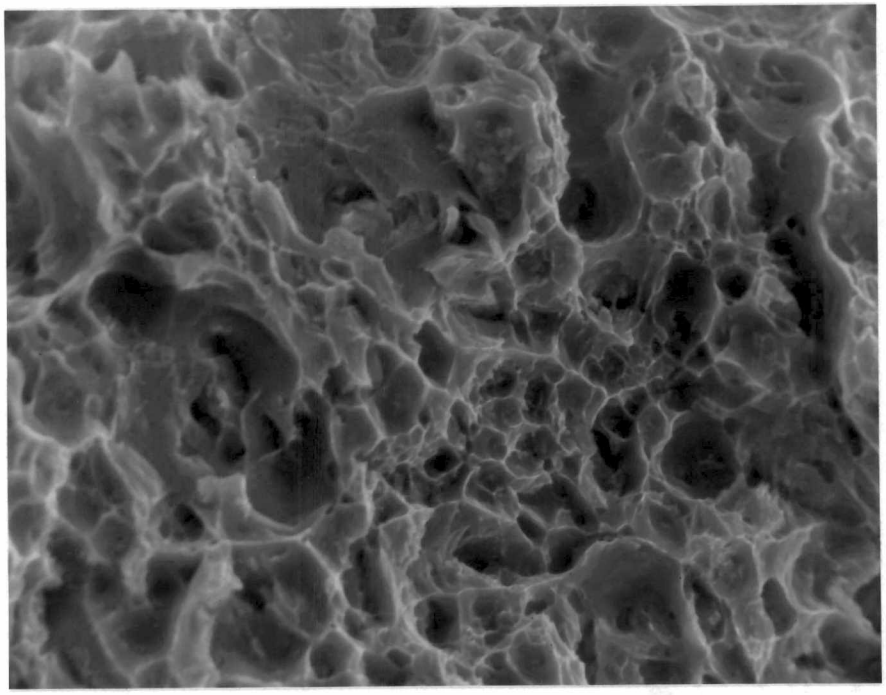

F) Tensile, Al-123, #3-6b, 2000X

Figure 37: Fracture surfaces of Al-123 and MB85 tensile specimens, (SEM) [400°C, 20 ksi, outgassed 30 min. at 400°C (750°F, 138 MPa, outgassed 30 min. at 750°F)] continued.

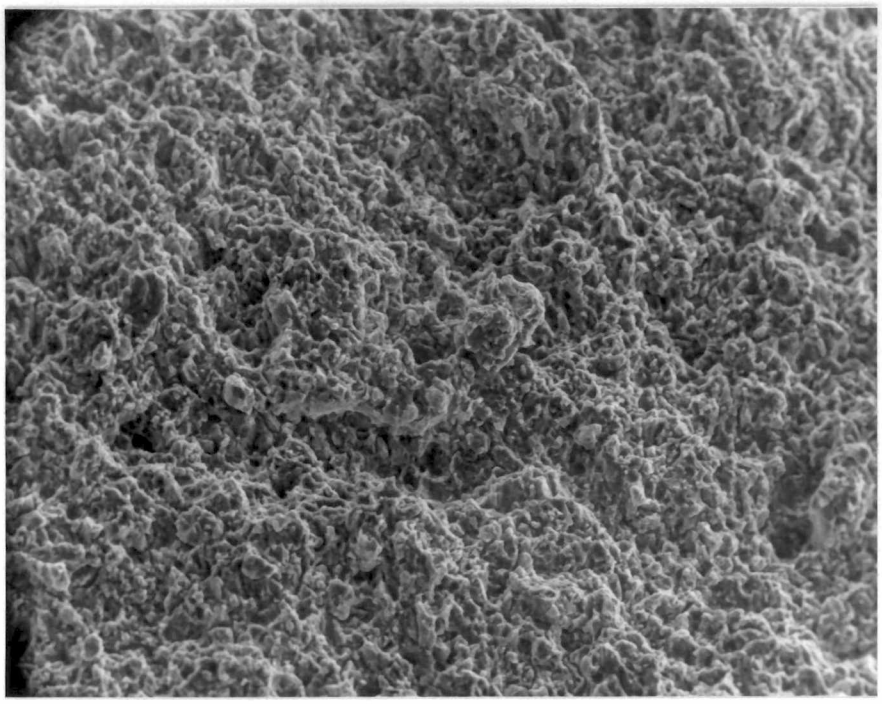

G) Tensile, MB85, #4-1a, 200X

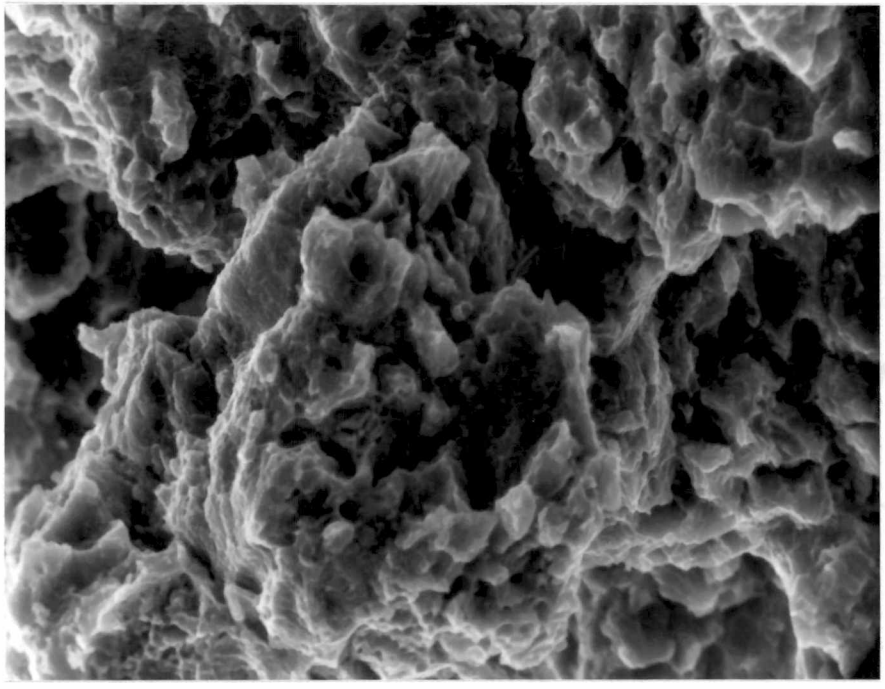

H) Tensile, MB85, #4-1a, 2000X

Figure 37: Fracture surfaces of Al-123 and MB85 tensile specimens, (SEM) [400°C, 20 ksi, outgassed 30 min. at 400°C (750°F, 138 MPa, outgassed 30 min. at 750°F)] continued.

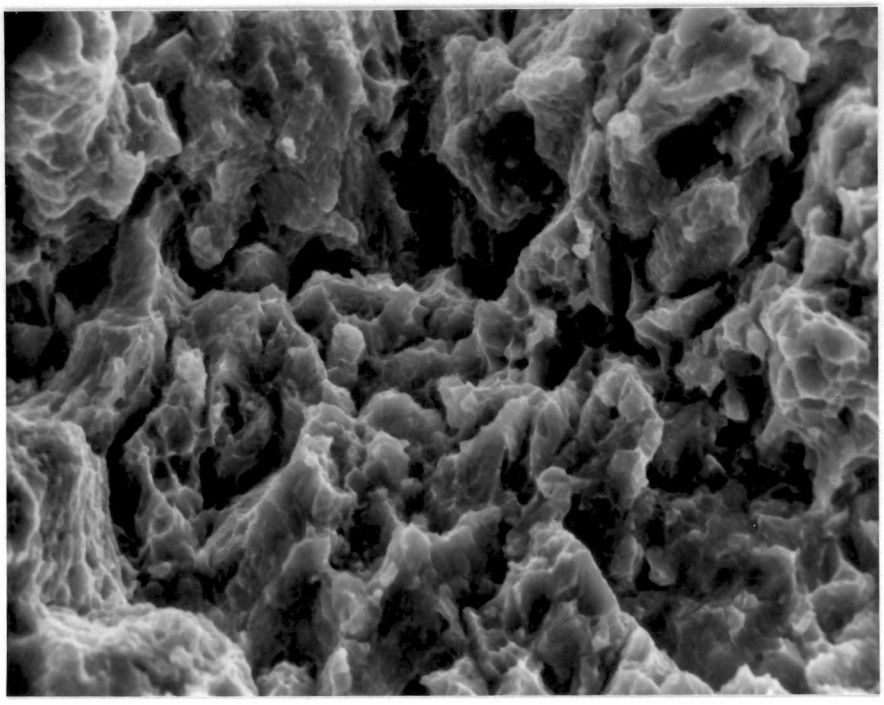

I) Tensile, MB85, #4-1b, 2000X (near edge of specimen)

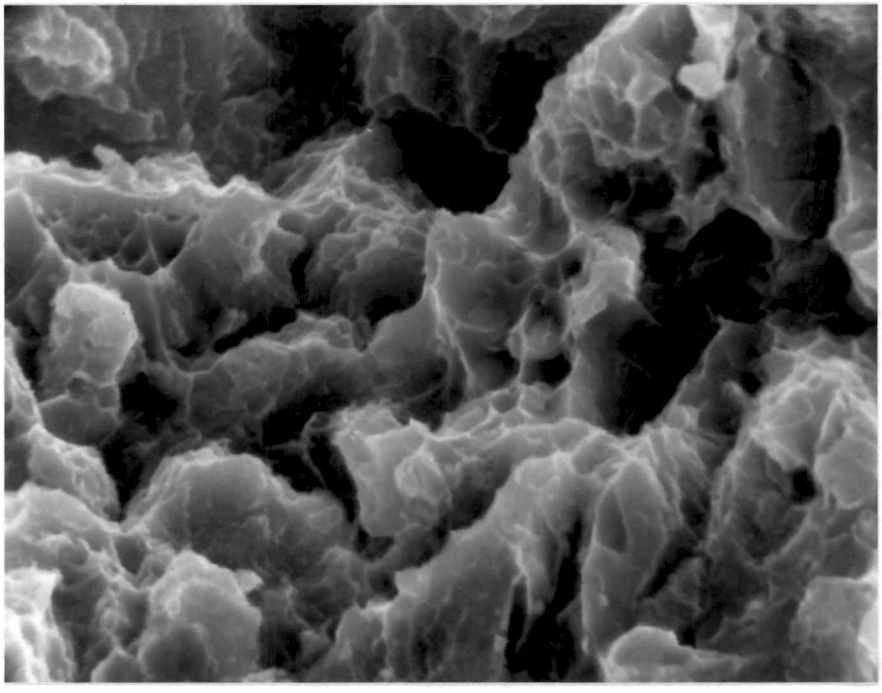

J) Tensile, MB85, #4-1b, 5000X (near edge of specimen)

Figure 37: Fracture surfaces of Al-123 and MB85 tensile specimens, (SEM) [400°C, 20 ksi, outgassed 30 min. at 400°C (750°F, 138 MPa, outgassed 30 min. at 750°F)] concluded.

For the MB85 specimens, the failure appears to be mixed mode. Both ductile-transparticle and brittle-interparticle failure is evident. The impact specimen shows a greater degree of interparticle failure. Limited ductility is evident for the tensile specimen even at the highest magnification. This failure surface may not be representative of a true tensile test failure, since a strong notch effect was present. More evidence of ductility would be expected if the failure had occured in the gauge section.

For the Al-123 specimens, very little evidence of brittle failure can be found. In such cases, the area is very small and isolated. The best explanation for them is a plate of oxide insufficiently broken up during consolidation. The cup-cone fracture of the tensile specimen is characteristic of ductile materials. The impact energy and ductility evident on the impact specimen failure surface indicates excellent interparticle bonding. Virtually no interparticle separation can be found on both impact and tensile specimen failure surfaces. The shear lips on the impact specimen are also indicative of good ductility.

The difference in failure of the MB85 and Al-123 specimens is obvious without magnification. The differences persist at the highest magnification as well. The MB85 tensile specimens retain a particulate appearance up

through 5000X magnification. The Al-123 tensile specimens appear to be a homogeneous bulk form of aluminum with little or no evidence of their prior particulate state. This disparity is more pronounced for the impact specimens.

Specimen Size

It was important to use as close to a standard specimen as possible to achieve acceptable repeatability. Statistically, a smaller specimen might prove less representative of the actual interparticle bond strength and integrity; one poorly bonded particle would represent a large fraction of the cross-section for a sub-standard specimen. This required a choice between specimen size and maximum pressure deliverable from the bidimensional compression aparatus. Exactly how the technique scales with specimen size was not able to be determined with the existing aparatus because of the limited force available in this system. It was decided that the specimen size was more important.

Aspect Ratio

In order to evaluate the differences between the mechanical properties of the MB85 and Al-123 specimens more completely, a longitudinal section was metallographically prepared from each test set. The microstructures are shown in Figure 38. It would be frivolous to make quantitative conclusions based on so few micrographs. However, the difference in average aspect ratio indicates that the Al-123 powder experienced a greater degree of consolidation via the upset mode. The well-established fact that this leads to greater ductility is in agreement with the results for bidimensional compression. The microstructure for #3-2 must be considered the resulatant microstructure for Al-123 specimens. The microstructure of #3-6 includes elongation during tensile testing, which adds considerably to the initial aspect ratio. Comparing the failure surfaces between impact specimens confirms the difference in energy absorbed. For the Al-123 impact specimen, the elongation of the individual particles increases toward the failure surface from the bulk, which would have required additional energy. The branching evident in the Al-123 specimen would also have increased the energy for fracture. The MB85 impact specimen micrograph, however, shows the interparticle nature of its failure. The corresponding energy was much lower than for the transgranular failure of the Al-123

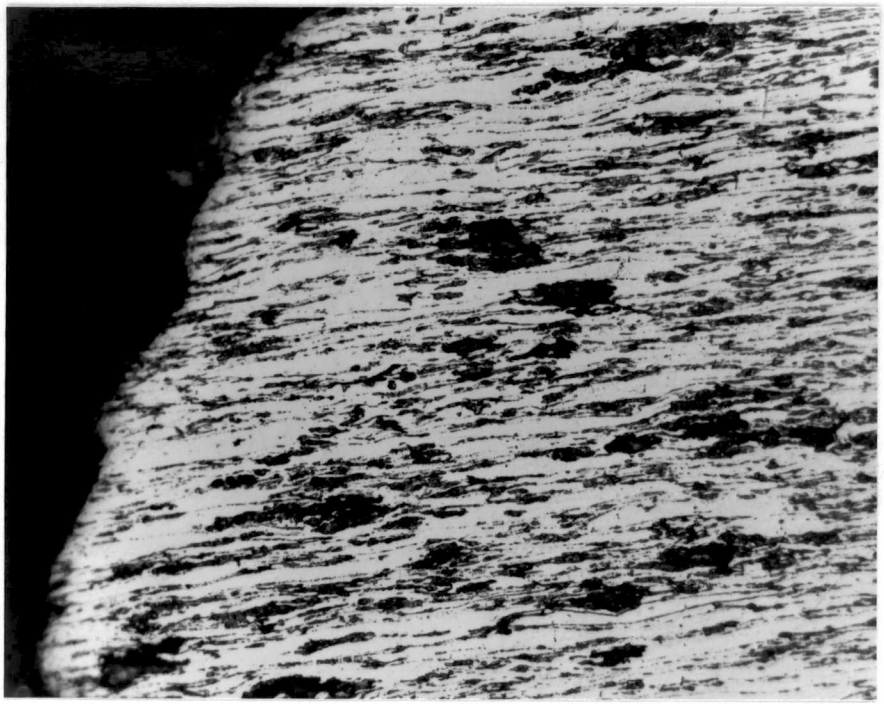

A) Tensile, Al-123, #3-6, 200X (at fracture)

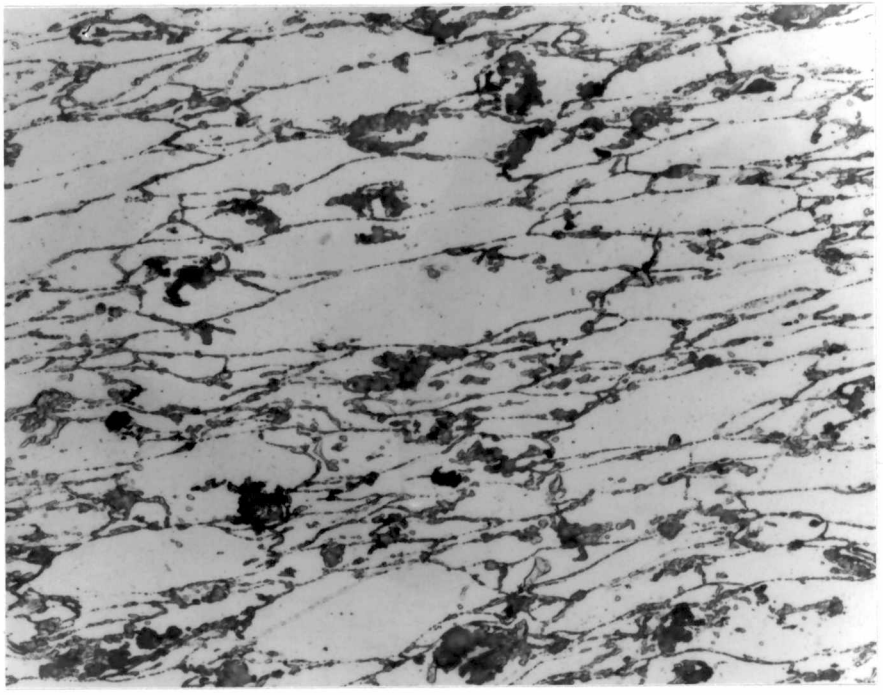

B) Tenslie, Al-123, #3-6, 400X (bulk)

Figure 38: Microstructures of mechanical property specimens, longitudinal views, (OPT).

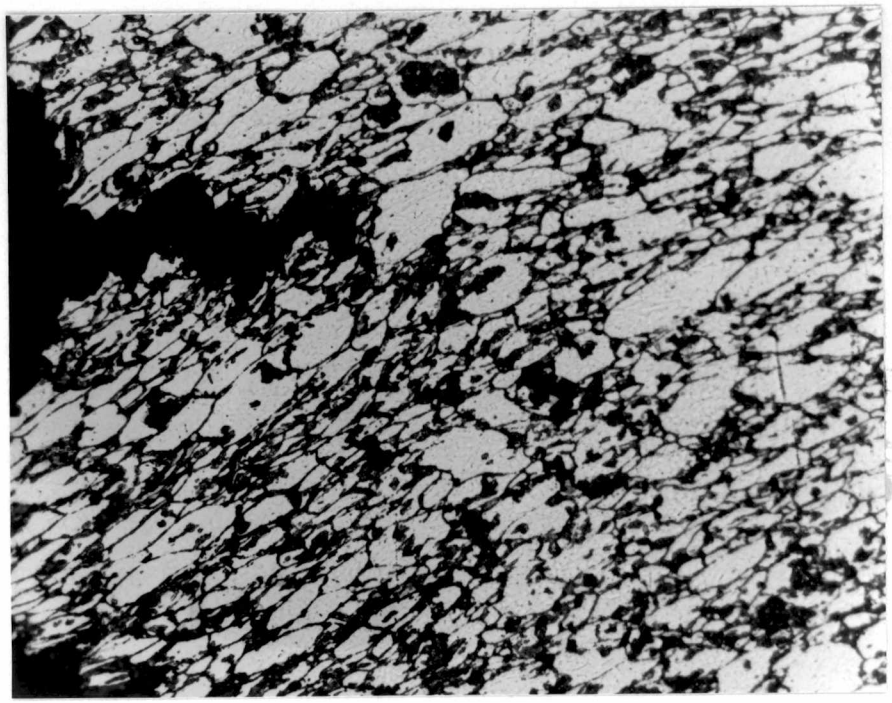

C) Impact, Al-123, #3-2, 200X (at fracture)

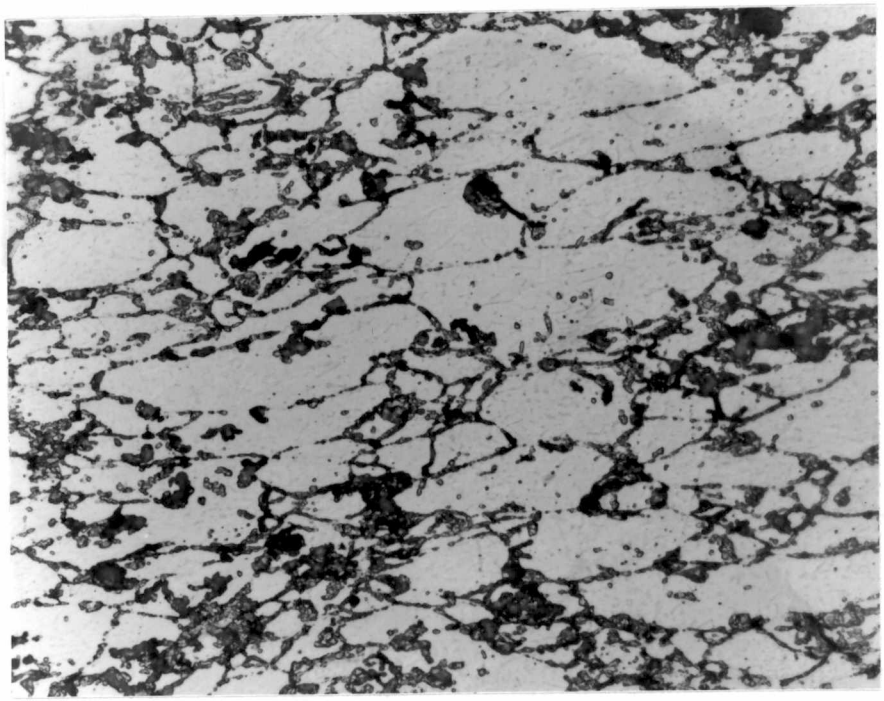

D) Impact, Al-123, #3-2, 400X (bulk)

Figure 38: Microstructures of mechanical property specimens, longitudinal views, (OPT) continued.

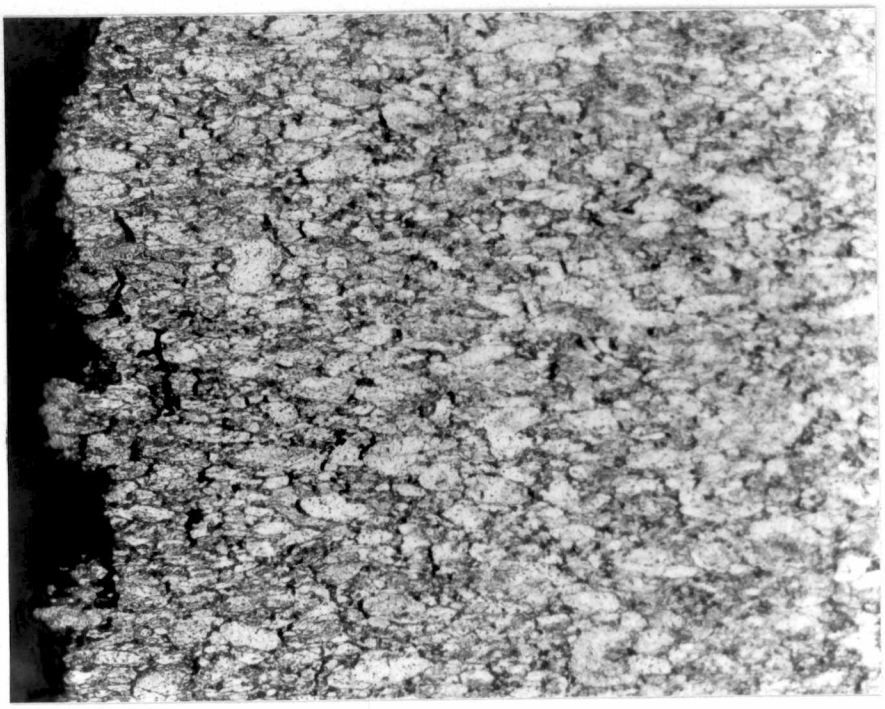

E) Impact, MB85, #4-5, 200X (at fracture)

F) Impact, MB85, #4-5, 400X (bulk)

Figure 38: Microstructures of mechanical property specimens, longitudinal views, (OPT) continued.

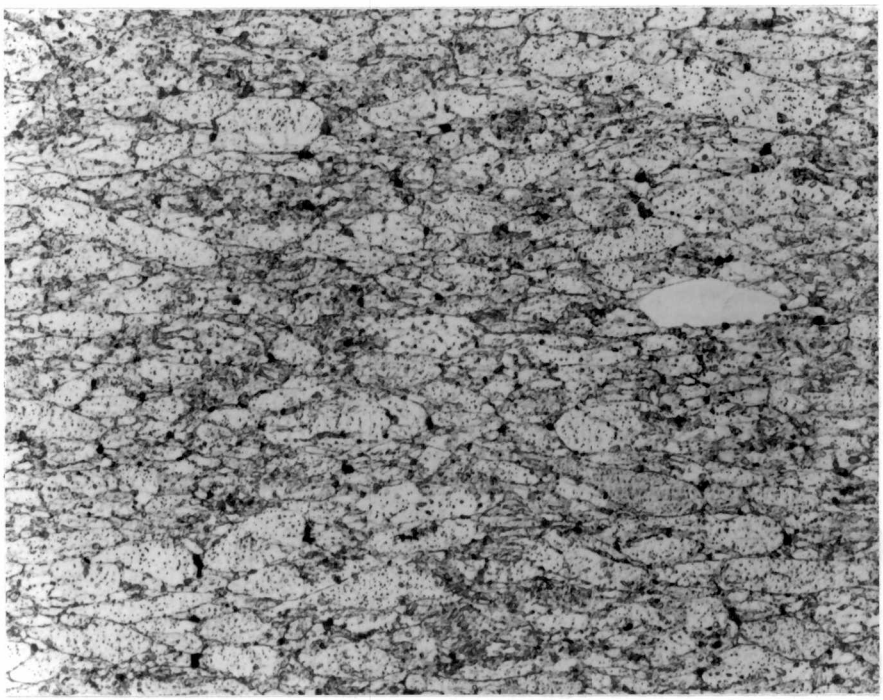

G) Tensile, MB85, #4-1, 400X (bulk)

Figure 38: Microstructures of mechanical property specimens, longitudinal views, (OPT) concluded.

impact specimen. Such a large difference in impact energy between Al-123 and MB85 specimens cannot be predicted by the difference in their aspect ratios alone. The differences in the nature of the oxide layers, between Al-123 and MB85 powder, and the amenability of the virgin-metal surfaces to cold welding must play a critical role.

Outgassing

The effect of outgassing parameters can not be specified. The same procedure was used for both powders. However, the combination of time, temperature, and pressure may have been inadequate for the MB85 powder. This effect could constitute an entire study on its own and was not pursued under the scope of this work.

CHAPTER V

CONCLUSIONS

THE BIDIMENSIONAL TECHNIQUE

The successful consolidation of the Al-123 powder demonstrates the feasibility of rigid die bidimensional compression. The difficulty in achieving ductility in the MB85 powder specimens must be attributed to inadequate powder preparation (outgassing) or inherent in this alloy. Mechanical properties of the Al-123 powder specimens were comparable to available literature values of similar purity aluminum. It is regretful that Alcoa could not provide data for direct comparison of mechanical properties with other consolidation techniques for the specific materials used in this study. Data concerning specific processes and materials is almost always considered proprietary.

The uniformity of residual porosity throughout the specimens suggests a possible application of this technique for fabrication of filters, oil impregnated bearings, and other controlled porosity materials. The potential application of this technique for fabrication of composite materials was demonstrated and deserves further study.

APPARATUS

An adequate rigid die bidimensional compression system has been developed sufficient for small scale, laboratory use. Lubrication was identified as a critical consideration requiring further study. Insufficient lubrication between the specimen and dies limited the ability to apply a purely bidimensional stress field. The actual stress field was much more complex than anticipated.

The need for position control for the advancement of the individual dies was repeatedly demonstrated. Use of this system for high strength materials or larger specimens would require increased maximum force to the dies from the hydraulic system. This, in turn, would require heavier construction of several components. Such a change would best be accomplished by construction of an entirely new apparatus.

LIST OF REFERENCES

1. A. Lawley, "Powder Consolidation," Advances in Powder Technology - 1981 Seminar, G. Y. Chin ed., ASM, Metals Park, OH (1982) 75.

2. H. F. Fischmeister, L. Olsson, and K. E. Easterling, "Powder Forging," Powder Met. Intl., Vol. 6, No. 1 (1974) 30

3. A. Squire, "Density Relationships of Iron-Powder Compacts," Metals Technology, 14 (1947) 485

4. M. E. Shank and J. Wulff, "Deterimination of Boundary Stresses During the Consolidation of Cylindrical Powder Compacts," Met. Trans., 185 (1949) 561

5. P. Duwez and L. Zwell, "Pressure Distribution in Compacting Metal Powders," J. of Metals, 1 (1949) 137

6. P. R. Sahm, "Pressure Sintering - A Versatile Method of Materials' Preparation (Part 1)," Powder Met. Intl. 3 (1971) [1] 45

7. R. Kamm, M. Steinberg, Students, and J. Wulff, "Plastic Deformation in Metal-powder Compacts," Metals Technology 14 (1947) 442

8. T. E. Tietz and I. G. Palmer, "Advanced P/M Aluminum Alloys," Advances in Powder Technology, ed. G. Y. Chin, ASM (1982) 189

9. H. F. Fischmeister, "Isostatic Hot Compaction - A Review," Powder Met. Intl., 10 (1978) [3] 119

10. Powder Metallurgy Equipment Manual, Powder Metallurgy Equipment Assoc., New York, NY (1968)

11. Broese van Groenou, "Pressing of Ceramic Powders. A Review of Recent Work." Powder Met. Intl. 10 (1978) [4] 203

12. F. V. Lenel, "Mechanical Fundamentals of Consolidation," Metals Handbook, 9th Edition, Vol. 7, ASM, Metals Park, OH (1984) 296

13. L. F. Hammond and E. G. Schwarts, "The Effect of Die Rotation On The Compaction of Metal Powders," Int. J. Powder Metall. 6 (1970) [1] 25

14. C. G. Goetzel, "Hot Pressing," Metals Handbook, 9th Edition, Vol. 7, ASM, Metals Park, OH (1984) 501

15. P. J. James, "Fundamental Aspects of the Consolidation of Powders," Powder Met. Intl., 4 (1972) [2] 82

16. U. S. Patent #3 687 842

17. P. E. Price and S. P. Kohler, "Hot Isostatic Pressing of Metal Powders," Metals Handbook, 9th Edition, Vol. 7, ASM, Metals Park, OH (1984) 419

18. P. E. Price and S. P. Kohler, "Cold Isostatic Pressing of Metal Powders," Metals Handbook, 9th Edition, Vol. 7, ASM, Metals Park, OH (1984) 444

19. W. J. Huppman and M. Hirschvogel, "Powder Forging," International Metals Reviews, 5 (1978) 209

20. H. A. Kuhn, "Deformation Processing of Sintered Powder Materials," Powder Metallurgy Processing - New techniques and Analysis, H. A. Kuhn and A. Lawley eds., Academic Press, New York (1978) 99

21. A. Lawley, "Analysis of Mechanical Property - Structure Relations in Powder Forgings," Powder Metallurgy Processing - New Techniques and Analysis, eds. H. A. Kuhn and A. Lawley, Academic Press, New York (1978) 139

22. P. W. Lee and H. A. Kuhn, "P/M Forging," Metals Handbook, 9th Edition, Vol. 7, ASM, Metals Park, OH (1984) 410

23. P. W. Lee and H. A. Kuhn, "Fracture In Cold Upset Forging," Met. Trans. 4 (1973) 969

24. R. W. Stevenson, "P/M Lightweight Metals," Metals Handbook, 9th Edition, Vol. 7, ASM, Metals Park, OH (1984) 741

25. B. L. Ferguson, "Forging and Rolling of P/M Billets," Metals Handbook, 9th Edition, Vol. 7, ASM, Metals Park, OH (1984) 522

26. F. V. Lenel, "Hot Pressing - Appendix: Hot Extrusion," Metals Handbook, 9th Edition, Vol. 7, ASM, Metals Park, OH (1984) 515

27. E. Y. Gutmanus, "Cold Sintering Under High Pressure - Mechanisms and Application," Powder Met. Intl., 15 (1983) [3] 129

28. R. M. Koerner, "Triaxial Stress State Compaction of Powders," Powder Metallurgy Processing - New Techniques and Analysis, eds. H. A. Kuhn and A. Lawley, Academic Press, New York (1978) 33

29. G. Bockstiegel and J. Hewing, "Critical Review of the Literature on the Densification of Powders in Rigid Dies," Archiv. Eisenhuttenwesen, 36 (1965) 751

30. M. Yu. Balshin, "Theory of Compacting," Vestnik Metalloprom., 18 (1938) 137

31. C. Torre, "Theory and Behavior of Pressed Powders," Montan. Hochschule Leoben, 93 (1948) 62

32. I. Shapiro and I. M. Kolthoff, J. Phys. and Colloid. Chem., 51 (1947) 483

33. R. W. Heckel, "An Analysis of Powder Compaction Phenomena," Trans. AIME, 221 (1961) 1001

34. P. J. James, "Particle Deformation During Cold Isostatic Pressing of Metal Powders," Powder Metall., 20 (1977) 199

35. B. O. Sundstrom and H. F. Fischmeister, "A Contiuum Mechanical Model for Hot and Cold Compaction," Powder Met. Intl., 5 (1973) [4] 171

36. P. R. Seelig and J. Wulff, "The Pressing Operation in the Fabrication of Articles by Powder Metallurgy," Trans. AIME, 166 (1946) 492

37. H. F. Fischmeister, E. Arzt, and L. R. Olsson, "Particle Deformation and Sliding During Compaction of Spherical Powders: A Study by Quantitative Metallography," Powder Metall., 21 (1978) [4] 179

38. A. R. Austen, W. L. Hutchinson, and W. H. Feilbach, "Cold Deformation Consolidation Process For Rapidly Solidified Metal Powders," Rapidly Solidified Materials [Proc. Conf.] San Diego, CA, ASM Metals Park, OH (1985) 45

39. G. Y. Onoda and M. A. Janney, "Application of Soil Mechanics to Ceramic Particulate Processing," Advances in Powder Technology, ed. G. Y. Chin, ASM (1982) 53

40. E. Arzt, M. F. Ashby, and K. E. Easterling, "Practical Applicaions of Hot-Isostatic Pressing Diagrams: Four Case Studies," Met. Trans. A, 14A (1983) 211

41. M. Stromgren, H. Astrom, and K. E. Easterling, "The Effect Of Interparticle Contact Area On The Strength Of Cold - Pressed Aluminum Powder Compacts," Powder Metall., 16 (1973) [32] 155

42. H. A. Kuhn and C. L. Downey, Int. J. Powder Met. 7 (1971) 15

43. D. C. Drucker and W. Prager, Q. Appl. Math., 10 (1952) 157

44. R. W. Hertzberg, "Deformation and Fracture Mechanics Of Engineering Materials," John Wiley & Sons, New York, 2nd Ed. (1983) 44.

45. D. S. Wilkinson and M. F. Ashby, "Pressure Sintering By Power Law Creep," Acta Met., 23 (1975) 1277

46. K. E. Easterling and A. R. Tholen, "The Role Of Surface Energy and Powder Geometry In Powder Compaction," Powder Metall., 16 (1973) [31] 112

47. ASM Heat Treater's Guide: Standard Practices and Procedures for Steel, ASM, Metals Park, OH (1982)

VITA

Steven M. Joslin was born in St. Louis, Missouri on June 7, 1961. He graduated from Central High School in Columbia, Tennessee in June 1979. He entered Tennessee Technological University majoring in Chemical Engineering and transferred to The University of Tennessee, Knoxville after two years. In the fall of 1983, he changed his major to Metallurgical Engineering and achieved his B. S. in March 1984.

In June 1984, he accepted a position in the Materials and Process Engineering department of McDonnell Douglas Astronautics Company in St. Louis, Missouri. In September 1986, he began an educational leave of absence returning to The University of Tennessee to obtain an M. S. in Metallurgical Engineering. He plans to continue in the Ph.D. program in Materials Science and Engineering at The University of Tennessee.

He is a member of ASM International and AIME.